VOLUME 34 MAY 1956 NUMBER 5

Canadian Journal of Physics

Editor: G. M. VOLKOFF

Associate Editors:

L. G. ELLIOTT, *Atomic Energy of Canada, Ltd., Chalk River*
J. S. FOSTER, *McGill University*
G. HERZBERG, *National Research Council of Canada*
L. LEPRINCE-RINGUET, *Ecole Polytechnique, Paris*
R. W. PRINGLE, *University of Manitoba*
B. W. SARGENT, *Queen's University*
Sir FRANCIS SIMON, *Clarendon Laboratory, University of Oxford*
W. H. WATSON, *University of Toronto*

Published by THE NATIONAL RESEARCH COUNCIL
OTTAWA CANADA

CANADIAN JOURNAL OF PHYSICS

(Formerly Section A, Canadian Journal of Research)

Under the authority of the Chairman of the Committee of the Privy Council on Scientific and Industrial Research, the National Research Council issues THE CANADIAN JOURNAL OF PHYSICS and six other journals devoted to the publication, in English or French, of the results of original scientific research. Matters of general policy concerning these journals are the responsibility of a joint Editorial Board consisting of: members representing the National Research Council of Canada; the Editors of the Journals; and members representing the Royal Society of Canada and four other scientific societies.

EDITORIAL BOARD

Representatives of the National Research Council

A. N. Campbell, *University of Manitoba*
G. E. Hall, *University of Western Ontario*
E. G. D. Murray, *McGill University*
D. L. Thomson, *McGill University*
W. H. Watson (Chairman), *University of Toronto*

Editors of the Journals

D. L. Bailey, *University of Toronto*
T. W. M. Cameron, *Macdonald College*
J. B. Collip, *University of Western Ontario*
G. A. Ledingham, *National Research Council*
Léo Marion, *National Research Council*
R. G. E. Murray, *University of Western Ontario*
G. M. Volkoff, *University of British Columbia*

Representatives of Societies

D. L. Bailey, *University of Toronto*
Royal Society of Canada
T. W. M. Cameron, *Macdonald College*
Royal Society of Canada
J. B. Collip, *University of Western Ontario*
Canadian Physiological Society
R. G. E. Murray, *University of Western Ontario*
Canadian Society of Microbiologists
H. G. Thode, *McMaster University*
Chemical Institute of Canada
T. Thorvaldson, *University of Saskatchewan*
Royal Society of Canada
G. M. Volkoff, *University of British Columbia*
Royal Society of Canada; Canadian Association of Physicists

Ex officio

Léo Marion (Editor-in-Chief), *National Research Council*
F. T. Rosser, Director, Division of Administration, *National Research Council*

Manuscripts for publication should be submitted to Dr. Léo Marion, Editor-in-Chief, Canadian Journal of Physics, National Research Council, Ottawa 2, Canada.
(For instructions on preparation of copy, see **Notes to Contributors** (inside back cover).)

Proof, correspondence concerning proof, and orders for reprints should be sent to the Manager, Editorial Office (Research Journals), Division of Administration, National Research Council, Ottawa 2, Canada.

Subscriptions, renewals, requests for single or back numbers, and all remittances should be sent to Division of Administration, National Research Council, Ottawa 2, Canada. Remittances should be made payable to the Receiver General of Canada, credit National Research Council.

The journals published, frequency of publication, and prices are:

Canadian Journal of Biochemistry and Physiology	Bimonthly	$3.00 a year
Canadian Journal of Botany	Bimonthly	$4.00 a year
Canadian Journal of Chemistry	Monthly	$5.00 a year
Canadian Journal of Microbiology	Bimonthly	$3.00 a year
Canadian Journal of Physics	Monthly	$4.00 a year
Canadian Journal of Technology	Bimonthly	$3.00 a year
Canadian Journal of Zoology	Bimonthly	$3.00 a year

The price of single numbers of all journals is 75 cents.

Canadian Journal of Physics

Issued by THE NATIONAL RESEARCH COUNCIL OF CANADA

VOLUME 34 MAY 1956 NUMBER 5

STRUCTURE OF THE MASS INCREMENTS OF ISOTOPES[1]

BY G. A. BAKER, JR. AND G. A. BAKER, SR.

ABSTRACT

A simple, accurate formula for the atomic masses of all isotopes is developed on the basis of a simplified nuclear model. It is shown theoretically and empirically that a formula which is linear in A and whose coefficients depend only on $N-Z$ with a term added for pairing effects accounts for the major portion of the structure in the present experimental data and predicts them with unexcelled accuracy.

INTRODUCTION

One major problem in physical research that is being extensively investigated is the creation of new elements in the very heavy region. In order to aid in this research it is very important to have as accurate a method as possible to predict unknown isotopic masses in the heavy region. A study of the literature reveals that the Weizsäcker formula, which is almost universally used, shows exactly the wrong behavior in this region. In view of these facts we feel that a different approach to the problem of predicting isotopic masses is necessary.

At the present time there exists a large amount of data concerning the isotopic masses of atoms. These data are concentrated primarily for low and high values of A (atomic mass number). As yet no one has developed formulas which give a detailed, really accurate description of these data. All previous such attempts as indicated by Green (Green and Edwards 1953; Green and Engler 1953) have used formulas patterned after the Weizsäcker formula, which has a major term involving A only, a correction term depending on A and $N-Z$, the neutron excess, and correction terms for the "pairing effect" and the "shell effects". We, on the other hand, have analyzed the mass increments of isotopes within groups of the same neutron excess as linear functions of A plus pairing effects plus shell effects.

We shall begin with a slightly naïve view of the nucleus and deduce in a qualitative way a simple expression for the nuclear-binding energy. We shall then empirically fit the constants involved and check the accuracy of the results, as a verification of the adequacy of the approximations made in our model of the nucleus.

[1]Manuscript received in original form September 26, 1955, and as revised January 18, 1956.
Contribution from the Department of Physics, University of California, Berkeley, California, and the Department of Mathematics, University of California, Davis, California.

I. MODEL

We know that the ground state of a nucleus is completely describable in terms of A and $N-Z$. Furthermore, we know that the nuclear forces are extremely short range and that they are probably saturated, that is, each nucleon does not interact simultaneously with all other nucleons in a nucleus. Thus, it is at least plausible to divide the nucleus into a core, whose characteristics depend only on the neutron excess, and a few nucleons stuck onto the surface of the core. We shall suppose that, to a first approximation, the extra-core nucleons do not appreciably interact with each other, aside from the pairing effect, and that the core binds all extra-core nucleons with the same binding energy. Hence, we should expect that

$$(1) \qquad E_{\text{binding}} = (b'(N-Z))A + a'(N-Z) + P'(A, N-Z, (-1)^N, (-1)^Z) + S'(A, N-Z) + R'(A, N-Z) .$$

In Eq. (1) E_{binding} is the binding energy, a' and b' depend only on the neutron excess, P' is the pairing correction whose sign is determined by the evenness and oddness of N and Z, S' is the correction for the shell effects, and R' is a small residual which may be zero. It should be remarked that one could hardly expect a well-established core for very light nuclei, and it is not surprising that the pairing and shell effects of this model are more important in the range of very small A. It is not claimed that Eq. (1) gives a completely detailed description of nuclear structure but it is a useful way of thinking of the nucleus for the purpose of predicting isotopic masses.

We have no *a priori* reason to expect that our linear formulas will be valid in regions far from the beta-stable isotopes. For values of A that are too small we will not have a complete core as, for example, the high A isotopes of krypton and xenon. If the values of A are too large we would expect the extra-core bonds to become saturated. It should be mentioned, however, that there are very few nuclear species and no mass data in such exceptional regions.

In fact, the linear part of Eq. (1) is found to be valid for ranges of A of about 30 to 40 mass numbers which is far greater than could be expected for a Taylor's expansion of any formula suggested heretofore. The reason that the region of validity cannot be extended further from the beta-stability line is that, since the lines of constant $N-Z$ are essentially parallel to the beta-stability line and the beta-stability line curves only slightly, then in order for the lines of Eq. (1) to be valid far from the beta-stability line and also in the stable region, validity ranges of A of more than 100 mass numbers would be required. Such wide ranges of validity cannot be expected for the reasons given above.

We emphasize that this approach is essentially different from a Taylor's series expansion of the Weizsäcker formula for several reasons. The linear functions of A are valid over a much longer range than could be expected from a series expansion. Also, the change of the slope with $N-Z$ which we have determined differs markedly in the region of the heaviest nuclei from that which would be predicted by the Weizsäcker formula.

II. PROCEDURE

The hypothetical model represented by Eq. (1) is checked against the experimental isotopic-atomic-mass data listed by Bainbridge (1953), Halsted

TABLE I

LINEAR ESTIMATING EQUATIONS FOR ΔM; $\Delta M = b(A + a/b)$

$N-Z$	n	r		b	a/b
−2	2	—		9739.868	−3.208556
−1	12	.99981222		9731.632	−2.803570
0	17	.99938479		9723.396	−2.305673
1	22	.99981915		9762.379	−2.434629
2	25	.99979453		9917.159	−2.933996
3	16	.99926190		9941.258	−3.099600
4	11	.99916264		9646.603	−1.664954
5	13	.99897630		9295.808	0.369128
6	16	.99933033		9197.294	1.143975
7	10	.99967762		9137.761	1.534615
8	10	.99954254		9257.919	0.672439
9	6	.99999758		9032.240	2.535592
10	12	.99958944		8871.489	4.106555
11	10	.99924600		8803.843	4.864401
12	11	.99955230		8590.722	7.339545
13	12	.99955875		8653.295	6.562900
14	9	.99975992		8606.887	7.170560
15	6	.99997399		8593.917	7.324621
16	10	.99945724		8591.184	7.232523
17	4	.99998592		8632.000	6.784059
18	9	.99946048		8197.333	13.224848
19	7	.99969004		8398.786	10.073858
20	6	.99928121		8235.244	12.767603
21	6	.99964323		8319.996	11.353991
22	5	.99868093		8281.250	12.045464
23	5	.99999454		8349.500	10.870771
24	5	.99974056		7998.708	16.982018
25	2			7928.842	18.419081
26	2			7928.842	18.444920
27	1		1	7928.842	18.184710
28	1			7928.842	18.586508
29	1			7928.842	17.501993
30	1			7594.000	24.890703
31	0			7594.000	25.051882
32	1		2	7594.000	25.213062
33	0			7594.000	25.097642
34	2			7594.000	24.982222
35	1			7594.000	24.839873
36	2			7467.868	27.993534
37	0		3	7341.736	31.537282
38	1			7215.604	35.081030
39	1			7089.472	39.086544
40	4	.99812776		6963.341	43.464160
41	5	.99945769		6284.500	70.856631
42	5	.99594769		6100.500	79.422342
43	11	.99882336		5645.054	102.609956
44	13	.99952121		5621.115	104.238283
45	15	.99977797		5740.875	97.556739
46	15	.99687445		5823.292	93.203467
47	15	.99993800		5930.692	87.521635
48	16	.99986828		6023.099	82.779407
49	15	.99992756		6086.088	79.614794
50	15	.99984103		6134.204	77.207445
51	9	.99981389		6198.050	74.108926
52	9	.99970880		6176.243	75.229481
53	6	.99988482		6287.857	69.728743
54	4	.99992945		6340.000	67.229022
55	4	.99991299		6458.000	60.577615

Note.—The sets of values of b marked 1 and 2 were obtained from the step structure observed in this table and shown in Fig. 1 as indicated in the text. The values of b marked 3 are obtained as linearly interpolated values between the values for $N-Z = 35$ and $N-Z = 40$. The corresponding values of a/b are estimated from the one or two observed values if there are any. If there are no observed values, the value of a/b is the average of the preceding and succeeding values.

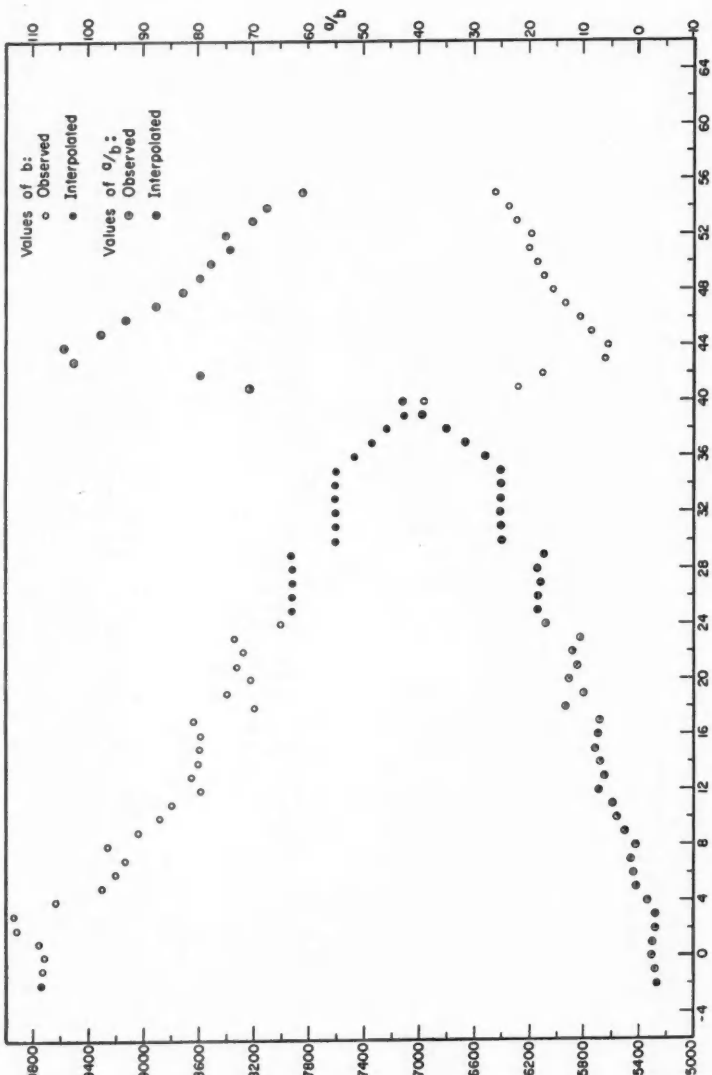

FIG. 1. Values of b and a/b of Table I plotted against the neutron excess $N-Z$. The observed and interpolated values are distinguished by different symbols.

(1952), and Collins *et al.* (1952, 1954) by means of the Einstein mass–energy relation. It is found that the gross aspects of the mass increments can be represented by straight lines with A as the independent variable, whose constants (slope and intercept) depend on N (number of neutrons) minus Z (number of protons). These lines are indicated by the first two terms of Eq. (1). The numerical values of the constants are given in Table I. (Of course, by the Einstein relation E_{binding} is proportional to the ΔM of Table I.) To indicate the extent to which the lines represent the observed data the correlation coefficients are also listed in Table I. The striking structure of the constants of Table I yields much insight into nuclear characteristics and enables us to fill in the gaps in existing experimental data in a reasonable way.

In order to emphasize the structure of the coefficients of Table I we prepared Fig. 1. The observed values are indicated to distinguish them from the interpolated values.

The simple linear estimates of the mass increments are surprisingly good. They account for about 99.88 per cent of the variation in the observed data as indicated by the correlation coefficients of Table I.

In Table II we compare the average absolute residuals from our linear estimates and those from the optimum semiempirical formula obtained by Green and Engler (1953), Fig. 1, page 41. These data are for beta-stable, odd-A

TABLE II

AVERAGE ABSOLUTE RESIDUALS IN MICRO-ATOMIC-MASS UNITS

Range of A	Number of observations		Average absolute residuals	
	This paper	Green*	This paper	Green*
10– 50	20	20	1562	2012
50–100	21	11	1955	1364
100–212	19	20	817	2200
212–246	16	15	511	3117
10–246	76	66	1263	2212

*Green and Engler (1953), Fig. 1. The residuals were read from the graph as closely as possible.

nuclei. The groups were chosen so as to divide the data into four approximately equal groups. The comparison in Table II shows that our linear estimates are as good as the Weizsäcker formula for A less than 100 and are far more accurate for A greater than 100. In the critical region of the heaviest elements our method gives an average absolute residual for odd-A, beta-stable isotopes of 511 as compared to Green's 3117 micro-atomic-mass units. This is a reduction in the average size of the residuals by a factor of more than 6. Also, our results are noticeably better in the region $10 \leqslant A \leqslant 50$ in which there is a sizable amount of experimental data. In the range of the heaviest isotopes the remaining structure, shell effects, can be removed in a fairly straightforward manner so that the residuals in this region can be further reduced to approximately the experimental error. We intend to do this in a future paper.

In the region of the heaviest nuclei our values agree quite well with the experimental values listed in a recent article by Glass *et al.* (1955). However, the extrapolations made by these authors for values of A greater than those for which measurements have been already made differ markedly from the values predicted by us on the basis of the coefficients of Table I.

Glass, Thompson, and Seaborg use a graphical procedure to extrapolate the alpha-decay energy into regions where there are no data, and by summing up mass differences are able to extrapolate the masses from a known mass in each decay series. We note, from a comparison with our results, that their extrapolated alpha-decay energy for the decay series with $N-Z = 42$ and containing $A = 218$ is about 3 Mev. higher than we obtain. An examination of the coefficients in Table I shows that in their extrapolation from high $N-Z$ down to 42, 40, etc., they have failed to take into account the precipitous decline of b with $N-Z$ in the transition between the regions of naturally stable and naturally unstable isotopes.

If the deviations of the mass increments from the fitted lines of Table I are considered, they are found to be distinctly nonrandom. One of the most striking features of the deviations of the observed ΔM (mass increments) from the linear estimates considered as a function of A is the pairing effect for A even. In order to assess the pairing effect represented by the third term in Eq. (1) as closely as possible we tabulated the deviations of the observed values from a series obtained by replacing y_i by $(y_{(i-1)/2}+y_i+y_{(i+1)/2})/2$. We find with Green and Edwards (1953) that the over-all pairing effect may be approximately represented as being inversely proportional to the square root of A. However, this representation completely overlooks the markedly stronger pairing for $N-Z = 0$ and the somewhat stronger pairing for $N-Z = 2$ especially for smaller A. After studying and averaging we arrived at the following easily applied formula for the pairing effect:

$$P = h(A, N-Z)((-1)^N+(-1)^Z) \tag{2}$$

where

$$h(A, N-Z) = \begin{cases} 2200, & 6 \leqslant A \leqslant 12, \quad N-Z = 0, \\ 1600, & 14 \leqslant A \leqslant 28, \quad N-Z = 0, \\ 1200, & 6 \leqslant A \leqslant 28, \quad N-Z = 2, \\ 800, & 30 \leqslant A \leqslant 88, \\ 600, & 90 \leqslant A \leqslant 206, \\ 400, & 208 \leqslant A \leqslant 246. \end{cases} \tag{3}$$

The linear and pairing effects corresponding to the first three terms of Eq. (1) can be fairly accurately assessed and applied to missing values. However, after these effects are removed, residuals are left which are also nonrandom but which cannot be described as easily as the linear and pairing effects. The size and importance of the deviations from linear estimates corrected for pairing effects may be indicated by regarding these second-order residuals as being without structure and quoting probable errors for specified

ranges of A. Thus, for the range $6 \leqslant A \leqslant 206$ the probable error is 2.86 electron masses for 288 observations, while for the range $A > 206$ the probable error is 0.99 electron masses for 148 observations.

However, the second-order residuals exhibit a relatively smooth, somewhat sinusoidal structure which is strongly suggestive of a nuclear shell structure and we shall identify at least the major part of these second-order residuals with the fourth term of Eq. (1). The fifth term of Eq. (1) may be very small or it may consist of stray elements of structure that cannot be identified with the first four terms. While the shell effects are not amenable to precise, predictive formulation some suggestive and summary comments will be made with regard to their most striking characteristics.

In order to summarize the shell effects we averaged the absolute values of the shell effects for each value of $N-Z$. The shell effects seem to be strong for $-1 \leqslant N-Z \leqslant 8$ with a considerable peak at $N-Z = 5$, and practically vanish at $N-Z = 9$. They are again strong for $10 \leqslant N-Z \leqslant 14$ with peaks at $N-Z = 11$ and 13. They fall away and appear to be of little importance for $17 \leqslant N-Z \leqslant 40$. The upper limit is in doubt because of lack of data. The shell effects become important again at $N-Z = 43$ at a much lower level than for small $N-Z$ and then drop away to nothing at $N-Z = 54$. The distances between very low points form the sequence 8, 6 for $N-Z < 25$.

To summarize the behavior of the shell effects for different values of A we averaged all absolute values for two adjacent values of A for A odd. For example, all absolute values of shell effects were averaged for $A = 9$ and $A = 11$ and entered opposite $A = 10$ etc. For even A, for example, one half the absolute values for $A = 10$ plus the absolute values for $A = 12$ plus one half the absolute values for $A = 14$ were averaged and entered opposite $A = 12$. The average values so obtained for A even and A odd fit together in a very striking pattern.

There was a small peak at $A = 14$, a larger peak at $A = 18$, a large peak at $A = 35$, a small peak at $A = 42$, a smaller peak at $A = 48$, a very large peak at $A = 62$, a smaller peak at $A = 76$, and the largest peak of all at $A = 90$. The shell effects then drop away and practically vanish at $A = 130$. There is no information for A between 130 and 204. At $A = 206$ the shell effects again become important in a minor sort of way and then fade away to small values as far as our information goes. The distances between peaks form the sequence 4, 14, 10, 6, 14, 14, 14, 14 for $A < 110$ and the sequence 14, 14 for $A > 206$.

III. CALCULATION OF LINEAR ESTIMATES

All possible data $6 \leqslant A \leqslant 246$ were used in fitting the straight lines of Table I which give estimates of ΔM, which is defined by the equation

$$\Delta M = 10^6(1.008142\,Z + 1.008982\,N - M_{ZN}), \tag{4}$$

as linear functions of A for particular values of $N-Z$. The lines are the usual least square lines, fitted without regard to the published errors, that is, all observed values were weighted equally. The obtained values for b (slope) and

a/b (intercept divided by slope) were used when n, the number of observations, was equal to or greater than 4. The other values of the constants were interpolated on the basis of the structure of the coefficients and such scanty information as is available.

A study of the values obtained for b and a/b given in Table I and portrayed in Fig. 1 shows that for $0 \leqslant N-Z \leqslant 23$ the values break up into blocks of 4, 4, 4, 6, and 6. The blocks 12 to 17 and 18 to 23 give the appearance of a descending staircase (for b) of tread 6 and step about 400 micro-atomic-mass units per atomic number. If we continue this structure we observe that the value of b for the block 30 to 35 is very close to the critical value for alpha stability. (If the masses were given exactly by the linear estimates without shell effects or pairing effects one could readily verify that the criterion for alpha stability is $b > \frac{1}{4}\Delta M(2, 2) = 7594$.) As we are approaching the transition region between alpha-stable and alpha-unstable nuclei, we assume that b for the 30 to 35 block is 7594.000 and we choose for the undetermined b's of the 24 to 29 block the value midway between this value and the average of the 18 to 23 block. The values of a/b were then adjusted to make the lines agree with observed data. It should be noted that the values of a/b seem to be level when the values of b are level. To get from $N-Z = 36$ to $N-Z = 40$ linear interpolation was used. It is further noted that beginning with $N-Z = 36$ blocks of 8 are indicated.

We mention that in order to reproduce the experimental results accurately the constants of the estimating equations must have more significant figures than the observations. We have given seven figures at least and then have been consistent on the number of decimal places carried.

In Table I we have used 42 lines to fit 436 observations. The correlation coefficients are so large that they clearly indicate the physical significance of the model used and the efficacy of the statistical techniques for predictive purposes. In addition, a striking structure is apparent in the values of the constants which enables us to bridge a gap in the existing data in a way that is valuable from a predictive viewpoint for further experimental work.

IV. SUMMARY

A mathematical model of the structure of atomic masses of the isotopes has been postulated and tested against all available observed data. The agreement between the model and the observed data is good enough to indicate that the model can be regarded as a useful approximation to reality as observed up to this time. This model can be used as a basis for guidance of further research both for intermediate masses and for heavier masses than have at present been observed. It is recognized, as additional observations are made, that adjustments in the values of the empirical constants will be necessary, but that can be done easily. It is expected that the over-all structure will remain essentially as pictured.

On the whole it is noted that the average of the squares of the correlation coefficients of Table I is 0.9988 which indicates good fits for the straight lines.

If we consider the frequency distributions of the residuals after the linear

estimates and the pairing effects are removed for the two regions of A, $6 \leqslant A \leqslant 206$ and $A > 206$, we find that they are very nearly normal. It seems appropriate to give probable errors for these distributions which have the usual interpretation. The probable error for the first region is 2.88 electron masses and for the second region, 0.99 electron masses. The shell effects are small and regular for large values of A so that especially in this region much closer estimates of known values are possible and such a project will be undertaken in a future paper.

The estimated and interpolated atomic masses follow very closely the observed beta-stability pattern.

Shell effects may seriously disturb the fitting of short series but this is more apt to happen for small A than for large A. Such disturbances appear as irregularities in Fig. 1 and tend to obscure an otherwise striking structure.

We reject the simple hypothesis of a constant binding energy per nucleon (approximately 7 Mev.) as being inadequate since b varies by a factor of more than 7/4 (from above 9900 to about 5600).

REFERENCES

BAINBRIDGE, K. T. 1953. *In* Experimental nuclear physics. Pt. V, Vol. I. *Edited by* E. Segrè. John Wiley & Sons, Inc., New York. p. 559.
COLLINS, T. L., JOHNSON, W. H., JR., and NIER, A. O. 1954. Phys. Rev. **94**: 398.
COLLINS, T. L., NIER, A. O., and JOHNSON, W. H., JR. 1952. Phys. Rev. **86**: 408.
GLASS, R. A., THOMPSON, S. G., and SEABORG, G. T. 1955. J. Inorg. Nuclear Chem. **1**: 3.
GREEN, A. E. S. and EDWARDS, D. F. 1953. Phys. Rev. **91**: 46.
GREEN, A. E. S. and ENGLER, N. A. 1953. Phys. Rev. **91**: 40.
HALSTED, R. E. 1952. Phys. Rev. **88**: 666.

PRODUCTION OF COSMIC RAY MESONS AT LARGE ZENITH ANGLES[1]

By D. Jakeman[2]

ABSTRACT

Events have been selected by coincidences between separated shielded trays of Geiger counters and it is shown that they arise from three types of phenomena, namely, extensive air showers, casual coincidences, and particles travelling in almost a horizontal direction. Selection of the last type of event has enabled the absolute intensity to be determined at zenith angles between 88° and 90°. Using a π meson production spectrum which gives consistency with the established underground absorption curve the intensity of particles in the horizontal direction has been calculated on the assumption that π–μ decay is the only source of μ mesons. The calculated intensity agrees well with the observations. Alternatively, by comparing the rate in the horizontal direction with the known rate underground, a value of $4.5\pm1.5\times10^{-3}$ sec. is obtained for the lifetime of the parents of μ mesons which, because of the depth of the atmosphere in the horizontal direction (362 m.w.e.), must have energy exceeding 10^{11} ev. This suggests that at this energy the parents of μ mesons can be identified with the π meson, and the number of μ mesons arising from the decay of a shorter lived meson (e.g. K meson) must be relatively small.

INTRODUCTION

It has long been established that most of the μ mesons which are observed in cosmic radiation arise from the decay of the π meson. With the discovery of other heavier types of mesons, it seemed possible that at higher energies other mesons might be formed which decayed directly into μ mesons and the observations of O'Ceallaigh (1951) supported this. More recent experiments by Daniel and Perkins (1954) suggest that heavy mesons (K-particles) of mass 1210 ± 40 m_e having a lifetime an order of magnitude smaller than π mesons are produced in nuclear interactions, their yield increasing with the energy of the primary initiating the event. These authors suggest that most of the K-particles are to be identified with particles classified phenomenologically as κ mesons which decay directly into a μ meson and probably two neutral particles.

In the present experiment we have attempted to measure the lifetime of the parents of μ mesons by comparing the rate of observed particles which are travelling in almost a horizontal direction at sea level with the rate underground at equivalent depths. This method makes use of the property of the atmosphere that it is not of a constant density. Barrett *et al.* (1952) have also tried to determine whether π–μ decay is the only mechanism whereby μ mesons are produced. In principle their experiment was to compare the rate underground at various depths and incident at various zenith angles up to about 60°. At this angle the density where the parents of μ mesons are produced differs from the density where the parents of vertical μ mesons are produced by a factor of 2. Because of this change in density, the number of μ mesons produced differs in the two directions although the difference is small and the

[1]Manuscript received November 10, 1955.
Contribution from the Division of Pure Physics, National Research Council, Ottawa, Canada. Issued as N.R.C. No. 3933.
[2]National Research Laboratories Postdoctorate Fellow; now with United Kingdom Atomic Energy Authority.

experiment of Barrett *et al.* was inconclusive. The corresponding ratio of densities for the vertical and horizontal directions is approximately 10 which suggests that there is a considerable advantage in making observations at large zenith angles.

The study of particles at large zenith angles was initiated by the observations by Broadbent and the present author of unusual events selected by the extensive air shower arrangement at Manchester, England. These events were clearly not normal extensive air showers but could possibly be explained by particles travelling horizontally. The experimental data were limited and the initial part of the present study was to verify that this explanation was correct.

EXPERIMENTAL ARRANGEMENT AND SELECTION OF EVENTS

The basic arrangement is shown in Fig. 1. It consists essentially of four trays of G.M. counters referred to as P_1, P_2, H, and E trays. The precise arrangement of counters in a particular tray was changed several times during the course of

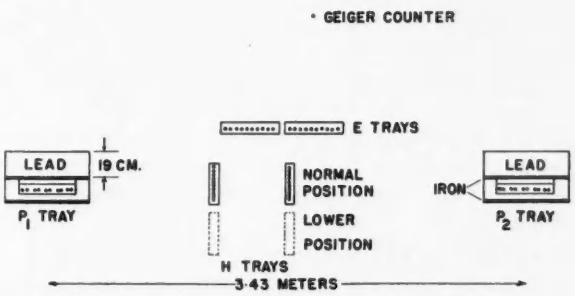

FIG. 1. Experimental arrangements, side elevation. (Plan elevation for similar arrangement is shown in Fig. 5.)

the experiment, but the function of each of the four trays remained the same. Coincidences between counters in P_1 and P_2, which were shielded on all sides by at least 20 cm. of lead, were always used to select events which fall into three groups.

Group 1: Extensive air showers.—Penetrating particles in extensive air showers can give rise to coincidences in P_1, and P_2. Since the number of penetrating particles (2%) in a shower is much smaller than the number of soft particles (98%) (e.g. Cocconi *et al.* 1949), the probability of a counter in the E tray being discharged is extremely high. This was clearly shown with the experimental arrangement at Manchester, where all the counters in the E tray were hodoscoped. It was found that frequently all counters in this tray were discharged with progressively fewer events in which some counters were not discharged. In the present experiment an ionization chamber situated between the P_2 and H tray was put in coincidence with the coincidence pulse from P_1 and P_2 and frequently when the E trays were discharged, a large burst was indicated. A coincidence between P_1, P_2, and E trays, therefore, showed the

presence of an extensive air shower. For all experiments described, the E tray contained 20 unshielded counters, each of area 100 cm.^{2}, divided into two groups of 10 counters in parallel. Showers in general discharged counters in the H tray since these also were unshielded. However, since they presented a smaller area to showers in the near vertical direction, as compared with the E tray, events were occasionally found in which they were not discharged. Any event in which the E tray was discharged is referred to as an E event. If it was not discharged, the event is referred to as a Q event.

Group 2: Particles travelling horizontally.—This group consists of all the Q events in which the H tray is discharged. The purpose of the first part of the experiment was to establish whether or not these events arose partly or entirely from particles travelling horizontally.

Group 3: Casual events.—This group consists of all the Q events in which the H tray was not discharged. Most of these events arise from casual coincidences. (See for example Table II.)

A 16-channel hodoscope arrangement was constructed and it was possible to get information on which of the individual counters or counter groups in the P_1, P_2, E, and H trays were discharged. The coincidence circuits and associated electronic apparatus were of the standard type used in the Cosmic Ray Laboratories at Ottawa and have proved themselves reliable over a period of many years. The recording of individual events was performed on a 20-pen Esterline Angus recorder which could be run at a speed such that the events were easily distinguishable.

CONFIRMATION OF PARTICLES TRAVELLING HORIZONTALLY

The first experiment was to check some of the Manchester work and to establish more definitely that the particles being detected were travelling horizontally. (We refer to these, for convenience, as horizontal particles.)

P_1 and P_2 each contained five pairs of counters, each pair having an area of 200 cm.^{2} Events were selected when two or more pairs of counters out of the five in each tray were discharged.

The selected events can be divided into two classes; an E event is one in which the E tray is discharged and a Q event is one in which it is not discharged. Each of these classes can be further subdivided according to whether or not the H tray is discharged. The number of events in each class is shown opposite "Normal position" in Table I.

TABLE I

	Running time, days	Type of event			
		$E+H$	$E-H$	$H-E$	$-E-H$
Normal position	86	56	6	38	17
Lower position	56	41	3	2	18

This confirms the existence of Q events and, since the number of $H-E$ events is appreciably greater than the number of $E-H$ events, the presence of particles

travelling in a horizontal direction is strongly suggested. (For showers, most of which are in the near vertical direction, the area of the E tray is very much larger than the H tray.) Further, the fraction of Q events which arise from particles travelling horizontally is $38/55 = 0.69 \pm 0.06$.

If the $H-E$ events arise from horizontal particles, the rate of events should be reduced if the H tray is moved to a lower position as shown in Fig. 1. The lower line ("Lower position") in Table I gives the number of the different types of events recorded.

It is seen that the number of $H-E$ events is considerably reduced as expected. The two $H-E$ events observed might still arise from particles travelling horizontally since it is shown below that secondaries accompany the horizontal particles and can have an appreciable spread at the position of the H tray.

More direct evidence that the $H-E$ events arise from horizontal particles was obtained with a slightly modified arrangement. The number of counters in each of P_1 and P_2 was reduced to eight equally spaced counters, each of area 100 cm.^{2} The alternate counters in each tray were connected together so that each tray consisted of two groups of counters. Fourfold coincidences between the two groups of P_1 and the two groups of P_2 were used to select events. The H tray was replaced by a tray as shown in Fig. 2. Each pair of counters of the

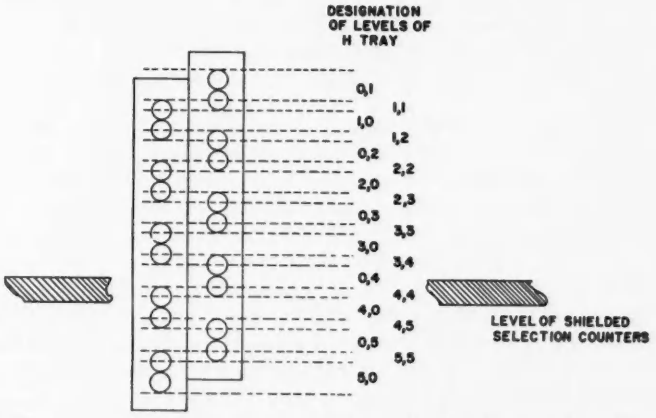

FIG. 2. Arrangement of H trays showing positions of pairs of counters in each tray.

H tray was attached to one channel of the pen recorder and hence, for every selected event, it was possible to determine which individual pairs of counters had been discharged.

As previously shown, horizontal particles produce events in which we have a coincidence between the counter in P_1 and P_2 and at least one counter in the H tray, but not one in the E tray, i.e., $H-E$ events. Forty-eight such events were recorded and, of these, 40 events were consistent with single particles passing through the H tray. For these 40 events, the height at which horizontal particles passed through the tray is known from the hodoscope arrangement

and Fig. 2 shows the different regions defined by the arrangement. The number of events observed falling in each of these regions is shown in Fig. 3. The level of the counters in trays P_1 and P_2 is also shown.

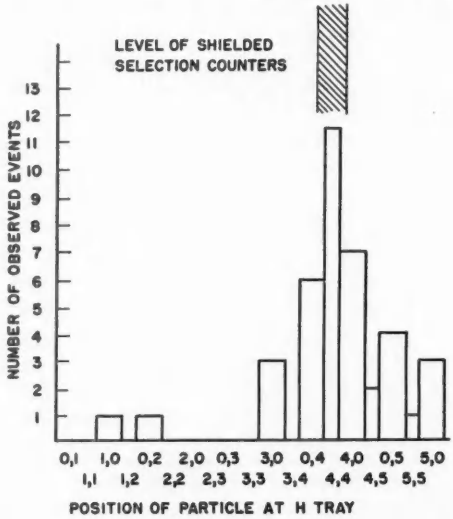

FIG. 3. Distribution in space of selected horizontal particles.

If the horizontal particles were to pass directly through the selecting counters in the P_1 and P_2, then half of the particles should hit the H tray in the region we have numbered 4,4 and the remainder in either 0,4 or 4,0. Hence 25 out of the 40 events are consistent with but do not necessarily indicate particles passing directly through the selecting counters, and the remaining 15 are definitely not consistent. This experiment shows a very high probability that horizontal particles are being recorded, some of them accompanied by secondaries, since Fig. 3 could not be explained otherwise. It also supports the Manchester work indicating that some of the horizontal particles do not pass directly through the selecting counters and that secondaries accompany the particle as it passes through the absorber.

The remaining 8 events out of the 48 recorded in this part of the experiment showed discharges in the H tray which could not be consistent with a single particle passing through the tray unless the particle was travelling at a very large angle from the horizontal. Particles at such a large angle could not produce the necessary discharges in the P_1 and P_2 tray. This suggests that secondaries accompany the particle as it traverses the air between the absorbers.

EXPERIMENTAL DETERMINATION OF THE ABSOLUTE RATE OF HORIZONTAL PARTICLES

In the experimental arrangement described in the previous section, many of the events arise from particles passing outside the solid angle defined by the selection counters, but secondaries associated with them discharge the counters.

It is difficult to estimate the frequency of such events and consequently the absolute rate of particles passing within the solid angle cannot be determined accurately. For this reason a more conventional arrangement was constructed for which the necessary corrections are much reduced. P_1 and P_2 were replaced by vertical trays (i.e., at right angles to the path of the horizontal particles) as shown in Fig. 4, and events were selected when coincidences occurred be-

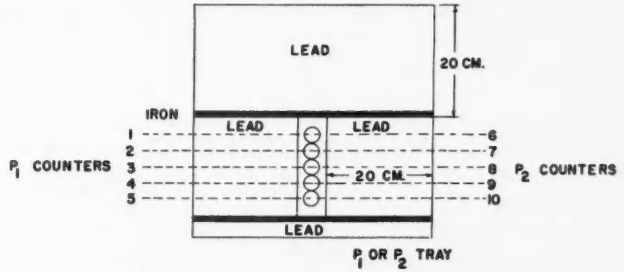

FIG. 4. Modification to P_1 and P_2 trays.

tween the discharges in any one of the five counters in P_1 (numbered 1–5 inclusive) and in any one of the five in P_2 (numbered 6–10 inclusive). This gives 25 counter telescopes and since each counter in the P_1 and P_2 trays had its own associated pen, it was possible from the recorder to determine which particular counters had contributed to the event.

The half angle defined by one of these telescopes is 0.2° and the most inclined direction at which particles may still pass through both trays is 2.0° from the horizontal. The H trays were replaced by four groups of counters, each group having an associated pen on the recorder. The E tray was split into two halves as in the previous experiment.

Initially the apparatus was set up with the line joining the centers of P_1 and P_2 trays almost in the E.W. direction and the topography was such that horizontal particles would not be obstructed from either the east or the west. Fenton, however, in discussion pointed out that the earth's magnetic field could appreciably alter the rates for horizontal particles in the E.W. direction. In order to reduce the effect of the earth's magnetic field, the arrangement was then set up with the centers of P_1 and P_2 in the direction along the horizontal component of the earth's magnetic field. In this direction, the Gatineau Hills, a few miles north, obstructed particles arriving from the northerly direction at zenith angles larger than 89.6°.

Most of the recorded events arose from casual coincidences between the P_1 and P_2 trays. The counting rate of these trays is 300 c.p.m. and with a resolving time of the coincidence circuits of 4 μsec. the number of expected casual events is 0.71 per hr. Table II shows the number of casual events expected and the number of events observed in which no counter other than those in P_1 and P_2 is discharged ($-E-H$ events). These are the same within the statistical error.

TABLE II

OBSERVED NUMBERS OF EVENTS COMPARED WITH NUMBERS EXPECTED FROM CASUAL COINCIDENCES

Direction of telescope	Running time, hr.	$-E-H$		$E-H$		$E+H$		$H-E$	
		Obs.*	Exp.†	Obs.*	Exp.†	Obs.*	Exp.†	Obs.*	Exp.†
E.W.	812.5	604	580	5	0.8	46	—	180	1.9
N.S.	2047.7	1424	1463	22	2.1	94	—	417	4.9
Total	2860.2	2028	2043	27	2.9	140	—	597	6.8

*Observed.
†Expected (casuals).

If we now consider the events when either the E or the H trays are discharged, then the number of events recorded which could arise from casual coincidences is very small. The main type of casual event is one in which a single particle passes through either the E or the H tray and a counter in P_1 (or P_2) and, within the resolving time, a counter in P_2 (or P_1) is discharged. Table II gives the observed number of the different types of events recorded and the calculated number which could arise from casual coincidences.

We consider now the $H-E$ events which we believe arise almost entirely from particles travelling in a horizontal direction, except for a small number of casual events as shown in Table II and perhaps a few events arising from extensive air showers as discussed below (correction (c)). Out of the 180 events recorded in the E.W. direction and 417 events recorded in the N.S. direction, 146 events and 339 events respectively gave single discharges in both the P_1 and the P_2 tray. These will be called single events and the remaining events in which more than one counter in either P_1 or P_2 is discharged will be called multiple events. For each of the single events the direction of the particle is known within the limits defined by a particular telescope. Each of the 25 telescopes can be designated by the number of the counter in the P_1 tray and the number of the counter in the P_2 tray and Tables III and IV give the number of single events recorded for each telescope for the E.W. and N.S. direction respectively. Numbers along the same diagonal line as shown refer to telescopes pointing in the same direction in space and the total number of events for each direction is given. The zenith angle refers to the line joining the centers of a particular counter telescope.

There is no evidence for differences in the number of observed events between telescopes pointing to the east and those pointing to the west (Table III) and the number of events for each zenith angle irrespective of whether the telescope is pointing to the east or the west is given in Table V(a). Tables IV and V(b) are similar tables for the N.S. direction. Table V also gives the average number of events per telescope for each direction and the absolute rate of particles per sec. per cm.^{2} per sterad. The number of telescopes pointing in a direction $\theta = 90°$ has been taken as 10 rather than 5 since particles can be recorded travelling from either the east or the west (north or south). This is discussed later (correction (d)).

TABLE III

NUMBER OF EVENTS PER TELESCOPE: E.W. DIRECTION

Counter number P_2 tray	Counter number P_1 tray 1	2	3	4	5	Total for telescopes pointing west	Mean zenith angle
6	5	6	6	5	6	6	88.4°
7	6	9	8	4	9	14	88.8°
8	5	1	6	5	7	17	89.2°
9	8	4	7	7	3	22	89.6°
10	8	7	4	5	5	32	90.0°
Total for telescopes pointing east	8	15	13	19	32		
Mean zenith angle	88.4°	88.8°	89.2°	89.6°	90.0°		

TABLE IV

NUMBER OF EVENTS PER TELESCOPE: N.S. DIRECTION

Counter number P_2 tray	Counter number P_1 tray 1	2	3	4	5	Total for telescopes pointing south	Mean zenith angle
6	10	12	12	19	24	24	88.4°
7	12	10	14	16	15	34	88.8°
8	19	11	12	17	12	40	89.2°
9	13	10	9	5	12	55	89.6°
10	23	18	11	11	12	49	90.0°
Total for telescopes pointing north	23	31	40	43	49		
Mean zenith angle	88.4°	88.8°	89.2°	89.6°	90.0°		

TABLE V

TOTAL NUMBER OF EVENTS, AVERAGE NUMBER OF EVENTS PER TELESCOPE, AND ABSOLUTE RATE FOR EACH DIRECTION

Direction	Number of telescopes	Total number of events	Average number of events per telescope	Absolute rate, particles $sec.^{-1}$ $cm.^{-2}$ $sterad.^{-1}$
(*a*) *E.W. direction*				
88.4°	2	14	7.0	$2.93\pm0.78\times10^{-5}$
88.8°	4	29	7.25	3.04 ± 0.46
89.2°	6	30	5.0	2.09 ± 0.31
89.6°	8	41	5.1	2.14 ± 0.27
90.0°	10	32	3.2	1.33 ± 0.19
(*b*) *N.S. direction*				
88.4°	2	47	23.5	$3.90\pm0.46\times10^{-5}$
88.8°	4	65	16.25	2.69 ± 0.34
89.2°	6	80	13.3	2.22 ± 0.23
89.6°	8	98	12.25	2.02 ± 0.17
90.0°	10	49	4.9	0.81 ± 0.09

The following corrections have to be made to the above rates.

(*a*) *Multiple events.*—Only single events in which one counter in each of the selecting trays has been discharged have been analyzed. The remaining 34 events in the E.W. direction and 78 in the N.S. direction must now be included. For these events the direction of the particle cannot be determined to within the angle defined by a single telescope but for 55 out of the total of 112 multiple events, it can be determined to within the angle defined by a single counter in one selecting tray and two adjacent counters in the other. An examination of these events and also of the remaining events suggests that the absolute rates given in Table V should all be increased proportionally by 23% ((34+78)/(146 +339) ×100%).

(*b*) *Particles not passing within solid angle defined by tray.*—It is possible that some of the recorded events arise from particles passing outside the solid angle defined by the P_1P_2 trays but which produce secondaries which then discharge the selecting counters. An exact evaluation of the correction to be made is not possible but a reasonable approximation can be found. The counter telescopes involving the end counters in a tray (Nos. 1, 5, 6, and 10) will be most affected whereas the telescopes defined by counters 3 and 8 will be least affected. If we assume that a particle passing outside the solid angle defined by the two trays could never discharge counters 3 and 8, then from a detailed examination of the discharged counters for each multiple event we arrive at the following approximate corrections which have to be deducted for each direction.

Direction (zenith angle)	88.2°–88.6°	88.6°–89.0°	89.0°–89.4°	89.4°–89.8°	89.8°–90.2°
Correction	12%	9%	6.5%	5%	4%

(*c*) *Background events.*—The H tray was moved from the position between the P_1 and P_2 trays and was placed as indicated in Fig. 5. $H-E$ events could not now arise from horizontal particles but only from casual coincidences and perhaps extensive air showers. In this position, the expected rate of casual coincidences was slightly smaller than the rate determined by the figures given

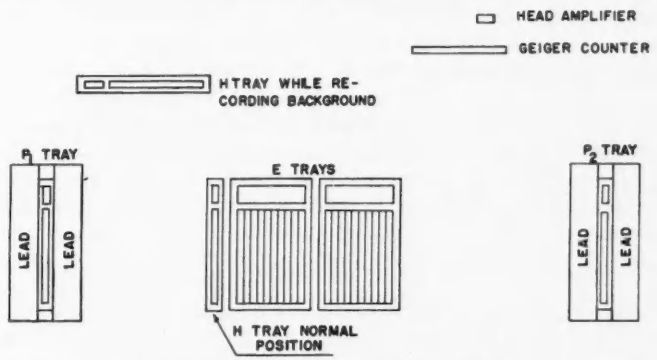

FIG. 5. Position of *H* tray while recording background events, plan elevation.

in Table II. The rate of showers would not be expected to be different. In a running time of 731.1 hr., only two such events were recorded, which indicates that the number of background events is extremely small and is no larger than that expected from casual coincidences.

(*d*) *Obstruction of the earth.*—In obtaining the absolute rates given in Table V we have assumed that the particles must be travelling in a downward direction for the four directions other than the 90° direction. For this direction we have assumed that particles can be received over the whole of the solid angle defined by the counters. That is not true—even in the E.W. direction particles travelling in the upward direction at an angle 0.2° from the horizontal would have passed through the earth. In the N.W. direction particles arriving from the north would have passed through the earth for directions having zenith angle larger than 89.6° so that for the horizontal telescopes (mean zenith angle 90°) only particles from the south can be recorded. Table VI gives the estimated fraction of the solid angle for which there is no obstruction due to the earth. The rates corrected for (*a*), (*b*), (*c*), and (*d*) are also given.

TABLE VI

FRACTION OF SOLID ANGLE FOR WHICH THERE IS NO OBSTRUCTION DUE TO THE EARTH; RATES CORRECTED FOR (*a*), (*b*), (*c*), AND (*d*)

Mean zenith angle	E.W. direction		N.S. direction	
	Fraction of solid angle	Rate corrected for (*a*), (*b*), (*c*), and (*d*), $\times 10^5$ sec.$^{-1}$ cm.$^{-2}$ sterad.$^{-1}$	Fraction of solid angle	Rate corrected for (*a*), (*b*), (*c*), and (*d*), $\times 10^5$ sec.$^{-1}$ cm.$^{-2}$ sterad.$^{-1}$
88.4°	1	3.17	1	4.20
88.8°	1	3.4	1	3.00
89.2°	1	2.40	1	2.55
89.6°	1	2.50	0.8	2.94
90.0°	0.8	1.95	0.4	2.40

In making correction (*d*) we are assuming that all the recorded particles are produced at large distances from the point of observation although we have

no experimental evidence to support this. Experiments could be made to test this point; here we tentatively assume that the particles are μ mesons which have been produced by the decay of other types of mesons near the top of the atmosphere.

Within the accuracy of the experiment there is no difference between the N.S. and the E.W. direction. The results of both directions have been combined and are shown in Fig. 13. The errors shown are slightly larger than the standard deviations of the counting rates in order to take into account the inaccuracies of the above corrections.

CALCULATED RATE OF HORIZONTAL PARTICLES

We first calculate the expected rate of μ mesons arising from the decay of π mesons which are produced near the top of the atmosphere in a direction such that the μ mesons are travelling horizontally when they reach sea level. For particles produced in the vertical direction Sands (1950) and Olbert (1954) have shown that an assumed π meson production spectrum in the range 10^8–10^{10} ev. leads to the observed μ meson spectrum at sea level. Barrett *et al.* (1952) use a theoretical production spectrum in agreement with this between 10^9 ev. and 4×10^9 ev. which, when extended to high energies, gives consistency with the underground absorption curve. The production spectrum for energies between 10^8 and 10^{13} ev. is shown in Fig. 6. Since the spectrum is based on the assumption that π meson decay is the only source of μ mesons, it could be incorrect in the region above 10^{10} ev. This is a point of considerable interest

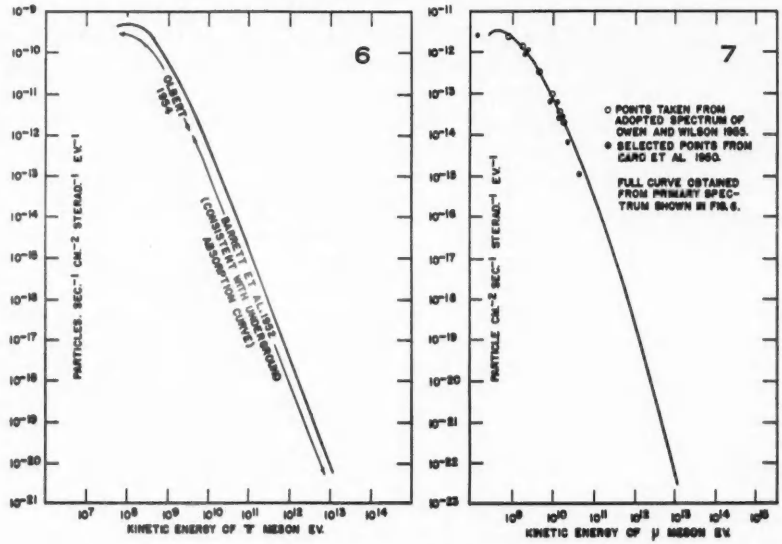
6
OLBERT 1954
BARRETT ET ALLKPER (CONSISTENT WITH UNDERGROUND ABSORPTION CURVE)
PARTICLES SEC⁻¹ CM⁻² STERAD⁻¹ EV⁻¹
KINETIC ENERGY OF π MESON EV.
7
○ POINTS TAKEN FROM ADOPTED SPECTRUM OF OWEN AND WILSON 1955.
● SELECTED POINTS FROM CARO ET AL. 1950.
FULL CURVE OBTAINED FROM PRIMARY SPECTRUM SHOWN IN FIG. 6.
PARTICLE CM⁻² SEC⁻¹ STERAD⁻¹ EV⁻¹
KINETIC ENERGY OF μ MESON EV.

FIG. 6. π meson production spectrum.
FIG. 7. Vertical μ meson energy spectrum at sea level.

and we make further comments on it in the next section. Figure 7 shows the sea level μ meson energy spectrum derived from the above π meson spectrum for energies between 10^8 and 10^{13}. The experimental results of Caro *et al.* (1950) and Owen and Wilson (1955) are shown indicating agreement up to energies of 2×10^{10} ev. Above this the experimental points of Caro *et al.* (1950) appear to be slightly lower than the expected curves.

The first step in calculating the spectrum at sea level of horizontal particles is to determine the μ meson production spectrum. The method of doing this for zenith angles up to about 60° has been given by Barrett *et al.* (1952). The assumptions made are:

(*a*) The intensity of π mesons of energy E' ev. at an atmospheric depth x gm. cm.$^{-2}$ produced by other types of particles in an atmospheric depth dx is equal to $F(E')\exp(-x/\lambda_p)dx/\lambda_p$ where λ_p is the mean free path of the producers of π mesons.

(*b*) The π mesons retain the direction of the producing particles which are isotropic at the top of the atmosphere. The μ mesons which arise from the π mesons' decay also retain this direction.

(*c*) If $\pi(E', x)$ is the differential π meson intensity at energy E' and atmospheric depth x there are two factors causing this to decrease.

(i) Nuclear interactions. The loss in depth dx is $\pi(E', x)dx/\lambda_\pi$ where λ_π is the absorption mean free path of π mesons. It will be assumed later that $\lambda_\pi = \lambda_p$.

(ii) π–μ decay. The loss in depth dx is $\pi(E', x)m_\pi c/p'dx/(\rho c\tau_\pi)$ where p' is the momentum of the π mesons, m_π is the mass of the π mesons, and τ_π its lifetime at rest, ρ is the density of air at the depth x. Since the energies under consideration are high $p'c = E'$.

Thus the differential π meson intensity $\pi(E', x)$ satisfies the following differential equation as a function of x:

$$(1)\qquad d(E', x)/dx = F(E')\exp(-x/\lambda_p)/\lambda_p - \pi(E', x)(1/\lambda_\pi + m_\pi c/E'\rho\tau_\pi)\,.$$

The μ mesons arising from the decay of π mesons of a fixed energy E' have a spread of energies between E' and $E'(m_\mu/m_\pi)^2$. Little error is introduced if we assume the μ mesons have a fixed energy equal to $E'(m_\mu/m_\pi)$.

The solution given by Barrett *et al.* to equation (1) for values of θ smaller than 90° assumes the equation

$$(2)\qquad \rho = kx\cos\theta,$$

where k is a constant equal to $1/6.46\times10^5$ cm.$^{-1}$, but this equation cannot hold for angles approaching 90°. The three equations governing the relation between ρ and x which are applicable at all angles are:

$$(3)\quad (a)\qquad x = \int_y^\infty \rho dy,$$

where y is the distance in cm. between a point P in space and the observation

point O at sea level such that OP is in the zenithal direction θ and x is the amount of matter traversed in the direction θ from P to infinity.

(4) (*b*) $$\rho = h_0 K \exp(-Kz),$$

where h_0 is the total depth of atmosphere in a vertical direction and z is the vertical height of the point P. This equation is not strictly true for small values of z but is valid in the region where π mesons are produced, i.e., $z > 8$ km. In order for equation (4) to give correct numerical values h_0 has to be taken as 1250 gm. cm.$^{-2}$ which is the extrapolated depth of the atmosphere if equation (4) were to be applied for all values of z. When we consider the energy loss and the decay of the μ mesons throughout the atmosphere this approximation for ρ is not sufficiently accurate and the correct form quoted by Rossi (1952), page 545, for the atmosphere has been used. Also in determining the total depth of the atmosphere in a horizontal direction the correct form has to be used.

(5) (*c*) $$y^2+2yS\cos\theta = Z^2+2zS, \qquad z \geqslant 0,$$

where S is the radius of curvature of the earth. Neglecting Z^2 in comparison with $2zS$ leads to extremely small errors and consequently this term has been dropped.

Equation (2) can be derived from (3), (4), and (5) if S is taken to be infinite, but at zenith angles near to 90° such an approximation is not possible. An exact solution to these equations shows that ρ/x is not a constant for zenith angles near to 90° but increases with increasing x as shown in Fig. 8. For comparison the values for $\theta = 0°$ and $\theta = 60°$ are also given, the deviations

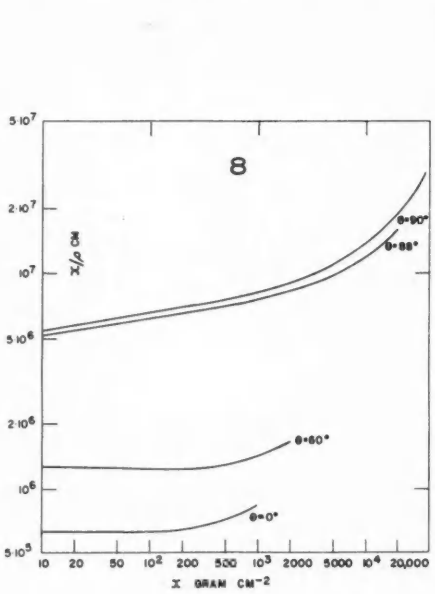

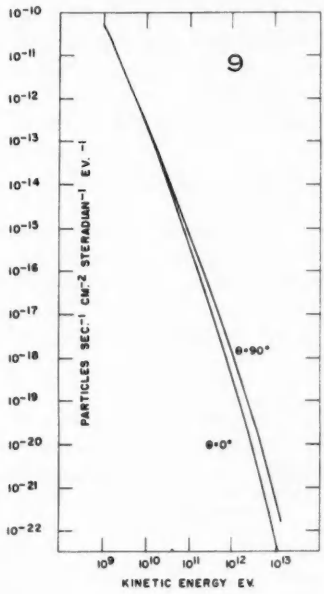

FIG. 8. Dependence of x/ρ on x.
FIG. 9. μ meson production spectra.

from ρ/x = constant in these cases being due to the deviations from equation (4) at small z. In the region where the π mesons are produced (90% are produced below $x = 270$ gm. cm.$^{-2}$) ρ/x does not vary appreciably and putting $(\rho/x)_{\theta=90} = 6.5\times10^6$ cm.$^{-1}$ introduces little error. By doing this we can use the solution of Barrett *et al.* to equation (1) and can finally derive a good approximation to the μ meson production spectrum $M(E, \theta)$ which gives the total number of μ mesons of energy E produced throughout the atmosphere at zenith angle θ:

$$M(E, \theta) = F(m_\pi/m_\mu E)m_\pi/m_\mu[E_0/(E_0+E/K(\rho/x)_\theta)] \tag{6}$$

where $E_0 = B(\lambda_\pi/(\lambda_\pi-\lambda_p))\cdot\ln(\lambda_\pi/\lambda_p)$ and $B = m_\mu c^2/c\tau_\pi K = 9\times10^{10}$ ev.

When $\lambda_\pi = \lambda_p$ the solution is exact and $E_0 = B$.

Equation (6) is shown in Fig. 9 for both $\theta = 0°$ and $\theta = 90°$. Below 10^{10} ev. there is no difference in the rate of particles produced in the two directions since almost all the π mesons decay into μ mesons. Above this value the ratio $M(E, 90°)/M(E, 0°)$ gets progressively larger and at an energy of 10^{13} ev. reaches its limiting value of $(\rho/x)_{\theta=0°}/(\rho/x)_{\theta=90°} = 10.2$.

We are interested in determining the μ meson spectrum, $M(E_0, \theta)$, at sea level. Particles of energy E_0 at sea level are derived from μ mesons of energy E produced near the top of the atmosphere, the value of E being dependent on the exact height. However, since 99% of μ mesons are produced within a depth of 550 gm. cm.$^{-2}$ whereas the total depth in the horizontal direction is 36,200 gm. cm.$^{-2}$ the range of values of E which gives rise to μ mesons of fixed energy E_0 at sea level is very small. Fig. 10 shows the energy at production, E, of a

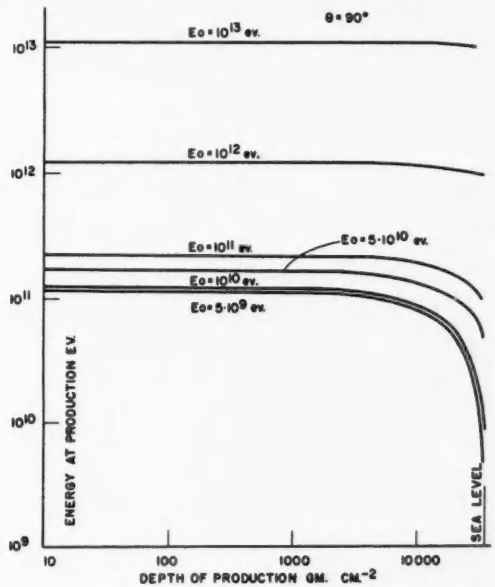

FIG. 10. Energy at production for mesons having energy E_0 at sea level produced at various depths.

μ meson which has energy E_0 at sea level, for μ mesons produced at various depths. These values have been computed assuming an energy loss of μ mesons given by

$$dE/dx = 1.9\times10^{6}+0.4\times10^{6} \log E/m_\mu c^2+5.38\times10^{-7}E \log 10^{-8}E.$$

This has been obtained by making appropriate modification to the figures, which refer to earth, given by Barrett *et al.* Thus the energy at any depth of the meson which has energy E_0 at sea level can be determined.

Because of μ meson decay only a fraction of the particles of energy E which produce particles of energy E_0 at sea level survive. The survival probability $w(x_1, x_2)$ for a μ meson produced at a depth x_1 to reach the depth x_2 is given by

$$-\ln w(x_1, x_2) = \int_{x_1}^{x_2} m_\mu/(\tau_\mu \rho(x)\, p(x)) \,.\, dx.$$

$\rho(x)$ and $p(x)$ have been determined above and the survival probability between a depth x_1 and sea level has been computed by numerical integration. Although the region of x_1 where μ mesons are produced is small when measured in units of gm. cm.$^{-2}$ it is not quite so small when measured in cm. and hence the survival probability depends to some extent on the exact depth where the μ meson is produced, as shown in Fig. 11.

From a knowledge of the above it is possible to determine the energy spectrum at sea level and this is shown in Fig. 12 for $\theta = 88°$ and $\theta = 90°$; the spectrum for $\theta = 0°$ is also shown for comparison. Above 4×10^{11} ev. the

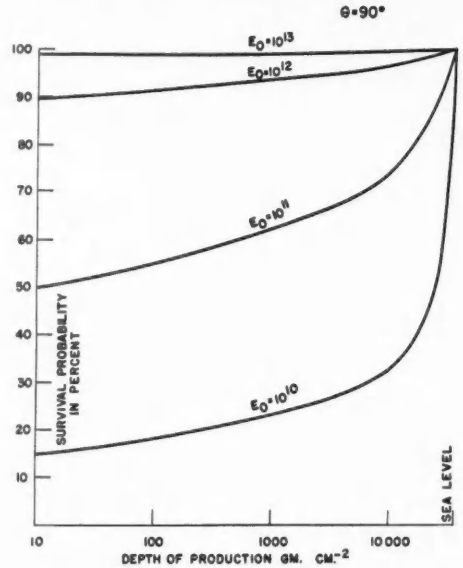

FIG. 11. Survival probability of μ mesons produced at various depths and having energy E_0 at sea level, horizontal direction.

number of particles in the horizontal direction exceeds that in the vertical direction and at an energy of 10^{12} ev. the rate is 2.5 times larger and is 5 times larger at 10^{13} ev. If one wishes to investigate the properties of μ mesons above 4×10^{11} ev. there is no advantage in observing them from the vertical direction.

Integrating the differential spectrum shown in Fig. 12, the total rate of particles can be found. The values for $\theta = 88°$ and $\theta = 90°$ are plotted in Fig. 13 on the line marked $\tau = \tau_\pi$. Intermediate values have not been calcu-

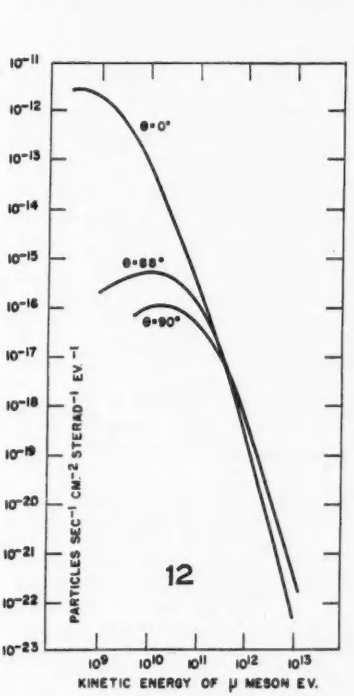

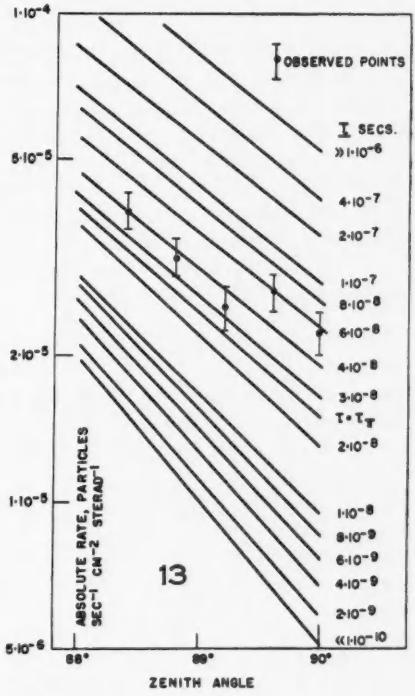

FIG. 12. μ meson energy spectra at sea level.
FIG. 13. Absolute rate at large zenith angles.

lated; the straight line joining the two calculated points is not necessarily the calculated rate at intermediate angles although it is unlikely that the correct form would be very different. Within the accuracy of the experiment this line is consistent with the observed rates.

NATURE OF THE PARENTS OF μ MESONS

Although in the previous section we were able to show that the observed rate of particles in the horizontal direction was consistent with the parents of μ mesons being π mesons having an energy spectrum as shown in Fig. 6, it is of interest to see if it is inconsistent with the assumption that some of the

parents are other types of mesons having a shorter lifetime. There appears to be ample evidence for the existence of κ mesons which decay directly into μ mesons (Daniel and Perkins 1954). It is suggested that their lifetime is of the order of 3×10^{-9} sec. and that their abundance relative to π mesons increases with increasing energy, and at energies large compared with the rest mass of the particle, the yield of π and κ mesons may be comparable. Thus at energies exceeding 10^{11} ev. which is the minimum energy of the parent of a μ meson which reaches sea level from the horizontal direction (see Fig. 10), it is not unreasonable to expect the presence of κ meson decay to manifest itself.

The primary energy spectrum shown in Fig. 6 is consistent with the observation underground if it is assumed that the π–μ decay is the only source of μ mesons. If at high energies μ mesons are derived from the decay of other particles, then the energy spectrum of Fig. 6 would have to be replaced by a series of energy spectra, one for each type of parent. The μ meson production spectrum shown in Fig. 9 for $\theta = 0°$ would not be different since it depends only on the observed underground absorption curve and the properties of μ mesons. The deduction of the μ meson production spectrum for $\theta = 90°$ would, however, depend on the nature of the parents. Now, in order to see how equation (6) depends on the properties of the π meson, we can replace

$$\frac{E_0}{E_0+E/K(\rho/x)_\theta} \text{ by } 1\Big/\left(1+\frac{E_\pi(\rho/x)_\theta}{m_\pi c^2 K c\tau_\pi}\right)$$

where E_π is the energy of the parent of a μ meson of energy E.

This expression, therefore, depends on E_π, m_π, and τ_π and by replacing them by E_κ, m_κ, and τ_κ we obtain the corresponding expression in the case of the parent being a κ meson.

In the case of π–μ meson decay, we assume $E_\pi/m_\pi = E_\mu/m_\mu$, which is a reasonable approximation. We cannot, however, replace the suffix π by κ to get the corresponding equation for κ–μ decay. Because the mass of the κ meson is large in comparison with the decay products, it is likely that on an average $E_\kappa = 3E_\mu$ and since $m_\kappa/m_\mu \sim 6$, we have $E_\kappa/m_\kappa \sim E_\mu/2m_\mu$.

For the general case, assuming that the parents of μ mesons of energy E_μ are produced by parents having energy E_x and rest mass m_x and lifetime τ_x, we can determine how the production spectrum at an angle θ differs from that at $\theta = 0°$ for various values of $E_x/m_x\tau_x$. From this we can calculate the expected rate of particles at sea level by the method adopted previously and Fig. 13 shows the rates at $\theta = 88°$ and $\theta = 90°$. In this figure we have chosen to make $\tau = (E_x/m_x)/(E_\mu/m_\mu)\tau_x$ so that for the case when $E_x/m_x = E_\mu/m_\mu$ (as in the case of π–μ decay) $\tau = \tau_x$. The case of μ mesons being produced entirely by κ mesons can be obtained by making $\tau = 2\tau_\kappa = 6\times10^{-9}$ sec.

It is seen that the value of τ which gives the best fit with the experimental points is $4.5\pm1.5\times10^{-8}$ sec. It is reasonable to identify this lifetime with that of the π meson.

In Fig. 14 we have assumed that the parents of μ mesons are π mesons and κ mesons which are produced in different proportions. The results suggest that the parents of μ mesons can be identified with the π meson although a small percentage of κ mesons cannot be excluded.

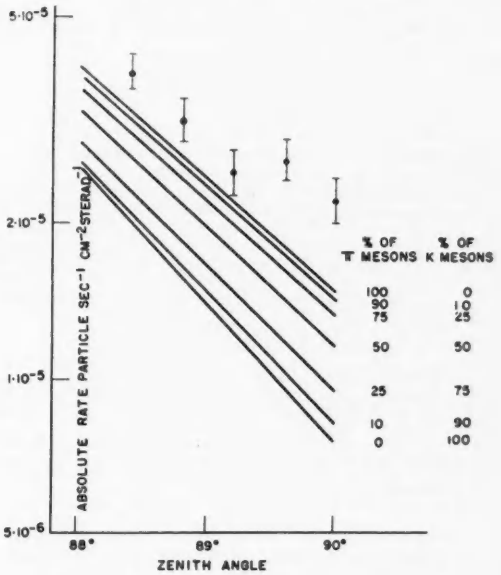

FIG. 14. Absolute rate at large zenith angles for various proportions of π and κ mesons.

PRODUCTION OF SECONDARIES

An indication that the observed horizontal particles are of high energy can be obtained from an examination of the events in which more than one counter in a tray is discharged (multiple events). It is natural to explain these events as arising from secondaries (knock-on electrons) produced in the lead by the horizontal particles.

The total number of $H-E$ events recorded was 597 and we believe that almost all of these arise from horizontal particles. In each event the particle traverses both the P_1 and the P_2 tray so that there is a total of 1194 traversals and, in 126 of these, multiple events are observed. The probability therefore of a particle traversing a tray and producing a multiple event is $10.6\pm0.9\%$. If the probability of producing a secondary in one of the selection trays is independent of what happens in the other, then the number of events in which both trays show multiple events is 13. In fact 14 such events were observed.

The probability of 10.6% is larger than is normally encountered for μ mesons in the vertical direction. For a short time the arrangement was turned through 90° so that vertical particles were being recorded with the same geometry as for the horizontal particles. The probability of a particle traversing a tray and producing a multiple event was found to be $3.54\pm0.41\%$ which is considerably less than that observed in the horizontal direction. It is reasonable to associate this high probability for producing secondaries in the horizontal direction with the high energy of particles which is expected in this direction.

Table VII shows the number of events in which more than one counter in a tray was discharged. The results suggest that the multiplicity is larger for horizontal particles than it is for vertical particles.

TABLE VII

ANALYSIS OF EVENTS INVOLVING SECONDARIES

Number of counters out of 5 discharged	Horizontal direction	Vertical direction
2	83	27
3	27	2
4	9	1
5	7	–

ACKNOWLEDGMENTS

The author wishes to express his gratitude to Dr. D. C. Rose and other members of the Cosmic Ray group for their assistance throughout the experiment and for providing many valuable discussions.

The author also wishes to thank the National Research Council of Canada for the award of a Fellowship.

REFERENCES

BARRETT, P. M., BOLLINGER, L. M., COCCONI, G., EISENBERG, Y., and GREISEN, K. 1952. Revs. Mod. Phys. **24**: 133.
CARO, D. E., PARRY, J. K., and RATHGEBER, H. D. 1950. Nature, **165**: 689.
COCCONI, G., TONGIORGI, V., and GREISEN, K. 1949. Phys. Rev. **75**: 1063.
DANIEL, R. R. and PERKINS, D. H. 1954. Proc. Roy. Soc. A, **221**: 351.
O'CEALLAIGH, C. 1951. Phil. Mag. **42**: 1032.
OLBERT, S. 1954. Phys. Rev. **96**: 1400.
OWEN, B. G., and WILSON, J. G. 1955. Proc. Phys. Soc. A, **68**: 409.
ROSSI, B. 1952. High energy particles. Prentice-Hall, Inc., New York.
SANDS, M. 1950. Phys. Rev. **77**: 180.

A STUDY OF NUCLEON FORCES WITH REPULSIVE CORES

II. LOW ENERGY PROPERTIES, PARTICULARLY CHARGE INDEPENDENCE[1]

By J. Shapiro[2] and M. A. Preston[3]

ABSTRACT

The low energy properties of two-nucleon potentials with infinite repulsive cores have been studied by numerical calculations using an electronic digital computer. The consequences of assuming charge independence for the nuclear force in the ^1S state have been examined by performing computations with several potential shapes for both the neutron–proton and proton–proton systems. It was found that this assumption severely restricts the possible potential shape. Charge independence occurs with the Yukawa potential for zero core radius. Potentials that are more singular at small distances than the Yukawa require larger core radii; less singular potentials are not charge independent.

A. INTRODUCTION

Because of the failure of the field theories to give a satisfactory two-nucleon law of force, many calculations have been performed using phenomenological potentials (e.g. Breit *et al.* 1936; Breit *et al.* 1939; Blatt and Jackson 1949; Jackson and Blatt 1950). In the phenomenological approach, a potential is assumed and physically observable quantities are calculated from the Schrödinger equation, and then are compared with the experimental results. This method involves lengthy computations; a large number of potentials must be tried, each of which involves either the numerical solution of differential equations or the use of approximate methods of doubtful accuracy. Nevertheless, a comprehensive phenomenological study of the two-nucleon system can be carried out with the aid of an electronic digital computer. As a start in such a study, the solution of the neutron–proton and proton–proton scattering equations for the ^1S state at low energies has been programmed for FERUT, the digital computer at the University of Toronto. For reasons outlined in Part I of this series (Bird and Preston 1955), these programs have been restricted to potentials with an infinite repulsive core,* surrounded by an arbitrary potential.

On the basis of an analysis of the early low energy NP and PP scattering experiments, Breit and collaborators (Breit and Feenberg 1935; Breit and Stehn 1937; Breit *et al.* 1939) introduced the hypothesis of charge independence of nuclear forces, which states that the force between two nucleons in a given total spin and orbital angular momentum state is independent of the charges of the two nucleons (except, of course, for the additional Coulomb repulsion

[1]Manuscript received January 12, 1956.
Contribution from Physics Department, Hamilton College, McMaster University, Hamilton, Ontario, and University of Toronto, Toronto, Ontario. Partially supported by a grant from the National Research Council.

[2]National Research Council Student 1951–52, Fellow 1952–53. This paper is based on work submitted for the degree Ph.D. in the University of Toronto. Now at Yale University, New Haven, Connecticut.
[3]Hamilton College.

*Professor Breit has pointed out that if one takes a "soft" core and if the electrostatic potential between two protons remains $1/r$ for very small distances, some of our results might be altered slightly.

between two protons). Since accurate experiments are available only at low energies, and the PP system can exist at low energies only in the ^1S state, the hypothesis of charge independence is based almost exclusively upon a comparison of the ^1S state of the NP and PP systems at low energies. One purpose of the present work was to determine to what extent the assumption of charge independence, together with current experimental results, limits the shape of the two-nucleon potential. It was found that this hypothesis severely restricts the possible potential shape.

From the point of view of meson field theory, charge independence means the same coupling constant and the same form of interaction with the meson field for both neutrons and protons. However, even such a charge independent theory would lead to slightly different force laws for the NP and PP systems, because (*a*) the mass of the neutral π-meson is different from that of the charged π-meson, and (*b*) there would be an interaction between the proton electromagnetic field and the meson field. Also self-energy terms such as vacuum polarization would be different. Such corrections would be expected to be small, however, so that a charge independent potential would be a valid first approximation from such a theory.

We have studied four different shapes of attractive well surrounding the core. Computations have been carried out for a wide range of the parameters appearing in each potential. The results obtained are discussed with particular emphasis on the possibility of obtaining potentials that are charge independent at low energies (i.e. fit both the neutron–proton and proton–proton experiments, for the same choice of parameters and same potential shape). The main conclusion is that in order to yield charge independence, the attractive well must be at least as singular at small distances as the Yukawa potential. The required core radius increases as the potential becomes more singular at small distances (the Yukawa potential is charge independent for zero core radius).

To simplify reference to the various states involved, the following notation will be used. The words "neutron–proton" will be abbreviated to NP, and "proton–proton" to PP. The following symbols will be used for the singlet state when no particular two-nucleon system is under consideration:

a_s singlet scattering length,
r_0 singlet effective range,
P_s singlet shape parameter,
r_c core radius.

When either the NP or the PP system is to be specified (the NN system has not been considered), the subscript n or p will be added to the above symbols, e.g. a_{sn} is the singlet scattering length in the NP system, r_{0p} is the singlet effective range for the PP system. For the triplet S state, which occurs only in the NP system, the symbols a_t, r_{0t}, P_t, r_{ct} will be used.

As discussed in Part I,* it has been shown that an S-wave NP phase shift δ_s (or δ_t) can be expanded as

*To the references given there, one may add Breit, Condon, and Present (1936) and Breit and Bouricius (1949).

$$k \cot \delta_s = -\frac{1}{a_{sn}} + \tfrac{1}{2} r_{0n} k^2 - P_{sn} r_{0n}{}^3 k^4 + Q_{sn} r_{0n}{}^5 k^6 + \ldots, \tag{A.1}$$

where only the first two terms are important at low energies, i.e., $k \cot \delta_s$ is a linear function of energy.

The approximation

$$k \cot \delta_s \simeq -\frac{1}{a_{sn}} + \tfrac{1}{2} r_{0n} k^2 \tag{A.2}$$

is called the Effective Range Theory. The quantities a_{sn} and r_{0n} are determined by the wave function u_0 at zero energy: a_{sn} by its asymptotic form

$$v_0 = 1 - r/a_{sn} \tag{A.3}$$

and r_{0n} by the integral

$$r_{0n} = 2 \int_0^\infty (v_0{}^2 - u_0{}^2) dr. \tag{A.4}$$

The quantity a_{sn}, called the singlet scattering length, was introduced by Fermi and Marshall (1948), who showed that the total incoherent scattering cross section at zero energy is

$$\sigma_0 = \tfrac{1}{4}(4\pi a_{sn}{}^2) + \tfrac{3}{4}(4\pi a_t{}^2). \tag{A.5}$$

The quantity r_{0n} is called the singlet effective range. Contributions to the effective range integral (A.4) occur only from within the range of the nuclear force.

In summary, the low energy NP scattering is completely determined by four quantities: the two scattering lengths, a_{sn} and a_t, and the two effective ranges, r_{0n} and r_{0t}. These quantities can be obtained for a given potential by solving the radial equations at zero energy. For the singlet case this equation is

$$-\frac{\hbar^2}{M}\frac{d^2 u_0}{dr^2} + V_s u_0 = 0 \tag{A.6}$$

where

$$M = 2M_N M_P/(M_N + M_P).$$

There are similar equations for the PP case. Owing to the exclusion principle, low energy PP scattering can occur only in the ^1S state. The radial wave equation for this state is

$$-\frac{\hbar^2}{M}\frac{d^2 u}{dr^2} + \left(\frac{e^2}{r} + V_s\right) u = Eu. \tag{A.7}$$

The asymptotic solution of (A.7) that is equal to unity at $r = 0$ is

$$v = C\,[F_0(kr) \cot \delta_s + G_0(kr)] \tag{A.8}$$

where F_0 and G_0 are the regular and irregular Coulomb functions (Breit *et al.* 1936) and δ_s is the ^1S phase shift. The "Coulomb penetration factor" C is defined by

$$C^2 = \frac{2\pi\eta}{e^{2\pi\eta} - 1}, \quad \eta = \frac{e^2}{\hbar v}, \tag{A.9}$$

where v is the relative velocity of the two particles. The formula for the cross section is rather complicated; it is given for S states by Breit *et al.* (1936).

It depends on only one parameter, the ^1S phase shift δ_s. An expansion for the phase shift, analogous to (A.1), exists for PP scattering; it is (Jackson and Blatt 1950)

$$\text{(A.10)} \qquad Ck \cot \delta_s + \frac{g(\eta)}{R} = -\frac{1}{a_{sp}} + \tfrac{1}{2} r_{0p} k^2 - P_{sp} r_{0p}^3 k^4 + Q_{sp} r_{0p}^5 k^6 + \ldots$$

where R is the "Coulomb length"

$$\text{(A.11)} \qquad R = \hbar^2/Me^2 = 2.882 \times 10^{-12} \text{ cm.}$$

and $g(\eta)$ is a slowly varying function of η, given by

$$\text{(A.12)} \qquad g(\eta) = -\ln \eta + \eta^2 \sum_{v=1}^{\infty} \frac{1}{v(v^2+\eta^2)}.$$

As in the NP case, the approximation of taking the first two terms is called the Effective Range Theory. The PP scattering length a_{sp} and effective range r_{0p} are determined by the solution u_0 of the radial equation (A.7) at zero energy. This equation is

$$\text{(A.13)} \qquad -\frac{\hbar^2}{M}\frac{d^2u_0}{dr^2} + \left(\frac{e^2}{r} + V_s\right)u_0 = 0.$$

The asymptotic solution of (A.13) can be written as

$$\text{(A.14)} \qquad v_0 = 2\sqrt{\frac{r}{R}} K_1\left(2\sqrt{\frac{r}{R}}\right) - \frac{\sqrt{rR}}{a_{sp}} I_1\left(2\sqrt{\frac{r}{R}}\right)$$

where K_1 and I_1 are the Bessel functions of purely imaginary argument (Watson 1952, p. 77). Equation (A.14) can be derived from the formulae in the appendix of Jackson and Blatt (1950). The effective range again is given by (A.4) except that now v_0 is given by (A.14) and u_0 is the solution of (A.13).

In summary, PP scattering for energies less than approximately 10 Mev. can be described by two parameters, the scattering length a_{sp} and the effective range r_{0p}.

The low energy PP scattering parameters can be obtained by plotting the left-hand side of (A.10), which contains the experimentally observed phase shifts, against k^2. The experimental points lie very nearly on a straight line. The intercept of this line determines a_{sp}, the slope determines r_{0p}. The experiments do not determine the quantity P_{sp} with any precision. The values obtained for a_{sp} and r_{0p} depend to some extent on the value assumed for P_{sp}, especially since PP scattering experiments cannot be carried out for energies less than approximately 100 kev. Yovits *et al.* (1952) have analyzed the experiments for four different values of P_{sp}. Their analysis suggests the following values:

$$a_{sp} = (-7.68 \pm 0.04) \times 10^{-13} \text{ cm.},$$
$$r_{0p} = (2.67 \pm 0.13) \times 10^{-13} \text{ cm.},$$
$$-0.04 < P_{sp} < 0.08.$$

For a specific potential, the computation of P_{sp}, which depends strongly on the potential shape, allows a more accurate analysis of the experiments. This will yield values of a_{sp} and r_{0p} consistent with that potential shape,

with much smaller errors than those quoted above. The analysis of Yovits *et al.* indicates that a_{sp} can be determined to within 0.01×10^{-13} cm., r_{0p} to within 0.02×10^{-13} cm., in this manner.

The NP scattering lengths quoted by Snow (1952) will be used:

$$a_{sn} = (-23.69\pm0.06)\times10^{-13} \text{ cm.},$$

$$a_t = (5.378\pm0.021)\times10^{-13} \text{ cm.}$$

These quantities do not depend on the potential shape. The triplet effective range can be obtained from the binding energy of the deuteron; the singlet effective range from the total scattering cross section at energies greater than zero. The values obtained for these quantities depend on the values assumed for the shape parameters P_{sn} and P_t (i.e., on the assumed potential shapes in the ^1S and ^3S states). The triplet effective range has been obtained for different values of P_t by Snow (1952); his results suggest

$$r_{0t} = (1.68\pm0.05)\times10^{-13} \text{ cm.}$$

An estimate of the singlet range based on the results quoted by Salpeter (1951), Hafner *et al.* (1953), and Snow (1952) gives

$$r_{0n} = (2.4\pm0.5)\times10^{-13} \text{ cm.}$$

Both effective ranges (in particular r_{0n}) can be estimated much more accurately for a particular assumed potential shape in the ^1S or ^3S state.

Magnetic interactions have been neglected in the theory outlined in this section. These will occur in both the NP and PP system, since both neutrons and protons have magnetic moments. Schwinger (1950) has evaluated the effect of magnetic interactions on the scattering lengths a_{sn} and a_{sp} for the square well and Hulthén ($V = V_0e^{-\beta r}/(1-e^{-\beta r})$) potentials without repulsive cores, assuming point nucleons. The Hulthén potential is similar in shape to the Yukawa potential, but leads to analytically soluble equations in the ^1S state. Schwinger found that magnetic interactions decreased a_{sn} and increased a_{sp} by small amounts which depended on the potential shape. When this effect was included, Schwinger found that the Hulthén potential agreed with charge independence; the square well did not. These conclusions are in agreement with results obtained in the present work.

Salpeter (1953) has extended Schwinger's calculations to the case of a Hulthén potential with a repulsive core, assuming that the nucleon magnetic moment is distributed uniformly over the core. He found that the magnetic correction decreased rapidly as the core radius was increased. He concluded that there is a definite discrepancy with charge independence if a core of any appreciable size is used. The present work shows that although this conclusion is true for the square well and Hulthén potentials, it is not true for more singular potentials.

B. NP SCATTERING BY AN EXPONENTIAL POTENTIAL WITH AN INFINITE REPULSIVE CORE

In Part I, the effects of finite cores with an exponential potential were discussed. Here we consider in detail the low energy properties of exponential potentials with infinite cores, i.e.

(B.1) $$V = \infty, \qquad r < r_c,$$
$$= -V_c \exp[-(r-r_c)/r_s], \qquad r > r_c.$$

Because of the notation used later in this paper we have replaced the symbol V_0 of Part I by V_c. The rest of the notation is unchanged. As can be seen by letting k_t approach infinity in (B.9) of Part I, the S-wave phase shift is given by

(B.2) $$\delta = \arg F(i\lambda)$$

where

(B.3) $$F(i\lambda) = (i\lambda)!\, J_{i\lambda}(\mu)(\tfrac{1}{2}\mu)^{-i\lambda}\exp(-i\lambda r_c/2r_s),$$
$$\lambda = 2r_s k, \quad \mu = 2r_s(MV_c/\hbar^2)^{\frac{1}{2}}.$$

Now $k \cot \delta$ can be obtained as a power series in k^2 by expanding $F(i\lambda)$ in a Taylor series around the origin. Comparison of this series with

$$k \cot \delta = -1/a + \tfrac{1}{2} r_{0k}{}^2 + \ldots$$

yields the results

(B.4) $$-1/a = F(0)/2r_s F'(0)$$

and

(B.5) $$r_0 = -\frac{2r_s}{F'(0)}\left[\frac{2}{3}\frac{r_s}{a}F'''(0) + F''(0)\right].$$

The problem is reduced to finding successive derivatives of $F(z)$ at $z = 0$. Introducing

(B.6) $$G(z) = \exp(zr_c/2r_s)\, F(z),$$

one has

(B.7) $$G(z) = 1 + \sum_{r=1}^{\infty} \frac{(-)^r}{r!}\left(\frac{\mu}{2}\right)^{2r} \prod_{n=1}^{r} \frac{1}{n+z},$$

$$G(0) = J_0(\mu),$$

$$G'(0) = \tfrac{1}{2}\pi N_0(\mu) - (C + \ln \tfrac{1}{2}\mu) J_0(\mu),$$

$$G''(0) = \sum_{r=1}^{\infty} \frac{(-)^r}{(r!)^2}(\tfrac{1}{2}\mu)^{2r}\left[\left(\sum_1^r \frac{1}{n}\right)^2 + \sum_1^r \frac{1}{n^2}\right],$$

$$G'''(0) = \sum_{r=1}^{\infty} \frac{(-)^r}{(r!)^2}(\tfrac{1}{2}\mu)^{2r}\left[\left(\sum_1^r \frac{1}{n}\right)^3 + 3\sum_1^r \frac{1}{n}\sum_1^r \frac{1}{n^2} + 2\sum_1^r \frac{1}{n^3}\right],$$

$$C = 0.5772\ldots.$$

In terms of these quantities

(B.8) $$a = r_c - 2r_s G'/G,$$

(B.9) $$r_0 = 2r_c\left(1 - \frac{r_c}{a} + \frac{1}{3}\frac{r_c^2}{a^2}\right) - 2r_s\left(1 - \frac{r_c}{a}\right)\left\{\frac{2r_s}{3a}\frac{G'''}{G'} + \left(1 - \frac{r_c}{a}\right)\frac{G''}{G'}\right\}.$$

(B.8) can also be obtained from (B.15) of Part I by letting $k_t \to \infty$.

(B.8) and (B.9) have been used to compute the effective range for NP scattering in the ^1S state for a wide range of the parameters. These equations

are particularly suitable for computation because G and its derivatives are functions of only the one variable μ. In addition, for singlet scattering, (B.8) severely limits the possible values of μ. Because of the large value of a_{sn}, the ratio G'/G must be large and positive, i.e. μ must be near a root of $J_0(x)$. In addition, this zero must be the first zero of $J_0(x)$, as can be seen by the following argument.

For the wave function at zero energy, one readily obtains from (B.17) and (B.18) of Part I

$$u_0 = -\frac{r_s\pi}{a}\left[N_0(y) - J_0(y)\frac{N_0(\mu)}{J_0(\mu)}\right]. \tag{B.10}$$

The range of y is $0 \leqslant y \leqslant \mu$. Since the singlet state of the NP system is unbound, the zero energy wave function cannot have any nodes (except at $r = r_c$, i.e. $y = \mu$). Thus the equation

$$J_0(y)\,N_0(\mu) - J_0(\mu)\,N_0(y) = 0 \tag{B.11}$$

must not have a solution in the region $0 \leqslant y < \mu$. From a table (Jahnke and Emde 1945) of the roots of

$$J_0(y)\,N_0(ky) - J_0(ky)\,N_0(y) = 0 \tag{B.12}$$

for $1 \leqslant k \leqslant \infty$, one sees that the roots y always satisfy $(k-1)y \geqslant 2.4048$, the first zero of $J_0(y)$. This means that if y is to be a root of (B.11), then $\mu - y \geqslant 2.4048$. Thus, if μ is less than the first zero of $J_0(y)$, u_0 can have no nodes in the interval $0 \leqslant y < \mu$.

Thus μ is restricted to values close to, and less than 2.4048. A similar argument shows that, in the case of triplet scattering, where the wave function u_0 must have one node (i.e. a bound state, the deuteron, exists), μ is restricted to values between the first and second zeros of $J_0(x)$, because for any value of k greater than unity, one and only one root of (B.12) satisfies

$$2.4048 \leqslant (k-1)y < 5.5201, \text{ the second zero of } J_0(x).$$

Equations (B.8) and (B.9) were used to obtain r_{0n} as follows. First, G and its derivatives were computed manually for the range $y_c = 2.30(0.01)2.40$. These values were used in a program for FERUT which operated as follows. The experimental value (-23.69×10^{-13} cm.) was assumed for a_{sn} and r_s calculated by means of (B.8), for given values of r_c and μ. This value of r_s was inserted in (B.9) to obtain r_{0n}. Computations were done for $\mu = 2.30(0.01)2.40$ and r_c (in units 10^{-13} cm.) $= 0(0.1)1.3$. The results are given in Figs. 1 and 2. Fig. 1 gives r_s as a function of μ and r_c, and Fig. 2 gives r_{0n} as a function of μ and r_c.

If V_c is expressed in Mev. and r_s in 10^{-13} cm., evaluation of the constant yields

$$V_c = 10.367\,\mu^2/r_s^2. \tag{B.13}$$

The equation (B.13) together with Figs. 1 and 2 allows values of any two of the quantities V_c, r_s, r_c, and r_{0n} to be obtained from the other two. The values obtained will fit the experimental value of the scattering length. The results of this section were used to check the NP program described in Section C.

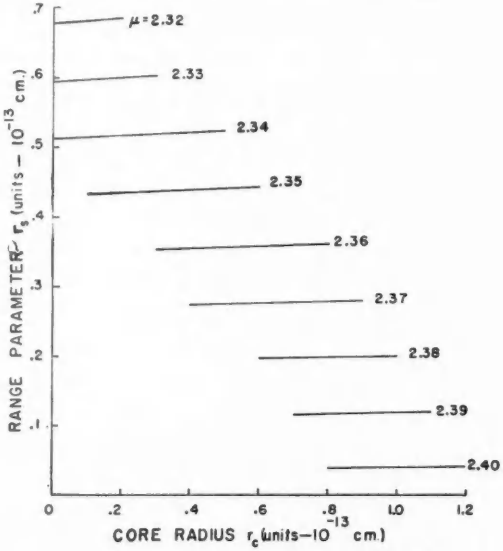

FIG. 1. Values of r_s plotted against core radius for ^1S NP scattering by an exponential potential. Each curve corresponds to a constant value of μ. All points fit the experimental scattering length $a_{sn} = 23.69 \times 10^{-13}$ cm.

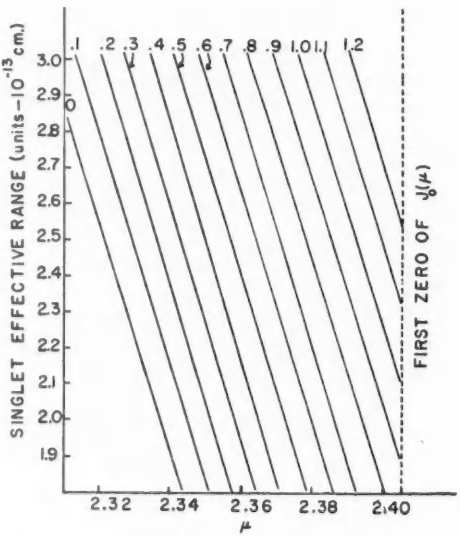

FIG. 2. Singlet NP effective range plotted against μ for an exponential potential with a hard core. Each curve corresponds to a constant value of core radius r_c (in units of 10^{-13} cm.)

C. THE COMPUTATIONAL PROGRAMS FOR LOW ENERGY ^1S SCATTERING

As has been pointed out, the contribution of the singlet states to low energy NP or PP scattering is given by two parameters, the scattering length and the effective range. Both of these are determined by the radial wave function at zero energy. Thus, the low energy singlet scattering for a given potential can be calculated by solving one differential equation, either (A.6) or (A.13).

FERUT has been programmed to compute these parameters for both the NP and PP systems for repulsive core potentials surrounded by an arbitrary attractive well. The radial equation was integrated inwards, starting with the asymptotic solution (A.3) or (A.14), and proceeding until the solution became negative. At this point, the core radius was determined by interpolating to find the zero of the solution. The effective range was determined by performing the integration (A.4). Only solutions corresponding to the experimental values of the scattering length, which was inserted into the asymptotic wave function, were obtained. For a given potential shape and value of the "range parameter" r_s (defined in (C.1)), different values of the strength of the potential were used to give a series of solutions covering the experimental uncertainties in the effective range. The final results for each equation consisted of the strength of the potential, the core radius, and the effective range. The programs gave both the core radius and effective range to an accuracy of better than five figures. In order to compute results with a new potential shape, only the subroutine that actually computed the potential at each point required changing.

The two programs (NP and PP) were used for several potential shapes in a search for charge independent potentials. The programs will be discussed in this section. The results obtained will be given in Section D. The complete programs, in the standard FERUT library form, may be found in Shapiro (1955).

The potentials considered always were of the form

$$\begin{aligned} V &= \infty, && r < r_c, \\ V &= -V_0 f(r/r_s), && r > r_c. \end{aligned} \tag{C.1}$$

The parameter V_0 will be called the strength of the potential; r_s will be called the "range parameter". For each potential shape, r_s and V_0 were varied over a two-dimensional net. With a few minor changes, the programs can handle more general potentials of the form

$$V = Af(r/r_s)+Bg(r/r_s)+Ch(r/r_s)$$

where A, B, C, and r_s are parameters that can be varied arbitrarily.

In nuclear problems, $f(x)$ is a short range function which is large and rapidly varying for small values of x and quickly becomes negligible as x increases. This causes difficulty in performing accurate numerical integrations, because a much smaller interval size is required for small x. Thus, either a non-uniform interval size or an extremely large number of points must be used in the integrations. This difficulty was avoided by making the substitutions (Bethe 1951)

(C.2) $$y = \log_e x, \quad U_0 = u_0 x^{-\frac{1}{2}}, \quad x = r/r_s,$$

and using a uniform net in y. The equations (A.6) and (A.13) become

(C.3) $$d^2U_0/dy^2 = [-Ge^{2y}f(e^y)+\tfrac{1}{4}]\,U_0 \qquad \text{NP}$$

(C.4) $$d^2U_0/dy^2 = [-Ge^{2y}f(e^y)+(r_s/R)e^y+\tfrac{1}{4}]\,U_0 \qquad \text{PP}$$

where

(C.5) $$G = MV_0r_s^2/\hbar^2.$$

The substitutions (C.2), which do not complicate the equations appreciably, considerably reduce the number of net points required, because (*a*) constant intervals in y correspond to intervals in x that continually decrease as x decreases, and (*b*) any singularity in the potential as $x \to 0$ is reduced by a factor $e^{2y} = x^2$.

On the other hand, $y \to -\infty$ as $x \to 0$, restricting the minimum core radius that could be handled by the program. This minimum was chosen at $y = -3.1$, corresponding to $x_c = 0.04505$. For a typical value of $r_s = 1\times10^{-13}$ cm., this gives $r_c \sim 0.045\times10^{-13}$ cm. Results for cores of this size will not differ appreciably from those for zero core radius, which have been treated in the literature.

With these substitutions, the asymptotic wave functions (which will be denoted by $\psi_0 = v_0x^{-\frac{1}{2}}$) become

(C.6) $$\psi_0 = e^{-y/2} - \frac{r_s}{a_{sn}}\,e^{y/2} \qquad \text{NP}$$

(C.7) $$\psi_0 = 2\sqrt{\frac{r_s}{R}}\left[K_1(z) - \frac{R}{2a_{sp}}\,I_1(z)\right] \qquad \text{PP}$$

where

(C.8) $$z = 2\left(\frac{r}{R}\right)^{\frac{1}{2}} = 2\left(\frac{r_se^y}{R}\right)^{\frac{1}{2}}.$$

The effective range integral, for both the NP and PP systems, becomes

(C.9) $$r_0 = 2r_s\int_{-\infty}^{\infty}[\psi_0^2(y) - U_0^2(y)]\,e^{2y}\,dy.$$

The programs for the NP and PP problems are similar in structure. The differential equation (C.3) or (C.4) was integrated inwards from the asymptotic solution, the solution being advanced one step at a time by Milne's method (Milne 1949, p. 140), which involves the use of the formula

(C.10) $$U_{n-1} = U_n + U_{n+2} - U_{n+3} + \tfrac{1}{4}h^2(5U_n'' + 2U_{n+1}'' + 5U_{n+2}'') + \tfrac{17}{240}h^6U^{(6)}$$

as a predictor, and

(C.11) $$U_{n-1} = 2U_n - U_{n+1} + \tfrac{1}{12}h^2(U_{n-1}'' + 10U_n'' + U_{n+1}'') - \tfrac{1}{240}h^6U^{(6)}$$

as a corrector. In this formula h is the interval in y. The last terms in these equations are estimates of the error. The difference of the values of U_{n-1} given by (C.10) and (C.11) is roughly 18 times the error of (C.11). These formulae require four previous values of U and three previous values of U''. The calculation is begun at some maximum value of y (say Y) at which the

potential is to be considered negligible. The four required starting values of ψ_0 are calculated at Y, $Y+h$, $Y+2h$, $Y+3h$ from (C.6) or (C.7) and the three required values of ψ_0'' are obtained by substitution in the differential equation (C.3) or (C.4) with the potential (G) set equal to zero. The program then operated as follows. (C.10) was used to "predict" U_{n-1}. This predicted value was inserted in the differential equation (C.3) or (C.4) to obtain a value of U_{n-1}'', which was used in (C.11) to obtain a corrected value of U_{n-1}.

For NP scattering, the integrations started at $y = 3.2$ (i.e. $r/r_s = x = 24.5$) and proceeded over a maximum of 64 steps with $h = 0.1$. Thus the minimum core radius that could be treated was $y = -3.1$ (i.e. $x = 0.04505$). For a typical value of r_s ($=1.0\times10^{-13}$ cm.), the starting value $y = 3.2$ corresponds to a value of $r = 24.5\times10^{-13}$ cm. Hence, the error due to cutting off the potential at this point is negligible. A run was performed with the exponential potential; comparison with the results obtained in Section B showed that the core radius and the effective range were obtained by the program to six-figure accuracy. For the potential $\exp(-x)/x^2$, where it appeared that a charge independent potential existed for a smaller core radius than $y = -3.1$, some runs were performed starting at $y = 2.5$ (i.e. $x = 12.18$) and continuing until $y = -3.8$ (i.e. $x = 0.02237$). Comparison of these results with those starting at $y = 3.2$ showed that the effect of cutting off the potential at $y = 2.5$ was still negligible. This potential, however, is very short tailed.

Since the above net did not give sufficient accuracy for the PP program, a net of 144 points, starting at $y = 3.25$ (i.e. $x = 25.8$) with an interval size $h = 0.05$, was used. The minimum possible core radius was $y = -3.95$ (i.e. $x = 0.01925$). Comparison of results obtained for $h = 0.1$ and $h = 0.05$ showed that the smaller net size gave six-figure accuracy for both effective range and core radius. The error was largest for r_s large, because the Bessel functions in (C.7) vary rapidly for large z (i.e. for r_s and y large).

For both the NP and PP programs, the difference between the "predicted" solution given by (C.10) and the "corrected" solution given by (C.11) was compared with a preset tolerance at each step. If the tolerance was exceeded, it was multiplied by four and printed. The enlarged tolerance was used for the remainder of the equation, in order to prevent excessive printing, but was reset to its original value before the next equation was solved. This procedure allowed an estimate of the accuracy of each solution to be made.

In each case the integration proceeded until either U became negative or until the net had been covered with U remaining positive. In the latter case, G was increased by a substantial increment, the new value of G was printed out and the integration routine re-entered. This device reduced the time spent on cases where the potential was too weak to give the experimental value of the scattering length. If U became negative during the integration, an inverse interpolation was performed to find y_c, using the last three values of U and U'', which were stored in the computer at that time. Then the core radius r_c was computed from y_c. The interpolation method used is described by Shapiro (1955). It is more accurate than inverse inrerpolation with a fourth-order polynomial.

The effective range integrals were obtained as follows. Since Y is the net

point at which it is assumed that U is given by its asymptotic form ψ, there is no contribution to r_0 for $y > Y$. Let y_0 be the first net point greater than y_c, the value of y corresponding to the core radius r_c. Equation (C.9) can be written as

$$(C.12) \qquad r_0 = 2r_s\left[\int_{-\infty}^{Y}\psi_0^2(y)e^{2y}dy - \int_{y_0}^{Y}U_0^2(y)e^{2y}dy - \int_{y_c}^{y_0}U_0^2(y)e^{2y}dy\right]$$

since $U_0(y) = 0$ for $y < y_c$.

The first integral of (C.12) can be evaluated analytically for both the NP and PP cases. The second integral was calculated numerically by the Euler–McLaurin summation formula (Whittaker and Watson 1927, p. 127), the summation being performed and preserved at each step in the solution of the differential equation. Since $U_0 = \psi_0$ at the upper limit, the correction terms at $y = Y$ could be evaluated explicitly. At the lower end of the range, it can be seen that the correction terms are negligible. In addition, the integrand of the third integral can be replaced by a straight line with negligible error and so readily be evaluated once $U_0(y_0)$ and y_c are found. These facts are demonstrated in detail by Shapiro (1955).

D. RESULTS FOR ^1S SCATTERING

The programs were used with the following shapes for the attractive well:

(D.1)	$f(x) = \exp(-x^2)$	Gaussian
(D.2)	$f(x) = \exp(-x)$	Exponential
(D.3)	$f(x) = \exp(-x)/x$	Yukawa
(D.4)	$f(x) = \exp(-x)/x^2$.	

The results obtained with scattering lengths of $a_{sn} = -23.69\times10^{-13}$ cm. and $a_{sp} = -7.68\times10^{-13}$ cm. are given in full in about 50 tables in Appendix C of Shapiro (1955). For each shape and a large range of values of r_s and G, the tables list the NP effective range r_{0n}, the NP core radius r_{cn}, the PP effective range r_{0p}, and the PP core radius r_{cp}. Figs. 3 to 6 have been constructed from these tables to illustrate the important points regarding charge independence. The criteria for charge independence may be stated as follows: A potential is charge independent if, for the same values of G and r_s, (*a*) the NP and PP core radii are the same, and (*b*) the NP and PP effective ranges are within the limits given by experiment. Since the NP effective range is not well known, criterion (*b*) in general is restrictive only through the PP effective range.

In Figs. 3 to 6, the difference Δr_c between the NP and PP core radii ($\Delta r_c = r_{cp} - r_{cn}$) is plotted as ordinate against the PP core radius as abscissa for the four potential shapes. The points on these curves correspond to equal values of r_s and G for the NP and PP potentials. Curves of constant range parameter r_s and of constant PP effective range r_{0p} are given. The two constant r_{0p} curves correspond to the experimental limits given in Section A. The region between these curves will be called the "allowed" region. Charge independence occurs whenever the allowed region intersects the line $\Delta r_c = 0$.

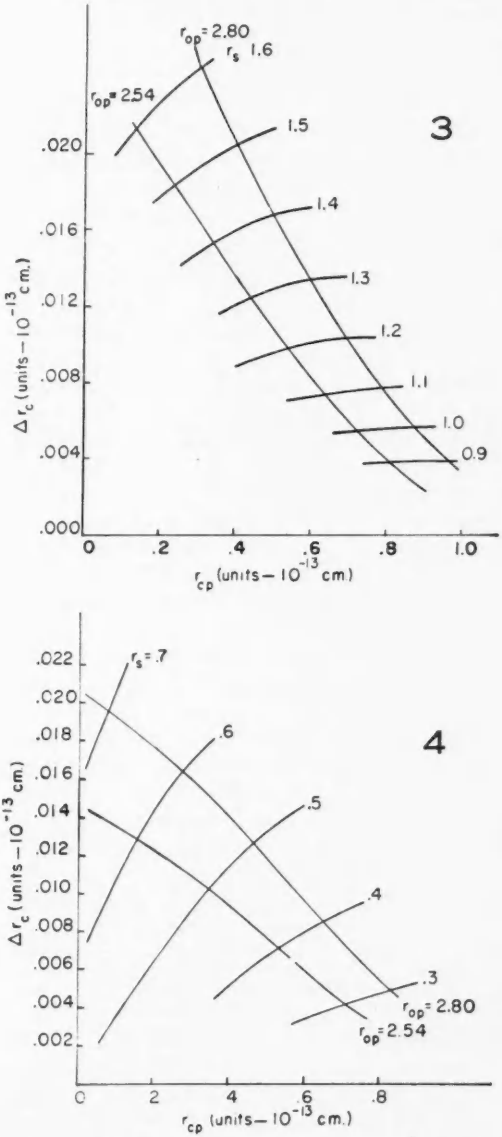

FIG. 3. Gaussian potential—Difference of PP and NP core radii plotted against PP core radius for NP and PP potentials with the same values of range parameter r_s and of V_0, the attractive potential strength (at $r = 0$). Curves of constant r_s and of constant PP effective range r_{0p} are shown (units 10^{-13} cm).

FIG. 4. Exponential potential—Δr_c vs. r_{cp} as in Fig. 3.

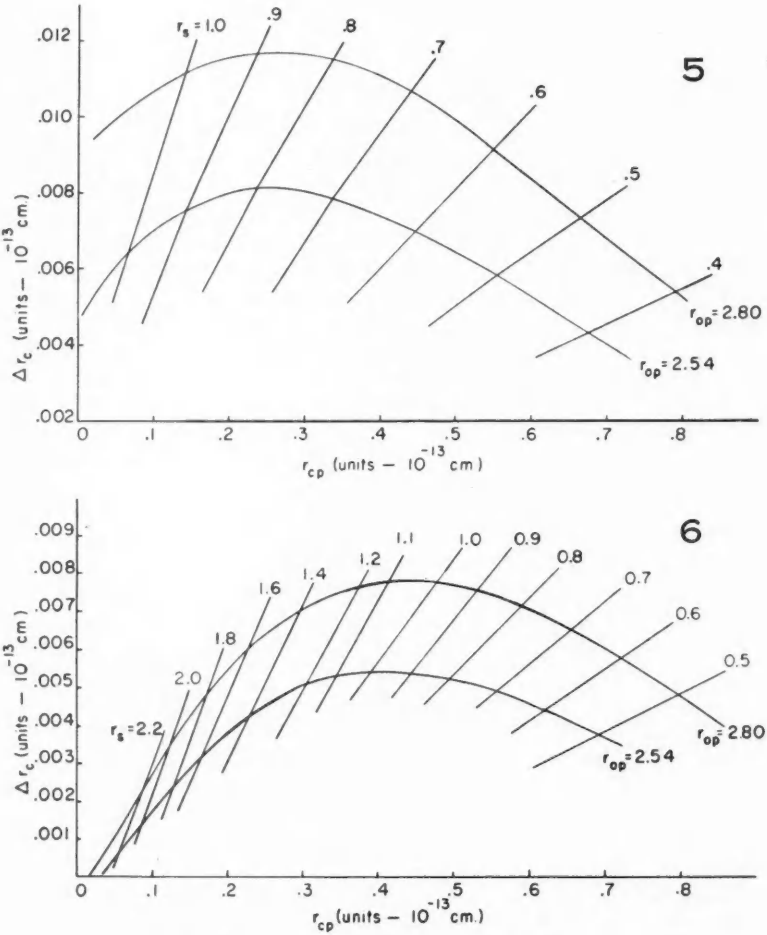

FIG. 5. Yukawa potential—Δr_c vs. r_{cp} as in Fig. 3.
FIG. 6. Potential e^{-x}/x^2—Δr_c vs. r_{cp} as in Fig. 3.

Examination of Figs. 3 to 6 suggests the following points:

(*a*) All four potentials appear to approach charge independence at large core radii. It will be shown below that this apparent charge independence at large core radii is a consequence of the method of plotting the curves and actually does not exist.

(*b*) At small distances, the allowed region bends down more and more as the order of the singularity of the potential at small distances increases. Charge independence finally occurs for the potential $\exp(-x)/x^2$ for the core radii

$r_c \sim 0.03\times10^{-13}$ cm. Thus, charge independence occurs only with potentials that are extremely singular (of the order of x^{-2} or greater) at small distances. The results suggest that charge independence will occur at larger core radii for potentials more singular than $\exp(-x)/x^2$.

(*c*) As the potential $\exp(-x)/x^2$ approaches charge independence, the allowed region becomes very narrow (it has a width $\Delta r_{cp} \sim 0.01$ to 0.02×10^{-13} cm. at $\Delta r_c = 0$). Thus, the assumption of charge independence restricts the core radius for a given potential to within very small limits.

The effect on Figs. 3 to 6 of experimental uncertainties in the scattering lengths was investigated by performing a few runs with slightly altered values of a_{sn} and a_{sp}. The uncertainty in r_{cp} due to this effect was found to be approximately six times the uncertainty in r_{cn}. The maximum possible error produced in Δr_c was always less than 0.001×10^{-13} cm. for zero core radius and decreased as the core radius increased. For the charge independent region of the potential $\exp(-x)/x^2$ the error obtained was 0.0002×10^{-13} cm. For the Yukawa at zero core it was approximately 0.0005×10^{-13} cm. These uncertainties are too small to affect appreciably any of the conclusions made above.

Thus, the experiments are accurate enough to make a critical analysis of the hypothesis of charge independence. This hypothesis either rejects a specific potential shape entirely or restricts the core radius to within very small limits ($\lesssim 0.02\times10^{-13}$ cm.). It should be pointed out that the method of analysis used here depends on extremely accurate computations since it is the difference between the two core radii which is used in Figs. 3 to 6.

The analysis used here can be refined further for a given potential by computing P_{sp} and using this value in fitting the experimental results. In this way the experimental errors in r_{0p} and a_{sp} for that particular potential can be reduced considerably from the values quoted in Section A. Both the width of the allowed region and the possible error in Δr_c due to errors in the scattering lengths will be reduced (by a factor of four to six). For the potential $\exp(-x)/x^2$, the charge independent core radius could be determined to approximately 0.004×10^{-13} cm. in this way. The PP experiments have been analyzed in the above manner for several potentials (without cores) by Yovits *et al.* (1952). Their results can be used to estimate a_{sp} and r_{0p} as functions of P_{sp}. The variation of P_{sp} with core radius will be approximately the same as for P_{sn}. The variation of the latter quantity has been calculated for several potentials by Preston (1954). His values of P_{sn} for zero core agree well with those of Yovits *et al.* for P_{sp}. Thus the values of a_{sp} and r_{0p} can be estimated approximately for the potentials treated here. This will be done below for cases of interest.

The allowed regions in Figs. 3 to 6 appear to approach charge independence at large core radii for all potential shapes. It will be shown now that charge independence does not occur in this region.

The points in Figs. 3 to 6 are plotted for equal values of r_s and V_0 in the NP and PP potentials. Thus, a particular point corresponds to equal potential strengths at the core only if the two core radii are the same, i.e. only along the

line $\Delta r_c = 0$. As the core radius increases, the potential strengths required to fit experiment become larger and larger, finally approaching a δ-function type of attraction at the core radius (this occurs in the limit $r_s = 0$). Thus, for large values of core radius, small values of Δr_c correspond to very large differences in the NP and PP potential strengths at the respective cores. Therefore, nothing can be deduced from Figs. 3 to 6 about charge independence in this region.

Calculations can be carried out for the limiting case of a δ-function type of interaction at the core. The maximum core radius, $\overline{r_c}$, at which the δ-function attraction occurs, is determined by the scattering length and effective range, as can be seen by writing

$$r_0 = 2\int_0^\infty (v_0^2 - u_0^2)dr = 2\int_0^{r_c} v_0^2 dr + 2\int_{r_c}^\infty (v_0^2 - u_0^2)dr, \tag{D.5}$$

since $$u_0 = 0 \text{ for } r < r_c.$$

In the δ-function limit, the second integral vanishes, so that

$$r_0 = 2\int_0^{\overline{r_c}} v_0^2 dr. \tag{D.6}$$

For the NP case, substitution of the value (A.3) for v_0 gives

$$\overline{r_{0n}} = 2\overline{r_{cn}}\left[1 - \frac{\overline{r_{cn}}}{a_{sn}} + \frac{\overline{r_{cn}}^2}{3a_{sn}^2}\right]. \tag{D.7}$$

The integral obtained for PP scattering by substitution of (A.14) into (D.6) is evaluated by Shapiro (1955). The result is

$$\overline{r_{0p}} = \frac{R}{6}\left[4 + (\overline{z_c}^2 - 4)\,\overline{z_c}^2\,A^2(\overline{z_c}) + 4\overline{z_c}^3\,A(\overline{z_c})\,B(\overline{z_c}) - \overline{z_c}^4\,B^2(\overline{z_c})\right] \tag{D.8}$$

where

$$\overline{z_c} = 2\left(\frac{\overline{r_{cp}}}{R}\right)^{\frac{1}{2}}, \tag{D.9}$$

$$A(z) = K_1(z) - \frac{R}{2a}\,I_1(z), \tag{D.10}$$

$$B(z) = -K_0(z) - \frac{R}{2a}\,I_0(z). \tag{D.11}$$

Equations (D.7) and (D.8) have been used to evaluate the maximum core radii as functions of the effective ranges in the ^1S state, using the experimental values of the scattering lengths. The results are given in Fig. 7.

Consider NP and PP potentials with the same values of r_s and potential strength at the core, but with different core radii. Let these approach the δ-function limit, keeping r_s and the potential strength at the core the same in the two cases. For such strong potentials, the Coulomb force is negligible in the neighborhood of the core, i.e. the NP and PP potentials are equal in this region except for the difference in core radii. Hence the relation

$$\left(\frac{u'}{u}\right)^{\text{NP}}_{r_{cn}+\epsilon} = \left(\frac{u'}{u}\right)^{\text{PP}}_{r_{cp}+\epsilon}$$

must hold, where ϵ is an infinitesimal. In addition, both the NP and PP wave

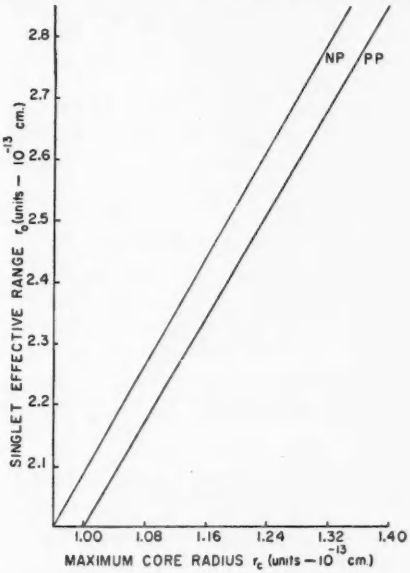

FIG. 7. Singlet effective range plotted against maximum core radius, for both NP and PP scattering, with $a_{sn} = -23.69\times10^{-13}$ cm., $a_{sp} = -7.68\times10^{-13}$ cm.

functions must match smoothly to their asymptotic forms. First taking the limit $r_s \to 0$ and then the limit $\epsilon \to 0$, one obtains for the limit of a δ-function type of interaction

$$\left(\frac{v'}{v}\right)^{NP}_{\overline{r_{cn}}} = \left(\frac{v'}{v}\right)^{PP}_{\overline{r_{cp}}} \tag{D.12}$$

where v is the asymptotic wave function. For zero energy, the wave functions in (D.12) are given by (A.3) and (A.14). Performing the differentiations in this case one obtains

$$\frac{1}{\overline{r_{cn}}-a_{sn}} = \frac{2}{R\bar{z}_c}\,\frac{K_0(\bar{z}_c)+(R/2a_{sp})I_0(\bar{z}_c)}{K_1(\bar{z}_c)-(R/2a_{sp})I_1(\bar{z}_c)}. \tag{D.13}$$

Values of $\bar{z}_c$ corresponding to the experimental PP effective range were determined from Fig. 7, and inserted in (D.13), together with the experimental value of a_{sp}. This determined $\overline{r_{cn}}-a_{sn}$. The results are given in Table I. Column

TABLE I

RESULTS OBTAINED BY FITTING EQUATION (D.13) TO THE LOW ENERGY PP SCATTERING PARAMETERS

(All lengths are in units of 10^{-13} cm.)

(1) $\bar{z}_c$	(2) $\overline{r_{cp}}$	(3) r_{0p}	(4) $\overline{r_{cn}}-a_{sn}$	(5) $\overline{r_{cn}}$
0.40	1.153	2.32	17.67	−6.02
0.42	1.271	2.57	16.78	−6.91
0.44	1.395	2.84	16.04	−7.65

(5) gives the values of $\overline{r_{cn}}$ obtained by replacing a_{sn} by its experimental value. It is seen that $\overline{r_{cn}}$ is a large negative number. But $\overline{r_{cn}}$ must be positive. Thus, if the constants in the δ-function interaction are fitted to the PP parameters a_{sp} and r_{0p}, the NP scattering length cannot be fitted. It follows that the limiting case of a δ-function interaction is not charge independent. Since the discrepancy in core radii is very large, we can also be confident that charge independence cannot occur for strong potentials near the limiting value.

The calculations of Schwinger (1950) and Salpeter (1953), described in Section A, give estimates of the changes δa_{sn} and δa_{sp} in the scattering lengths produced by magnetic interactions. Multiplying these by the quantities $\partial r_{cn}/\partial a_{sn}$ and $\partial r_{cp}/\partial a_{sp}$ obtained from runs with different values of scattering length yields the change in Δr_c required to fit experiment when magnetic interactions are taken into account. Both δa_s and $\partial r_c/\partial a_s$ decrease rapidly in magnitude as r_c increases. The results obtained for zero core radius are given in Table II, together with estimates of a_{sp}, r_{0p} obtained from the work of

TABLE II

ESTIMATES OF (*a*) EFFECT OF MAGNETIC INTERACTIONS ON Δr_c AND (*b*) LOW ENERGY PP SCATTERING PARAMETERS, FOR VARIOUS POTENTIALS WITHOUT CORES

(All lengths are in units of 10^{-13} cm.)

Potential	Change in Δr_c produced by magnetic interactions	PP scattering length a_{sp}	PP effective range r_{0p}
Gaussian	0.005	−7.67	2.59
Exponential	0.009	−7.684	2.655
Yukawa	0.0090	−7.707	2.743
$\exp(-x)/x^2$	0.003	−7.72	2.80

Yovits *et al.* (1952) and Preston (1954). The numbers given in Table II are rough estimates only, because (*a*) the results in the literature did not include all the potential shapes used here, and (*b*) the calculations on magnetic interactions are based on very crude models. A fairly accurate estimate of the change in Δr_c could be made only for the Yukawa potential.

Comparison of Table II with Figs. 3 and 4 shows that the effect of magnetic interactions is not large enough to yield charge independence at zero core radius for either the Gaussian or exponential potentials. Since the magnetic correction decreases much more quickly with increasing core radius than the curves of constant r_{0p} in Figs. 3 and 4, these potentials do not yield charge independence for any core radius.

For the Yukawa potential, Table II gives $r_{0p} = 2.74 \times 10^{-13}$ cm. which corresponds to $\Delta r_c \simeq 0.0080$ for $r_{cp} = 0$ in Fig. 5. Thus, the effect of magnetic interactions is large enough to give charge independence at zero core radius. Since the constant r_{0p} curves of Fig. 5 slope upwards and the effect of magnetic interactions decreases with increasing core radius, charge independence cannot occur for $r_c \gtrsim 0.04 \times 10^{-13}$ cm. Values of the potential constants and derived effective range, as obtained by extrapolations from the results in the tables in the thesis, are given in Table III. These were obtained by assuming

TABLE III

PARAMETERS AND EFFECTIVE RANGES FOR CHARGE INDEPENDENT YUKAWA POTENTIAL, AFTER MAKING CORRECTIONS FOR (*a*) MAGNETIC INTERACTIONS, AND (*b*) THE EFFECT OF P_{ap} ON EXPERIMENTAL VALUE OF r_{0p}

(All lengths are in units of 10^{-13} cm.)

r_c	r_s	G	V_0 (Mev.)	r_{0p}	r_{0n}
0	1.140	1.57	50.1	2.74	2.657
0.02	1.116	1.65	54.9	2.74	2.663
0.04	1.092	1.73	60.2	2.74	2.670

$r_{0p} = 2.74\times10^{-13}$ cm. Thus, if it is assumed that Schwinger's calculation of the effect of magnetic interactions is approximately correct, the charge independent Yukawa potential must have parameters in the range given in Table III.

The results at small core radii for the potential $\exp(-x)/x^2$ are given on an enlarged scale in Fig. 8. Since the core radius at which charge independ-

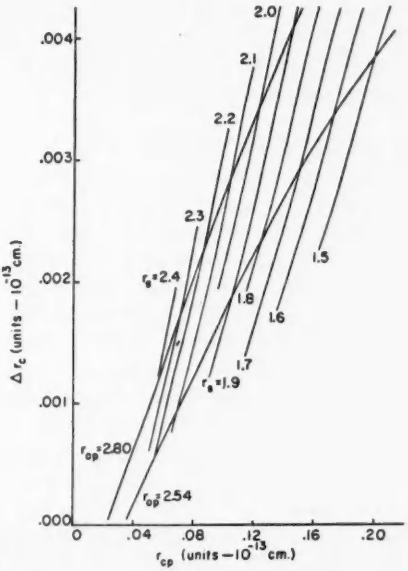

FIG. 8. Potential e^{-x}/x^2. An enlargement of a portion of Fig. 6, Δr_c vs. r_{cp} as in Fig. 3.

ence occurs is small, the corrections for zero core can be used. Table II gives $r_{0p} = 2.80\times10^{-13}$ cm. This is a rough estimate obtained by extrapolating the results of Yovits *et al.* (1952) and Preston (1954) to more singular potentials. The $r_{0p} = 2.80\times10^{-13}$ cm. curve of Fig. 8 and the result quoted in Table II show that charge independence will occur at a core radius of $r_c \sim 0.11\times10^{-13}$ cm. where magnetic interactions are taken into account. The potential parameters obtained by extrapolating the results in the tables in Shapiro (1955)

TABLE IV

PARAMETERS AND EFFECTIVE RANGES FOR CHARGE INDEPENDENT POTENTIAL OF THE FORM $\exp(-x)/x^2$ (*a*) WITHOUT AND (*b*) WITH CORRECTIONS FOR MAGNETIC INTERACTIONS
(All lengths are in units of 10^{-13} cm.)

r_c	r_s	G	V_0 (Mev.)	r_{0p}	r_{0n}
0.02	2.66	0.60	3.5	2.80	2.50 (*a*)
0.11	2.06	1.02	10.0	2.80	2.62 (*b*)

are given in Table IV for the magnetic interaction (*a*) excluded and (*b*) included. The value $r_{0p} = 2.80\times10^{-13}$ cm. was used in obtaining these results. It is seen that the potential parameters are quite different in the two cases. However, in this particular case, the core radii involved are very close to a singularity of the potential. Because of this, small changes in the core radius require large changes in the other potential parameters to maintain agreement with experiment.

Values of the charge independent parameters (without corrections for magnetic interactions) for the potential $\exp(-x)/x^2$ have been published elsewhere (Preston and Shapiro 1954). The values quoted there differ slightly from those given in the first line of Table IV because a less accurate method of analysis had been used. In particular, the values quoted for the NP effective range are too low.

The main results obtained will be summarized briefly.

(*a*) If magnetic interactions are neglected, the hypothesis of charge independence places severe restrictions on the potential shape. For example, the core radius for the potential $\exp(-x)/x^2$ can be determined to within approximately 0.004×10^{-13} cm., if the effect of the shape parameter P_{sp} is taken into account. The method of analysis used here could be applied equally well to potentials that are not charge independent, provided a specific form of charge dependence is assumed. Potentials with known charge dependence can arise from meson theories.

(*b*) If a specific form of charge dependence is assumed, the factor limiting the accuracy of the present method of analysis is the uncertainty in the calculations of the effect of magnetic interactions, not experimental errors.

(*c*) Although the size of the magnetic corrections is not well known, the charge independent core radius is determined fairly well (to within approximately 0.05×10^{-13} cm. for $\exp(-x)/x^2$), because the slope of the allowed region is large. For (more singular) potentials that are charge independent at larger core radii, the allowed region will have an even greater slope, allowing the core radius to be determined more accurately.

(*d*) To be charge independent, the potential must be at least as singular at small distances as the Yukawa.

(*e*) The core radius required for charge independence increases as the order of the singularity of the potential at small distances increases. (The Yukawa potential is charge independent for zero core radius.)

(*f*) Charge independence cannot occur for extremely large core radii ($\gtrsim0.8\times10^{-13}$ cm.).

Both charge independent potentials obtained in this work have large positive values of shape parameter. It is conceivable that more accurate PP scattering experiments, or even an extremely careful analysis of existing ones, will reject such potentials. Thus, it may be possible to show that no static charge independent potential with an infinite repulsive core can explain the low energy properties of the two-nucleon system.

We would stress that the question of magnetic interactions between nucleons should be studied carefully. The sensitivity of this effect to various assumed distributions for the magnetic moment of a nucleon should be examined.

Finally we shall make some remarks about the pseudoscalar meson theory of nucleon forces, as derived by Lévy (1952) and Klein (1953 *a*, *b*). It has been shown by Blatt and Kalos (1953) and also in Part III of this series (Shapiro and Preston 1956) that this potential will not fit experiment for both triplet and singlet states. However, these calculations assumed that the potentials derived from pseudoscalar meson theory had equal cores in the singlet and triplet states. Since the relativistic terms represented by the core may be spin dependent, this is not a necessary consequence of the theory. Thus, the fact that they could not fit the experimental results does not reject the potential. The pseudoscalar meson potentials behave at small distances as r^{-3}. The results of this paper suggest that charge independence for such a potential will occur at core radii of approximately $(0.2\text{–}0.4)\times10^{-13}$ cm. This is the size of core predicted by the theory. In addition, the Lévy potential is charge independent, except for small corrections (e.g. π^+–π^0 mass difference). Thus, it appears that the pseudoscalar meson theory may give a better fit to experiment than currently is believed, provided different core radii are assumed in the singlet and triplet states. Therefore, the coupling constant should be obtained by fitting the ^1S states of the NP and PP systems, rather than the ^1S and $^3S+^3D$ states of the NP system. In addition, such a fit will give the singlet core radius. Fitting the deuteron binding energy then will give the triplet core radius. The derived quantities (e.g. NP and PP effective ranges, quadrupole moment) will give a critical test of the potential, particularly if the shape parameters P_{sn}, P_{sp}, P_t are calculated.

REFERENCES

BETHE, H. A. 1951. Phys. Rev. **82**: 60.
BIRD, J. R. and PRESTON, M. A. 1955. Can. J. Phys. **33**: 399.
BLATT, J. M. and JACKSON, J. D. 1949. Phys. Rev. **76**: 18.
BLATT, J. M. and KALOS, M. H. 1953. Phys. Rev. **92**: 1563.
BREIT, G. and BOURICIUS, W. G. 1949. Phys. Rev. **75**: 1029.
BREIT, G., CONDON, E. V., and PRESENT, R. D. 1936. Phys. Rev. **50**: 825.
BREIT, G. and FEENBERG, E. 1935. Phys. Rev. **48**: 203.
BREIT, G. and STEHN, J. R. 1937. Phys. Rev. **52**: 396.
BREIT, G., THAXTON, H. M., and EISENBUD, L. 1939. Phys. Rev. **55**: 1018.
FERMI, E. and MARSHALL, L. 1949. Phys. Rev. **75**: 578.
HAFNER, E. M., HORNYAK, W. F., FALK, C. E., SNOW, G., and COOR, T. 1953. Phys. Rev. **89**: 205.
JACKSON, J. D. and BLATT, J. M. 1950. Revs. Mod. Phys. **22**: 77.
JAHNKE, E. and EMDE, F. 1945. Tables of functions. 4th ed. Dover Publications, New York. p. 205.
KLEIN, A. 1953*a*. Phys. Rev. **89**: 1158.
——— 1953*b*. Phys. Rev. **90**: 1101.

LÉVY, M. M. 1952. Phys. Rev. **88**: 725.
MILNE, W. E. 1949. Numerical calculus. Princeton Univ. Press, Princeton, N.J.
PRESTON, R. L. 1954. A study of repulsive core potentials in the neutron–proton system at low energies. M.Sc. Thesis, McMaster University, Hamilton, Ontario.
PRESTON, M. A. and SHAPIRO, J. 1954. Phys. Rev. **96**: 813.
SALPETER, E. E. 1951. Phys. Rev. **82**: 60.
——— 1953. Phys. Rev. **91**: 994.
SCHWINGER, J. S. 1950. Phys. Rev. **78**: 135.
SHAPIRO, J. 1955. Ph.D. Thesis, University of Toronto, Toronto, Ontario.
SHAPIRO, J. and PRESTON, M. A. 1956. Unpublished.
SNOW, G. 1952. Phys. Rev. **87**: 21.
WATSON, G. N. 1952. A treatise on the theory of Bessel functions. 2nd ed. Cambridge University Press, London.
WHITTAKER, E. T. and WATSON, G. N. 1927. A course of modern analysis. 4th ed. Cambridge University Press, London.
YOVITS, M. C., SMITH, R. L., JR., HULL, M. H., JR., BENGSTON, J., and BREIT, G. 1952. Phys. Rev. **85**: 540.

KINETICS OF SOLIDIFICATION[1]

By K. A. Jackson and Bruce Chalmers

ABSTRACT

The kinetic theory of melting and freezing is developed from consideration of atom movements at an interface between solid and liquid. The equations developed are shown to have the same form as the corresponding thermodynamic equations. The homogeneous nucleation of a solid phase in a liquid is then considered from the point of view of this theory. Agreement with experimental observation is obtained on the following points. (1) The supercooling at which homogeneous nucleation occurs is proportional to the absolute equilibrium temperature. (2) The surface free energy per atom used in the quasi-thermodynamic treatment of nucleation should be equal to one-half the latent heat per atom. (3) The amount of liquid supercooled has a very small effect on the temperature at which homogeneous nucleation occurs.

INTRODUCTION

In discussions of the kinetics of change of state, and other phase changes, it has been customary to consider only the net rate of the process; this is zero when equilibrium exists. Following this approach, the net rate of a reaction can be related to the change of free energy which accompanies it. The application of this method to the growth of crystals from the melt has been discussed by Turnbull (1950a). The main result is that $\bar{R}$, the net rate of freezing or melting, is a function of the temperature of the interface; the actual relationship can be calculated by making reasonable assumptions; but it appears that the further development of this approach is inherently limited.

The alternative approach, which is discussed in the present paper, is to consider explicitly the two rates, the difference between which is the net rate of the process. It has been suggested (Chalmers 1949) that the process of melting (or liquid formation) and the process of freezing (or solid formation) both occur at a solid–liquid interface at any temperature at which the interface exists; the interface moves if the rates of melting and of freezing are not equal. This again shows $\bar{R}$ to be a function of the temperature, but the two rates can be considered in terms of the geometry and crystallography of the interface rather than the free energy of the phases.

In the present paper, quantitative expressions are found for the rates of melting and freezing. From these expressions, the net rate of movement of a solid–liquid interface is calculated as a function of temperature by the use of reasonable assumptions. A relationship between the latent heat of fusion and the equilibrium temperature is derived. The dependence of the relationship on the crystallography of the solid is explained. It is shown that a curved interface should have a different equilibrium temperature from a plane one, and this leads to a detailed analysis of the equilibrium temperature as a function of radius of curvature. This is extended to the derivation of the critical size of a homogeneous nucleus and calculations are made of the abundance

[1]Manuscript received in original form August 8, 1955, and as revised February 20, 1956. Contribution from the Division of Engineering and Applied Physics, Harvard University, Cambridge 38, Massachusetts.

and size distribution of solid-like clusters in the liquid. A combination of these two analyses defines the conditions for homogeneous nucleation.

EQUILIBRIUM TEMPERATURE

We will define P_M and P_F as the probability that an atom will make a transition from solid to liquid, or liquid to solid, across the interface in one vibrational cycle of the atom. We know from experiment that there is, for a given system at a given pressure, only one temperature at which $\bar{R}$, the net rate of movement of an interface, is zero, i.e. only one temperature of equilibrium between solid and liquid; it follows that either P_M or P_F or both must be temperature dependent.

TEMPERATURE DEPENDENCE OF RATES

The energy of an atom in the solid may be considered as made up of two parts:

(1) E_S, the cohesive energy. This is the energy associated with the formation of the lattice from isolated atoms at absolute zero.

(2) Thermal energy, which is present when the lattice is at a temperature other than absolute zero.

When an atom leaves a lattice site to become part of the liquid, it must pass through a state where its energy is greater than at the lattice site. In making the transition from solid to liquid, some paths will be easier to follow than others. The maximum energy along the easiest path from solid to liquid will be called E_T. This is the least energy the atoms can possess and make the transition from solid to liquid.

The fraction of solid atoms at an interface at temperature T possessing an energy equal to or greater than E_T will be given by:

$$\exp[(E_S-E_T)/kT] = \exp(-Q_M/RT),$$

where $(E_T-E_S)/k = Q_M/R$. The quantity Q_M may be called the activation energy for melting.

According to the principle of detailed balancing, or of microscopic reversibility, an atom going from the liquid to the solid must have the same minimum energy, E_T, as an atom going the other way. The lowest energy possible for a transition from solid to liquid will be the lowest energy possible for a transition from liquid to solid.

The fraction of atoms having sufficient energy to make the transition from liquid to solid is given by

$$\exp[(E_L-E_T)/kT] = \exp(-Q_F/RT),$$

where E_L is the binding energy of the liquid and Q_F is the activation energy for freezing.

The latent heat of fusion is the heat evolved when a gram of liquid solidifies. It is the difference between the energies of the solid and the liquid at the equilibrium temperature. The latent heat is approximately the difference between the internal energies of the liquid and solid. Thus,

$$(E_L-E_S)/k = L/R.$$

These energy relationships are shown schematically in Fig. 1. A statement that is entirely equivalent to the one above is that

(1) $$L = Q_M - Q_F.$$

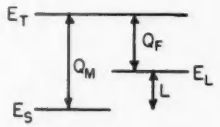

FIG. 1. Energy relationships for a pure metal.

OTHER FACTORS DETERMINING RATES

An atom at an interface will not cross the interface every time it has sufficient energy to do so. If an atom is vibrating obliquely to the interface, it must have a higher energy in order to escape from the solid, since only the components of its momentum normal to the interface determine whether or not it can escape from the solid. The fraction of the vibrations in which an atom has a sufficient component of its momentum normal to the interface we shall define as the geometric factor G. There will be two geometric factors; G_M for atoms leaving the solid, and G_F for atoms leaving the liquid.

Only a certain fraction, A_M, of the solid atoms at the interface which satisfy the above conditions will be in a position at which they are able to enter the liquid. This fraction is referred to as the accommodation coefficient. Similarly, A_F is the accommodation coefficient for freezing.

EQUILIBRIUM OF A PLANE INTERFACE

The probability of an atom at the interface making a transition from solid to liquid during one vibrational cycle of the atoms in the solid is:

(2) $$P_M = A_M G_M \exp(-Q_M/RT).$$

The corresponding probability from liquid to solid is:

(3) $$P_F = A_F G_F \exp(-Q_F/RT).$$

The probability per second is ν times this, where ν is given approximately by kT/h, the Debye frequency. The total number of atoms crossing the interface per square centimeter per second is given by

$$N_S \nu_S P_M \qquad \text{solid to liquid}$$

and

$$N_L \nu_L P_F \qquad \text{liquid to solid}$$

where N_S and N_L are the numbers of atoms at the interface per square centimeter in the solid and liquid respectively.

For equilibrium:

$$N_S \nu_S P_M = N_L \nu_L P_F$$

or

$$\exp[(Q_M - Q_F)/RT_E] = A_M G_M N_S \nu_S / A_F G_F N_L \nu_L,$$

but

$$Q_M - Q_F = L,$$

(4) $$L/RT_E = \ln(A_M G_M N_S \nu_S / A_F G_F N_L \nu_L),$$

where T_E is the equilibrium temperature.

ACCOMMODATION COEFFICIENT

The number of atoms per square centimeter of interface is very nearly the same for both solid and liquid. The direction in which an atom must be moving to leave either the solid or the liquid will be confined to a solid angle which will be approximately equal for the solid and for the liquid when the interface between them is plane. Hence

$$N_S G_M / N_L G_F = 1.$$

Equation (4) becomes essentially

$$L/RT_E = \ln(A_M \nu_S / A_F \nu_L).$$

Thus the equilibrium temperature depends principally on the latent heat of fusion and the probability of an atom being accommodated at the surface of the solid and the liquid, and the relative frequencies in the solid and the liquid. The effect of frequency has been discussed by Mott and Jones (1936) and we will not discuss it further here. In general, the variations in the liquid structure are small compared to the variations in the crystal structure of solids, and so may be ignored in most cases. The accommodation of atoms on the solid surface would seem to be the major factor determining the relationship between the latent heat and the equilibrium temperature.

The coefficient A_F should be the same for all solid–liquid interfaces having the same arrangement of atoms at the solid surface. In Fig. 2 latent heats of

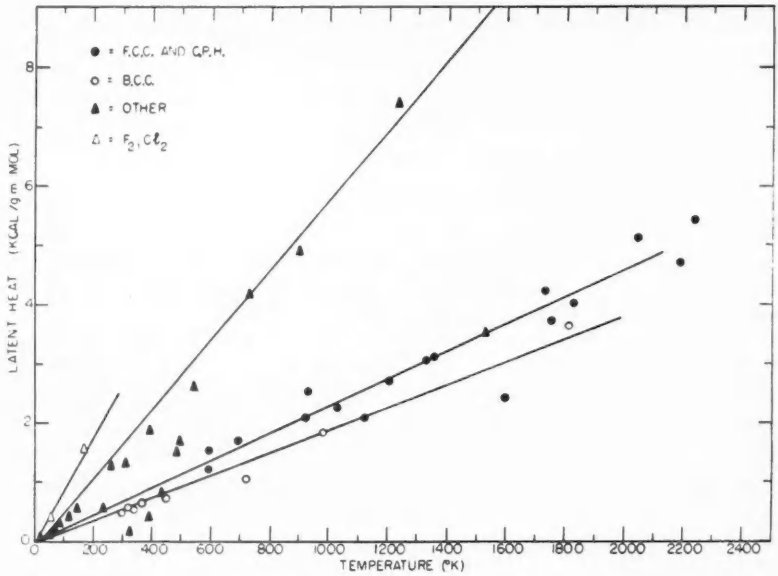

FIG. 2. Latent heats of fusion as a function of the absolute melting temperatures of various elements.

fusion in kcal. per gm. mol. have been plotted against the equilibrium temperature for many elements.*

The values for both face-centered cubic and hexagonal close-packed metals lie roughly on a straight line. Both these structures have planes which have the same (maximum) closeness of packing. The body-centered cubic metals, both the alkali metals and others, lie below the close-packed metals on this plot. This indicates that the accommodation coefficient on the solid surface is higher, as would be expected since these metals are less closely packed.

Other crystal structures which have predominantly covalent bonding and whose structure satisfies the "8-N rule" lie roughly on another straight line of considerably greater slope. These atoms can only be accommodated on the solid at sites where they will satisfy the correct bonding of the solid, whereas no such condition exists for atoms that are leaving the solid. Thus they have a lower accommodation coefficient for freezing, and a resultant lower equilibrium temperature than would be the case for a metallically bonded crystal with the same latent heat.

Substances which are molecular in the liquid, and freeze as molecules, such as fluorine and chlorine, are subject to an extra restriction. The molecules can only be accommodated on the solid if they are oriented properly. These halogens have a very low accommodation coefficient on the solid.

TABLE I

	$\frac{N_S A_M G_{MV_S}}{N_L A_P G_{PV_L}}$	$\frac{L}{RT_E}$
f.c.c., c.p.h.	3.16	1.12
b.c.c.	2.54	0.93
8–N	18.2	2.90
F_2, Cl_2	85	4.45

Table I shows approximately the ratio of the accommodation coefficients for the four main types discussed above.

ESTIMATION OF ACTIVATION ENERGIES

A liquid may be pictured as an aggregation of atoms, some of which form transient "clusters". These small clusters may be similar to small elements of the solid, but their orientations are random. As will be seen later, most of the atoms in the liquid are single, not part of any cluster, at or above the equilibrium temperature. The ease with which the atoms and clusters move in the liquid depends on temperature.

The same energy "barriers" that limit the movement of atoms in diffusion in a liquid, and the transfer of momentum in viscous flow, may also control the movement of atoms from liquid to solid. The activated state in all these

*The values plotted have been taken from Smithells' "*Metal Reference Book*". For some of these elements, the equilibrium temperatures, or the latent heats, are not known accurately. For many other elements, there is no value given in Smithells' for the latent heat of fusion. Moreover, the latent heats quoted in other handbooks differ as much as 5 or 10% from some of the values in Smithells'. However, the values are accurate enough to show distinct trends.

three cases should be the same. It will be assumed that the temperature dependence of the rate of freezing is the same as that for viscous flow or liquid diffusion. Although most measurements for the activated energies of these last two do not agree too well, some recent measurements for sodium show excellent agreement. We will use measured values of the "activation energies" for viscosity (Table II) as the transition energy for freezing.

TABLE II

VALUES OF VISCOSITY ACTIVATION ENERGIES

Metal	Q_η/RT_E
Cu	0.60
Pb	1.96
Sn	1.47
Hg	1.29

Selecting $Q_\eta/RT_E = 1.5$ as a representative value, we will estimate $Q_F/RT_E = 1.5$. Hence $Q_M/RT_E = 2.65$, since $L/RT_E = 1.15$ for a close-packed metal.

ESTIMATION OF ACCOMMODATION COEFFICIENT

The factor that remains undetermined is $A_M G_M$. We will estimate G_M as the order of one-sixth the total solid angle, and G_F about the same. We know the ratio A_M/A_F, so it is only necessary to determine one accommodation coefficient. Certainly neither can be greater than unity; or, since $A_M/A_F = \exp(L/RT) = \exp 1.15 = 3.16$, A_F must be less than 1/3.16 for close-packed metals. To set a lower limit on A_M we will consider the change in the net rate of solidification with temperature.

Let $\bar{R}$ be the net rate of melting; then

$$(5) \quad \bar{R} = N_S V_0 A_M G_M \nu_S \exp(-Q_M/RT) - N_L V_0 A_F G_F \nu_L \exp(-Q_F/RT),$$

where V_0 is the atomic volume in the solid;

$$(6) \quad (d\bar{R}/dT)_{T_E} = N_S V_0 A_M G_M \nu_S (Q_M/RT_E^2)\exp(-Q_M/RT_E) - N_F V_0 A_F G_F \nu_L (Q_F/RT_E^2)\exp(-Q_F/RT_E).$$

Substituting $A_M/A_F = 3.16$, $G_M = G_F = 1/6$, $\nu_S = \nu_L = 2.8\times10^{13}$ sec.$^{-1}$,

$$N_F = \tfrac{1}{2}(3\times10^8)^2 V_0 = (3\times10^{-8})^3/\sqrt{2},$$

$$Q_M/RT_E = 2.65, \quad Q_F/RT_E = 1.5, \quad T_E = 1356° \text{ for copper},$$

$$(d\bar{R}/dT)_{T=T_E} = 8.4\, A_M \text{ cm./sec./deg.}$$

In the absence of experiments designed to give the value of $d\bar{R}/dT$, we can set limits on it by considering the accuracy associated with the use of melting or freezing points of metals as temperature standards.

Consider a melting and freezing point determination of a pure metal. Let us assume that the metal is in the form of a cylinder 6 cm. in diameter and takes 10 min. to freeze or melt. Experience suggests that under such conditions the difference between the melting and freezing temperatures would not be more than 1/10 degree.

Using this limit we find that:

$$d\bar{R}/dT \geqslant 3\times 10/600 = 1/20 \text{ cm./sec./deg.}$$

This means that

$$8.4\, A_M \geqslant 1/20,$$

$$A_M \geqslant 1/168.$$

We also know that $A_M \leqslant 1$, and $A_M/A_F = 3.1$.

Thus

$$1 \geqslant A_M \geqslant 1/168,$$

$$1/3.1 \geqslant A_F \geqslant 1/532 \text{ for copper.}$$

Carrying through this same calculation for sodium gives

$$d\bar{R}/dT_{T_E} = 94\, A_M.$$

PREDICTED CURVES

We are now in a position to draw the individual curves for the rate of freezing, rate of melting, and net rate of solidification as a function of temperature.

These curves are shown in Figs. 3 and 4. These curves were plotted for copper, taking $A_M = 1/5$. This numerical value may be in error by a factor of 5. The rate at which atoms cross the interface at the equilibrium temperature corresponds to a growth rate of solid and liquid of 1700 cm./sec. An order of magnitude here will not alter the conclusion that atoms are moving very rapidly across the interface at the equilibrium temperature. The slow rates of freezing and melting obtainable in a laboratory correspond to the difference between two large rates. At absolute zero of temperature all rates are zero. A liquid would solidify very slowly if its temperature were low enough. Unfortunately, it does not seem possible to cool a liquid metal rapidly enough to observe this effect. Let us examine copper, for example. Copper nucleates homogeneously at about 1120°K. (Turnbull and Cech 1950). From Fig. 4 we see that at 1000°K. the net rate of freezing will be about 250 cm./sec. The sample would have to be cooled through this region in a very small fraction of a second. In fact the sample would have to be cooled right down to about 100°K. (where the rate of freezing is very small) in much less than a second to keep it in a liquid state. Such rates of cooling are clearly unobtainable in a laboratory today for bulk samples, and it seems improbable that they could be obtained even for fine particles.

Two alternatives present themselves. The first is to go to materials other than metals. The temperature of the minimum T' in Fig. 4 (corresponding to the maximum net rate of freezing) can be shown to be given by:

$$\ln(Q_M/Q_F) = L\Delta T'/RT_E T', \tag{5a}$$

where

$$\Delta T' = T_E - T'.$$

For a given value of the latent heat, $\Delta T'$ decreases as Q_M and Q_F increase. It can also be shown that the maximum net rate of freezing decreases simultaneously. We might expect to be able to cool materials with Q_M and Q_F large compared to L into the region of low temperature immobility. This has been done by Tamman (1922) with some organic compounds. He was able to super-

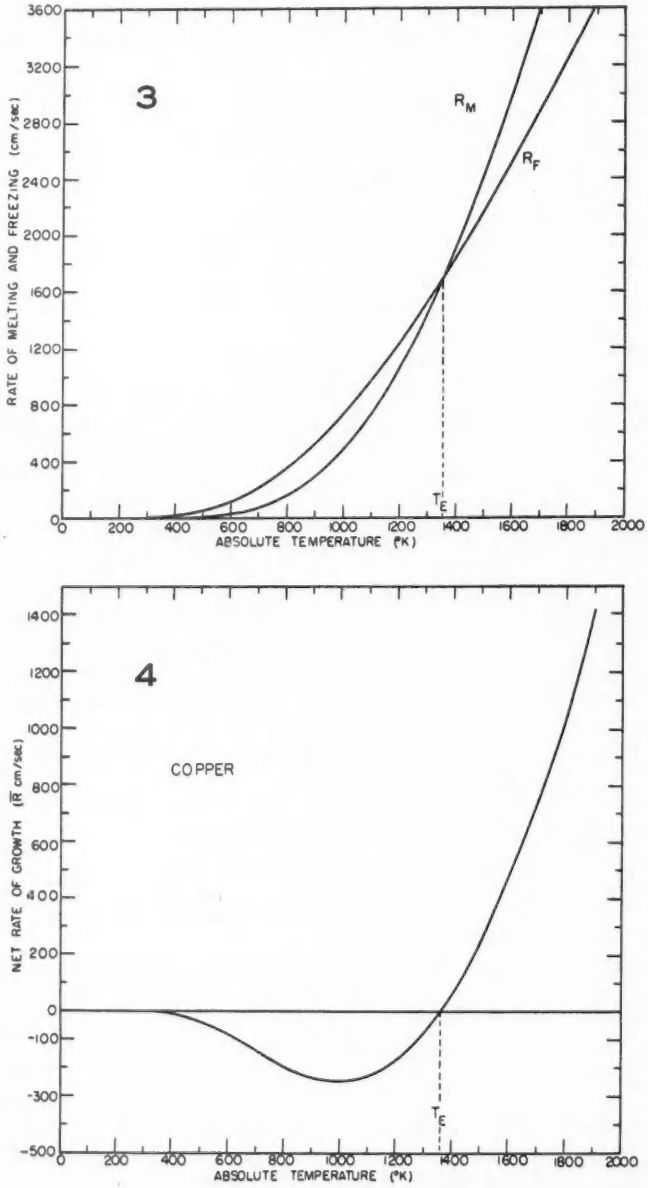

FIG. 3. Rate of production of solid or liquid as a function of temperature for copper.
FIG. 4. Net rate of production of solid or liquid as a function of temperature for copper.

cool these liquids rapidly enough to get into the low temperature range where the rate of solid growth was inappreciable. The liquids were observed to "freeze" on slow heating.

A similar phenomenon can be observed with selenium (Turnbull and Cech 1950). Selenium can be cooled rapidly enough so that it is in a "glassy" state far below its equilibrium temperature. It evidently has a high activation energy for viscous flow, which means that the rates at which freezing and melting occur will be lower than for normal metals, and one would expect to be able to "freeze in" the liquid.

The second alternative would be to construct a liquid at a very low temperature by vapor deposition on a very cold substrate. This would be particularly useful for metals since direct information about the rate of freezing alone could be obtained. If the rate of propagation of an interface could be measured in such a sample, for various temperatures, a good estimate of Q_F and the product $A_F G_F \nu_L N_L V_0$ could be obtained. Using copper as an example again, the rate of freezing R_F in the region 150°K. to 200°K. is the order of 1 mm./min. from equation (5) and R_M is less than one per cent of this rate in this temperature region. At the boiling point of liquid nitrogen (77°K.) the rate of freezing is 10^{-9} mm./min.

ENERGY OF ATOMS AT THE SURFACE OF THE SOLID

We have neglected the interfacial energy in the previous sections. The interfacial energy influences the equilibrium when the area of the interface is changing and only has an appreciable effect if the surface to volume ratio of the solid is large. The interfacial energy may be thought of as arising largely because the solid atoms at the interface have fewer than normal number of nearest neighbors. The missing neighbors are replaced by liquid. These missing neighbors of an atom on the solid surface give rise to an interfacial energy which is some fraction of the latent heat of fusion. We will make the assumption that the interfacial energy is linear with the number of missing nearest neighbors. For example, a single atom sitting on a (111) plane of a face-centered cubic structure with coordination three has nine missing nearest neighbors or a "surface energy" equal to $\frac{3}{4}L$. When such an atom leaves the solid, it loses three nearest neighbors; and each of the three atoms in the plane with which it was in contact lose one nearest neighbor, thereby raising their energy. An energy equal to one half the latent heat is associated with moving this atom from the solid to the liquid. Similarly a surface atom with coordination six has a surface energy $\frac{1}{2}L$, but has a total energy L associated with its melting. Such an atom is in a so-called "repeatable step" position.

We can see that our considerations in the previous sections apply *on the average* over the interface.

DETAILED STRUCTURE OF THE INTERFACE

A plane interface, say a (111) plane in a close-packed structure, will not be in equilibrium with a liquid at the equilibrium temperature. Every solid atom at the interface would have a coordination nine, or three halves the latent heat of fusion associated with melting. These atoms will leave the solid more

slowly than atoms are arriving from the liquid. As soon as atoms freeze singly, or in groups on the solid, the average coordination of the interface will be reduced, and this will go on until equilibrium is reached. The interface will no longer be plane. The interface will not depart too drastically from a plane, since large peaks or holes would be preferred melting or freezing sites. The interface will have an equilibrium number of atoms of each coordination on it. Under circumstances such as these, the nucleation of a new layer of solid will not be difficult because of the rapid rate of arrival of atoms from the liquid, even though the nucleus of critical size is large.

During growth, an interface will tend to approximate to the close-packed planes (Elbaum and Chalmers 1955). If the interface is inclined slightly to such a plane, it will be terraced. Each terrace forms a line of preferred growth sites which will produce growth by lateral movement. The net rate of arrival of atoms at such preferred sites is much greater than it would be on a plane, so that these atomic steps are an important aspect of the growth mechanism.

If a solution or a vapor is in contact with a solid surface, atoms will arrive at the solid much less frequently than they will cross a liquid–solid interface. In the former case the atoms have sufficient time to migrate on the solid surface and settle in a preferred site as discussed by Frank (1952).

INTERFACIAL ENERGY OF SMALL CLUSTERS OF SOLID ATOMS

For small clusters of solid atoms it is possible to construct a model and count the number of missing nearest neighbors. In this way one may estimate, on the basis of the simple linear assumption relating surface energy and the number of missing nearest neighbors, the surface energy associated with such a cluster. The surface energy obtained in this way, when divided by the total number of atoms present, varies as $n^{-1/3}$ where n is the total number of atoms present. This we would expect, since the total number of missing bonds depends on the number of surface atoms which varies as $n^{2/3}$, or the surface energy per atom in the cluster varies as $n^{-1/3}$.

We will assume that a small cluster of solid atoms has an effective latent heat given by:

$$L^n = (1-\beta/n^{1/3})L \tag{7}$$

where β from counting missing bonds on a model is 1.33 for face-centered cubic materials.

GEOMETRIC FACTOR

The "geometric factor" of an atom will also depend on its coordination. The geometric factor has been defined as the fraction of time that an atom is vibrating in a direction in which it has a sufficient component of its velocity normal to the interface. If an atom has low coordination, it will have a much larger angle in which to escape. The average escape angle over the whole interface will depend on the radius of curvature of the solid interface. Or we can write:

$$G_M{}^n = (1+\alpha/n^{1/3})G_M. \tag{8a}$$

There will also be a change in the geometric factor for the liquid, positive if the liquid surface is convex, negative if concave, or

$$G_F^n = (1-\alpha/n^{1/3})G_F \tag{8b}$$

if we are considering a solid crystal in a liquid.

It will be seen that these geometric factors add to the effect of surface energy, that is, they give an atom of low coordination which is energetically favored for melting, a still higher probability of melting.

STRUCTURE OF THE LIQUID

The same interatomic forces act between atoms in the solid and in the liquid. At sufficiently low temperatures, these forces produce an ordered array of atoms. This ordering tendency is present above the melting temperature. This results in the occurrence of small solid-like "clusters" of atoms in the liquid. In the present section we wish to calculate the size distribution of the clusters.* We will assume that each of these clusters can be treated as a small element of solid. From the expressions we have developed above we know the rate at which atoms will join, or leave, such clusters from the rest of the liquid.

If there were but one cluster in the liquid, it would be unstable. Actually there will be many "pairs" of atoms in the liquid. Some of these will break up, but some will be joined by a third. Some of these trios of atoms will lose an atom, and some will gain one, and so on. If this process goes on long enough (actually a very short time, since the atoms could change their allegiance every 10^{-14} seconds) the liquid will reach a state where the rate at which clusters of, say, three atoms gain an atom is the same as the rate at which clusters of four atoms lose an atom. Thus an equilibrium distribution of clusters will exist in the liquid.

The rate at which clusters of a given size will gain or lose atoms depends on the number of such clusters and the number of atoms per unit time that join or leave these clusters. If the number of clusters of n atoms is N_n and the rate at which a cluster of size n gains an atom is R_F^n, and loses an atom is R_M^n, then:

$$N_n R_F^n = N_{n+1} R_M^{n+1}, \tag{9}$$

for all values of n, is the condition that equilibrium exists between clusters.†

This condition results (see Appendix I) in a size distribution of clusters given by:

$$\ln \frac{N_n}{N} = -\ln \frac{N}{N_1} + \ln B + (n-2)\frac{L\Delta T}{RT_E T} - \frac{3}{2}\left(\frac{\beta L}{RT} + 2\alpha\right)[(n-1)^{2/3} - 2^{2/3}] \tag{10}$$

where N is the total number of atoms, and N_1 is the number of single atoms in the sample of liquid. This equation predicts that 90% of the total number of

*For the standard treatment of the size distribution of clusters see, for example, Hollomon and Turnbull (1953).

†This assumes that the atoms join and leave the clusters as separate atoms, not in pairs or trios. This assumption is justified because the probability of a "molecule" making a transition is an order of magnitude less than the probability of a single atom making a transition, and the number of pairs in the liquid is an order of magnitude less than the number of single atoms.

atoms are single atoms. This means that the term in $\ln(N/N_1)$ is small. The second term is also small. Equation (10) can be written essentially as:

$$N_n = N \exp(nf_1\Delta T - n^{2/3}f_2) \tag{11}$$

assuming $n \gg 1$, and where f_1 and f_2 are slowly varying functions of temperature in the region of the equilibrium temperature. At the equilibrium temperature the number of clusters decreases as $\exp(-n^{2/3})$. Above the equilibrium temperature ΔT will be negative, the number of clusters will drop off more rapidly with cluster size. For supercooling, ΔT will be positive. For small cluster sizes $\exp(-n^{2/3})$ dominates, and the number of clusters decreases with cluster size. However, for large cluster sizes, the number of clusters will increase with cluster size, since for large n the linear term will dominate the $n^{2/3}$ term.

Thus for a supercooled liquid, we should find a minimum number of clusters for some finite cluster size. This is shown in Fig. 5. The cluster size

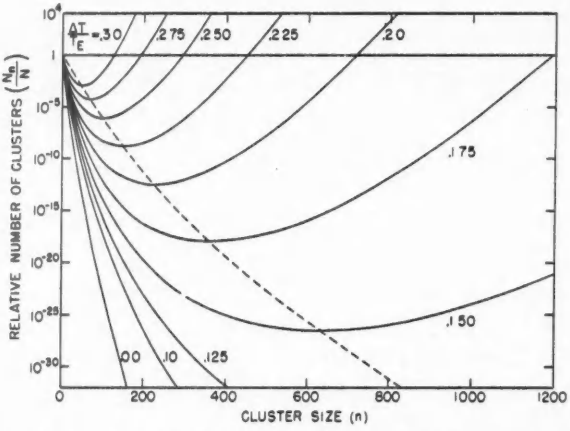

FIG. 5. Size distribution of clusters in a liquid for various temperatures. The dotted line represents the critical nucleus size (the locus of the minima).

corresponding to this minimum is the critical nucleus size for homogeneous nucleation.* The critical size nucleus becomes smaller with increasing supercooling, and the number of such nuclei increases. As can be seen from Fig. 5, the number of critical nuclei that exist at small supercooling, say $\Delta T/T_E = 0.1$, is so small that it is safe to say there are none. In supercooling a liquid, we start from somewhere above the equilibrium temperature where no large clusters exist. As we cool the sample below the equilibrium temperature there should be some very large clusters of solid atoms in equilibrium with the small clusters in the liquid. For the small clusters to become large, they would

*The critical nucleus size is usually defined as the size of a cluster that has an equal probability of increasing or decreasing in size. The two definitions are shown to be equivalent in the next section.

have to pass through the intermediate size where they is virtually zero probability of a cluster existing, so the clusters remain small. The supercooled liquid is thus in a metastable state. Homogeneous nucleation will occur when there is a finite probability that a nucleus of critical size exists.

HOMOGENEOUS NUCLEATION

At the equilibrium temperature, atoms will cross a plane solid–liquid interface at equal rates in both directions. The effect of the radius of curvature is such that a solid with a convex interface will be in equilibrium with the liquid at a lower temperature than would be the case for a plane interface. This will, of course, be unimportant for macroscopically curved interfaces. However, for every temperature below the equilibrium temperature there will be a cluster size having a radius of curvature such that atoms will join it and leave it at equal rates.

In nucleation theory such a cluster is termed a "critical nucleus". The critical size n^* of the nucleus can be calculated for any temperature. The condition for a critical nucleus is that

$$R_M^n = R_F^n$$

or

$$A_M G_M^n \nu_S N_S / A_F G_F^n \nu_L N_L = \exp(L^n/RT^*), \tag{12}$$

where T^* is the temperature at which n^* is the critical nucleus size. Substituting from equation (4), we may write

$$(G_M^n/G_M)(G_F/G_F^n)\exp(L/RT_E) = \exp(L^n/RT^*). \tag{13}$$

Using (7) and (8) and taking logarithms,

$$\frac{L}{RT_E} = \ln\frac{1-\alpha/n^{1/3}}{1+\alpha/n^{1/3}} + (1-\beta/n^{1/3})\frac{L}{RT^*}. \tag{14}$$

To a close approximation:

$$\ln\frac{1-\alpha/n^{1/3}}{1+\alpha/n^{1/3}} = -\frac{2\alpha}{n^{1/3}}. \tag{15}$$

Or equation (12) becomes

$$n^{*1/3}\frac{L\Delta T^*}{RT_E T^*} = \left(2\alpha+\beta\frac{L}{RT^*}\right) \tag{16}$$

where $\Delta T^* = T_E - T^*$.

It may be seen that equation (16) is the position of the minimum in equation (10) if we assume $n \gg 1$. The variation of n^* with ΔT^* is shown in Fig. 6 as predicted from equation (16). Combining equation (10) with equation (16), we obtain an equation for the number of critical nuclei as a function of temperature. Using $\beta = 1.33$ for face-centered cubic materials and setting $\alpha = 0$, we can obtain the number of critical nuclei as a function of temperature for various size liquid samples (Fig. 7). It is evident that the homogeneous nucleation temperature is influenced little by the number of atoms in the liquid sample, in agreement with observations made by Turnbull and Cech (1950). Changing the number of atoms in the liquid sample by 10 orders of

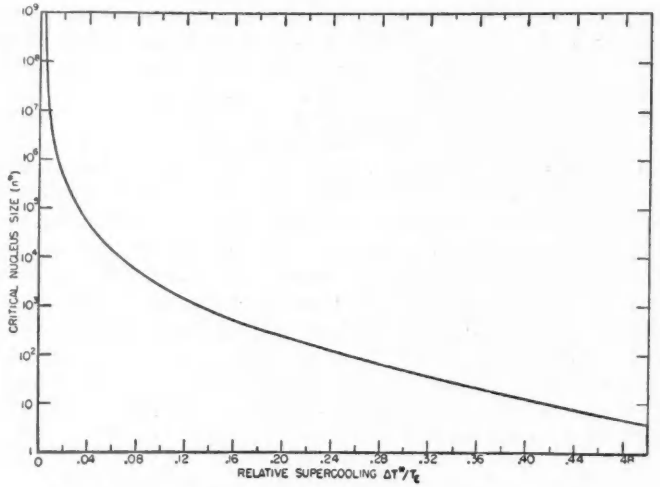

FIG. 6. Size of a critical nucleus as a function of supercooling.

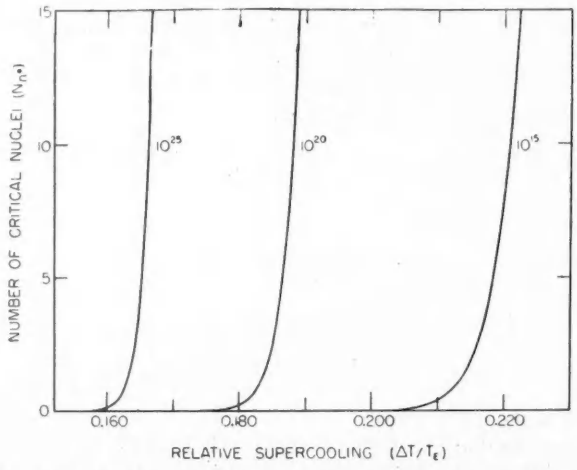

FIG. 7. Number of critical nuclei in liquid samples of various sizes as a function of supercooling. The number beside each curve is the total number of atoms in the liquid sample.

magnitude changes the homogeneous nucleation temperature 5%. For the particle experiments of Turnbull, the total number of atoms was of the order of 10^{15}, so that the homogeneous nucleation temperature is $\Delta T^*/T_E = 0.21$ and $n^* = 267$.

The experimental values for the homogeneous nucleation temperature give $\Delta T^*/T_E = 0.18$ for most metals (Turnbull and Cech 1950). If we had chosen

$\beta = 0$ and $\alpha = \frac{1}{2}$, we would have obtained in principle the same curves, the only difference arising because in equation (10) the β term is temperature dependent and the α term is not. It is known that counting bonds on a model overestimates the surface energy of a solid or liquid in contact with a vapor by a factor of two. The estimate is probably better for a liquid–solid interface; however the predicted homogeneous nucleation temperature is slightly high. The correct value of β is probably $0.65 < \beta < 1.33$, so that $\frac{1}{4} > \alpha > 0$.

COMPARISON WITH PREVIOUS THEORIES OF NUCLEATION

Previous theories of homogeneous nucleation have been developed by many workers (see for example the excellent review article by Hollomon and Turnbull 1953). These theories have been based on the free energy of the cluster of the solid atom given by:

$$\Delta F = 4\pi \frac{r^2\sigma}{0.8a^2} - \sqrt{2}\frac{4}{3}\pi \frac{r^3}{a^3}\frac{L\Delta T}{T_E}, \tag{17}$$

assuming that L is independent of temperature, $L\Delta T/T_E$ is the volume free energy per atom, σ is the surface free energy per atom, $0.8a^2$ is approximately the surface area of an atom in square centimeters for a close-packed metal, a is the interatomic spacing.

For a nucleus of critical size $d/dr\ (\Delta F) = 0$, or

$$\frac{L\Delta T^*}{T_E} = \frac{\sqrt{2}}{0.8}\frac{\sigma a}{r^*}. \tag{18}$$

Comparing with equation (16),

$$\frac{L\Delta T^*}{kT_E T^*} = \left(2\alpha + \frac{\beta L}{kT^*}\right)\frac{1}{n^{*1/3}}.$$

Assuming again $\beta = 1.33$, $\alpha = 0$, and using $1.81/n^{1/3} = a/r$ for a sphere of close-packed metal, we find:

$$\sigma/L = 0.52.$$

Turnbull (1950*b*) has observed that the surface free energy for most systems studied is approximately one half the latent heat of fusion.

EXTENSIONS OF THE PRESENT THEORY

The theory of melting and freezing presented here can be extended to alloys, as is discussed elsewhere (Chalmers 1954). Further development of this aspect of the theory will be published in a later paper.

The nucleation theory has been presented above to account for homogeneous nucleation in terms of interface kinetics. Heterogeneous nucleation can be considered by studying the case where the nuclei do not form a complete sphere, but form a spherical cap on a substrate. Such a cap will have a larger radius of curvature for the same number of atoms in a cluster, and a stable cluster will exist on a suitable substrate at a higher temperature than if the nuclei are spherical drops. The stability of such a spherical cap depends on the angle of contact at the solid–liquid–substrate line of contact.

DISCUSSION

It will be evident from the foregoing discussion that the concept of the equilibrium of two phases can be looked at from two points of view. We may follow the classical thermodynamic method and discuss the equality of the free energies of the two phases; if these are not equal, then there is a thermodynamic potential *tending* to cause a change. The change can not occur, however, unless another condition is satisfied; that is, unless both phases exist in contact with each other. The creation of the initial interface requires a different "equilibrium" condition, namely that for nucleation of the new phase.

The alternative view is to recognize that some transformations can take place only at an interface and to consider equilibrium in such cases entirely in terms of processes that take place at interfaces. The spontaneous occurrence of an interface, such as when a "solid-like" cluster forms in a liquid, then allows the same analysis to be used as at any other interface. The result is expressed as the net rate of increase of amount of one of the phases.

A further feature of the "interface kinetics" treatment is that the atomic arrangement at the interface can be introduced; this is not the case when free energies of phases are compared but it is evident from the experiments, for example, of Elbaum and Chalmers (1955) that different crystallographic faces behave differently when in contact with the liquid.

It follows that the same physical condition, that of equilibrium, can be described in two different ways; it remains to demonstrate their equivalence.

The thermodynamic criterion ignoring the PV term is:

$$U_S - T_E S_S = U_L - T_E S_L \tag{19}$$

and the kinetic expression is

$$N_S A_M G_M \nu_S \exp(-Q_M/RT_E) = N_L A_F G_F \nu_L \exp(-Q_F/RT_E). \tag{20}$$

From (19):

$$T_E = (U_L - U_S)/(S_L - S_S).$$

From (20):

$$T_E = \frac{(Q_M - Q_F)}{R \ln(A_M G_M N_S \nu_S / A_F G_F N_L \nu_L)}.$$

But $$(U_L - U_S) = (Q_M - Q_F) = L,$$

therefore $$S_L - S_S = R \ln(N_S A_M G_M \nu_S / N_L A_F G_F \nu_L);$$

but $$S = R \ln p,$$

$$\ln(P_L/P_S) = \ln(N_S A_M G_M \nu_S / N_L A_F G_F \nu_L),$$

or

$$P_L/P_S = N_S A_M G_M \nu_S / N_L A_F G_F \nu_L \tag{21}$$

where P_S and P_L are the probabilities of finding an arrangement equivalent to solid, or liquid, among all possible arrangements.

We therefore conclude that the probability P of the existence of a state is proportional to the probability of an atom of sufficient energy entering that

state; or that the entropy of a state is proportional to the logarithm of the probability of an atom entering it across an interface, if the atom has high enough energy.

APPENDIX

The condition for an equilibrium distribution of cluster sizes in the liquid is:

$$N_n R_F^n = N_{n+1} R_M^{n+1}, \tag{9}$$

$$\frac{N_{n+1}}{N_n} = \frac{A_F G_F^n \nu_L N_L}{A_M G_M^{n+1} \nu_S N_S} \exp\left(\frac{Q_M^{n+1} - Q_F^n}{RT}\right). \tag{22}$$

Substituting from equation (4),

$$\frac{N_{n+1}}{N_n} = \frac{G_F^n}{G_F^\infty} \cdot \frac{G_M^\infty}{G_M^{n+1}} \exp\left(\frac{Q_M^{n+1} - Q_F^n}{RT} - \frac{L}{RT_E}\right).$$

Now

$$\frac{N_n}{N_1} = \frac{N_n}{N_{n-1}} \cdot \frac{N_{n-1}}{N_{n-2}} \cdots \frac{N_2}{N_1} \tag{23}$$

or

$$\begin{aligned} \frac{N_n}{N_1} &= \prod_{n=2}^{n} \frac{G_F^{n-1}}{G_F} \cdot \frac{G_M}{G_M^n} \exp\left(\frac{Q_M^n - Q_F^{n-1}}{RT} - \frac{L}{RT_E}\right) \\ &= B \prod_{n=2}^{n-1} \frac{G_F^n}{G_F} \cdot \frac{G_M}{G_M^n} \exp\left(\frac{Q_M^n - Q_F^n}{RT} - \frac{L}{RT_E}\right) \end{aligned} \tag{24}$$

where $$B = \frac{G_F^1}{G_F} \cdot \frac{G_M}{G_M^n} \exp\left(\frac{Q_M^n - Q_F^1}{RT} - \frac{L}{RT_E}\right).$$

Using equations (7) and (8),

$$\frac{N_n}{N_1} = B \prod_{n=2}^{n-1} \frac{1-\alpha/n^{1/3}}{1+\alpha/n^{1/3}} \exp\left(\frac{L}{RT} - \frac{L}{RT_E} - \frac{\beta}{n^{1/3}} \frac{L}{RT}\right). \tag{25}$$

Using $\ln[(1-x)/(1+x)] = -2x$ for small x, defining $T_E - T = \Delta T$, and taking logarithms, we get

$$\begin{aligned} \ln \frac{N_n}{N_1} &= \ln B + \sum_{n=2}^{n-1} \left(\frac{L\Delta T}{RT_E T} - \frac{\beta}{n^{1/3}} \frac{L}{RT} - \frac{2\alpha}{n^{1/3}}\right) \\ &= \ln B + (n-2) \frac{L\Delta T}{RT_E T} - \left(\frac{\beta L}{RT} + 2\alpha\right) \int_2^{n-1} \frac{1}{n^{1/3}} dn \\ &= \ln B + (n-2) \frac{L\Delta T}{RT_E T} - \frac{3}{2}\left(\frac{\beta L}{RT} + 2\alpha\right)[(n-1)^{2/3} - 2^{2/3}]. \end{aligned} \tag{26}$$

The total number of atoms

$$N = \sum_{n=1}^{\infty} n N_n, \tag{27}$$

$$\ln \frac{N_n}{N} = -\ln \frac{N}{N_1} + \ln B + (n-2) \frac{L\Delta T}{RT_E T} - \frac{3}{2}\left(\frac{\beta L}{RT} + 2\alpha\right)[(n-1)^{2/3} - 2^{2/3}],$$

which is equation (10).

REFERENCES

CHALMERS, B. 1949. Proc. Roy. Soc. **196**: 64.
——— 1954. Trans. Am. Inst. Mining Met. Engrs. J. Metals, **200**: 519.
CHALMERS, B. and MARTIUS, U. M. 1952. Phil. Mag. (7), **43**: 686.
ELBAUM, C. and CHALMERS, B. 1955. Can. J. Phys. **33**: 196.
FRANK, F. C. 1952. Phil. Mag. Suppl. 1. 91.
HOLLOMON, J. H. and TURNBULL, D. 1953. Progr. Metal Phys. IV: 333.
MOTT, N. F. and JONES, H. 1936. Theory of the properties of metals and alloys. Oxford at the Clarendon Press.
TAMMAN, G. 1922. Aggregatzustände. Leopold Voss, Leipzig.
TURNBULL, D. 1950*a*. Thermodynamics in physical metallurgy. Am. Soc. Metals. 282.
TURNBULL, D. 1950*b*. J. Chem. Phys. **18**: 769.
TURNBULL, D. and CECH, R. E. 1950. J. Appl. Phys. **21**: 804.

THE ELECTRICAL CONDUCTIVITY OF CHLOROBENZENE[1]

By John Hart and A. G. Mungall

ABSTRACT

Measurements of the conductivity of chlorobenzene in evacuated cells of identical geometry but with different electrode metals have shown that the conductivity measured is dependent on the electrode metal employed. The degree of dependence is more marked and the conductivities are one or two orders of magnitude larger in the presence of air. Preliminary measurements of small discharge currents in a cell with monel metal electrodes are also described.

INTRODUCTION

Experiments dealing with the direct-current electrical conductivity of polar organic liquids such as chlorobenzene and chloroform have in the past given rise to a series of disconnected results (Eck 1949). A typical observation has been that a direct potential difference placed across a set of electrodes immersed in the liquid has caused a current to flow which is dependent on time, usually decreasing. However, the magnitude of the conductivity and the shapes of the current–time curves have differed widely in different experiments. Experiments performed at the National Research Council a year ago (Hart and Simmons 1955) indicated the possibility that the conductivity measured was connected in some way not only with the liquid itself, and the impurities in it, but also with the electrodes.

EXPERIMENTAL RESULTS

Preliminary measurements made with monel electrodes, immersed in chlorobenzene, indicated the likelihood that electrode effects were much more important than had previously been thought. A conductivity cell was inserted in the condensing arm of an evacuated continuous distillation system made entirely of glass. Distilled liquid passed continuously through the cell and the overflow from the cell was returned to the distilling flask. Since air pressure in the system was of the order of 10^{-6} mm. of mercury, the effects of gaseous impurities in the liquid were probably small. The electrodes were circular, of 1 cm.^{2} effective area, and the distance between them was 0.3 cm. A guard ring was employed to reduce edge effects. D-c. current–time curves (Fig. 1) obtained from this cell during continuous distillation indicated that the limiting conductivity, after a potential of 100 volts had been applied during distillation for about 28 hr., was about 1.2×10^{-11} reciprocal ohm centimeters. Typical values quoted (Scheflan and Jacobs 1953; Weissberger and Proskauer 1935; Weissberger *et al.* 1955) are in the range 10^{-9} to 1.3×10^{-10} reciprocal ohm centimeters, between one and two orders of magnitude larger. In Fig. 1 the sudden initial rise in conductivity probably indicates that impurities from the condenser walls are being carried into the cell; the subsequent rapid fall indicates that these impurities and also those originally in the cell are

[1]Manuscript received November 25, 1955.
Contribution from the Division of Applied Physics, National Research Council, Ottawa, Canada. Issued as N.R.C. No. 3941.

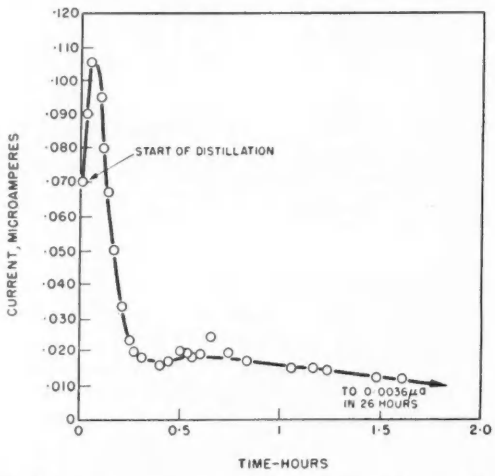

FIG. 1. Cell current as a function of time during continuous distillation.

later carried away. Short-term (four-minute) current–time measurements, with a sample of the liquid stationary in the cell, indicate a recovery during current flow apparently not previously mentioned in the literature (Fig. 2). This recovery may be due to electrode effects.

The existence of a very small discharge current after the electrode potential had been removed was also found. The direction of this current was initially

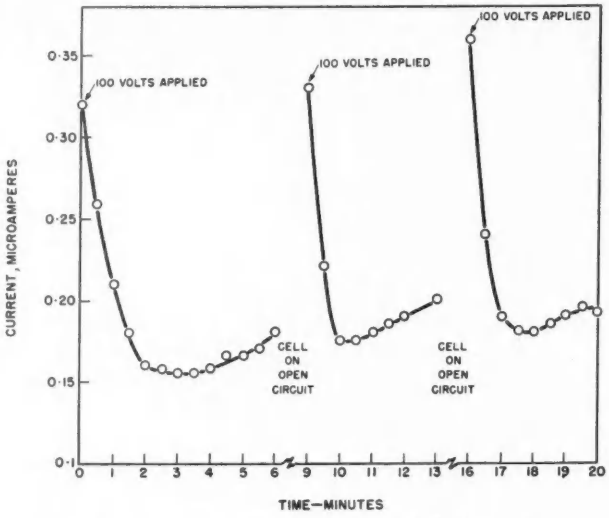

FIG. 2. Cell current as a function of time with liquid stationary.

dependent on the polarity immediately before discharge and subsequently changed in a manner dependent on the polarity of previous potentials, and the length of time they had been imposed. Figure 3 shows a typical discharge

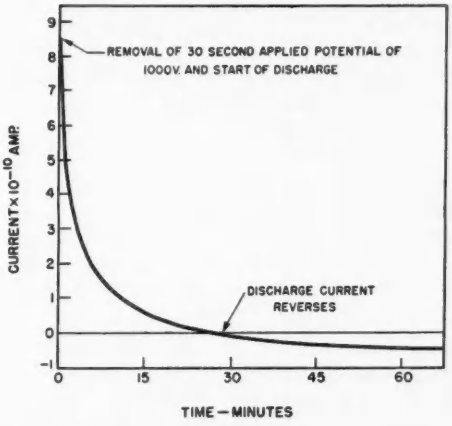

FIG. 3. Dependence of discharge current on time.

current–time curve of the cell indicating this effect. In the first half of the curve the discharge current flows in such a direction as to discharge the effect of the most recently applied potential; in the second half it flows in such a direction as to discharge the effects of potentials which had been applied in reverse polarity intermittently during previous weeks. Figure 4 indicates the effect of starting a flow of pure liquid through the cell during discharge; the current suddenly rose and then dropped to a new limiting value shortly afterwards.

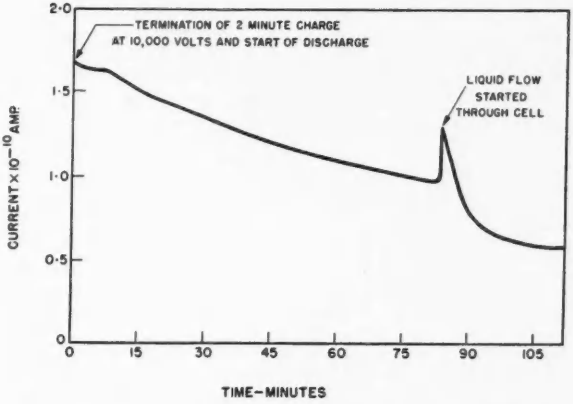

FIG. 4. The effect on the discharge current of passing liquid through the cell.

These experiments suggest that there is perhaps the formation of a charged dipole layer in the immediate vicinity of the electrode surfaces, and that part of this layer can be removed by washing. Further, reversal of the electrode

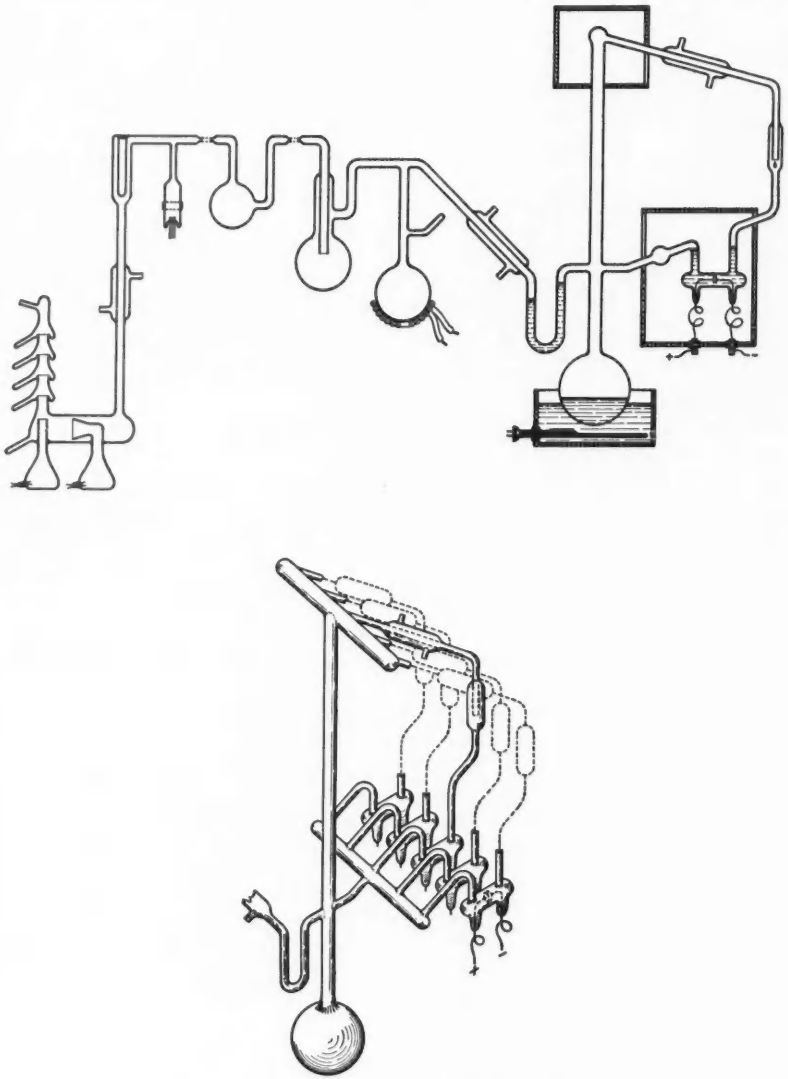

FIG. 5. The five-cell continuous distillation system.

potentials does not appear to reverse the entire layer of dipoles, but either reverses some or deposits others in the reverse direction. There is also chemical change at the electrodes involving reactions between the electrode metal and the products of electrolytic dissociation of the liquid.

It was apparent from these experiments that the electrodes themselves play an active part in determining the current flow for a given applied potential. Consequently, a further experiment was devised in which the conductivity of chlorobenzene in a closed distillation system was measured in five cells of identical geometry, but with different electrode metals. Each cell consisted of two rectangular electrodes of 0.5 cm.^{2} area, 0.15 cm. apart. No guard rings were used in this experiment since edge effects in the previous one were small. Figure 5 shows a drawing of this equipment, the five cells being fed separately by five condensers, with the liquid divided evenly between them in the vapor phase. The cells are enclosed in a thermostated plexiglass box, and all cell leads pass out through the bottom of the box to a plexiglass switchboard. Each cell can then be connected in either polarity to the voltage supply and a recording micromicroammeter.

The liquid was allowed to distill through the cells for several days, a total of about 5 liters passing through each cell. The total volume of liquid in the system was about 400 cc. and the volume of each cell was about 20 cc. Some preliminary current–time curves were then taken with no liquid flow through the cells. These showed considerable differences between cells; much more than could be explained by the small differences in cell geometry. Figure 6 shows a typical set of curves. However, the conductivities indicated from these curves were somewhat higher than those measured previously and the presence of impurities in the liquid was suspected. Consequently, a three and a half week continuous distillation period was undertaken. Current–time curves (Fig. 7) taken at the end of this period indicated a significant decrease in conductivity although the shapes of the curves were very similar. The conductivity remained practically constant over a two-week period, at the end of which time air was admitted to the system. The effect on the conductivity was striking. Figure 8 shows current–time curves for the five cells with air present. The average conductivities for the five cells taken over one-minute intervals increased as shown in Table I. A-c. measurements at 4 c.p.s. (square wave) were also taken and are shown in the same table.

TABLE I

Electrode metal	D-c. conductivity, $\times 10^{-11}$ recip. ohm cm.		A-c. conductivity, $\times 10^{-10}$ recip. ohm cm.	
	In vacuum	In air	In vacuum	In air
Tantalum	3.0	240	1.2	24
Monel	3.2	27	1.1	3.9
Nickel	1.8	56	1.0	8.4
Platinum–rhodium	1.9	570	1.1	33
Platinum	2.2	300	1.2	35

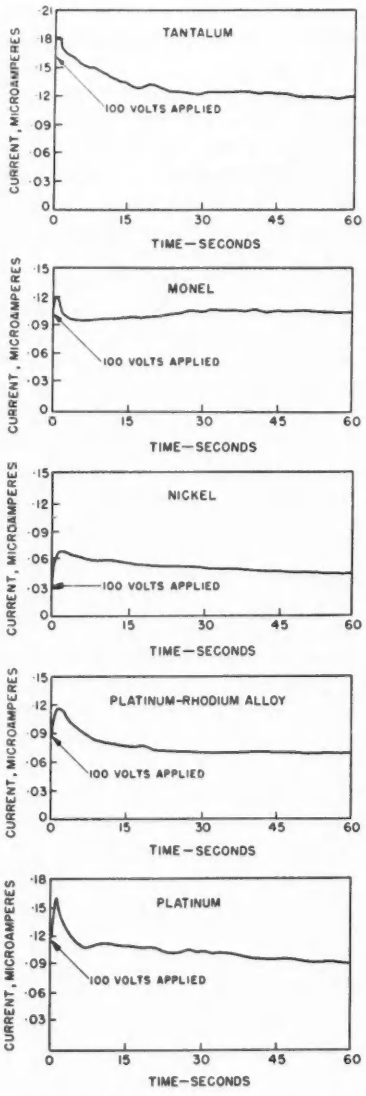

FIG. 6. Cell current as a function of time for five different electrode metals; liquid relatively impure, no air present.

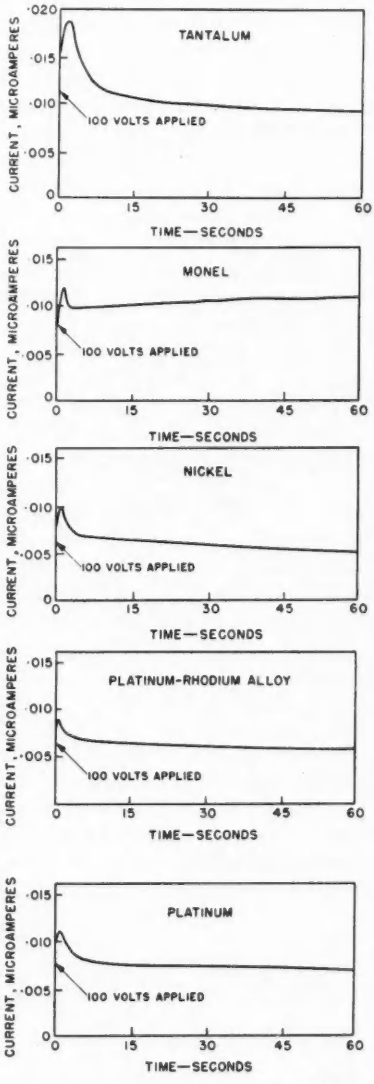

FIG. 7. Cell current as a function of time for five different electrode metals; liquid relatively pure, no air present.

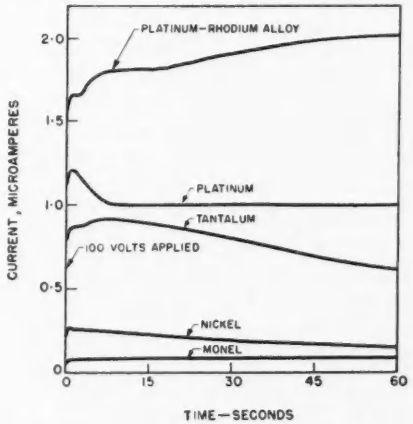

FIG. 8. Cell current as a function of time for five different electrode metals; air present.

The shapes of the current–time curves were not significantly altered by the large change in conductivity except, perhaps, for the platinum–rhodium electrode. This suggests that the form of the curve is chiefly dependent on the electrode metal whereas the amplitude is dependent on the liquid itself with its included impurities. The a-c. measurements show somewhat smaller increases, and in general, the a-c. conductivity in pure or impure liquid did not appear to be time dependent. It is, however, important to note that even the a-c. measurements show large electrode effects in the presence of air.

CONCLUSIONS

Most previous experiments on the electrical conductivity of polar liquid dielectrics have been carried out with air present (Eck 1949; Hart and Simmons 1955; Rider 1955) and with little or no attention paid to possible existence of electrode effects, it being assumed that the liquid alone determined the current flow in a conductivity cell. The above experiments point emphatically to the necessity of making all conductivity measurements in cells free of air and further indicate that the measurements may be strongly affected by the electrode metal employed. Further experiments in connection with this problem are continuing.

REFERENCES

ECK, J. L. 1949. Ann. phys. **4**: 13.
HART, J. and SIMMONS, D. A. 1955. Can. J. Phys. **33**: 54.
RIDER, J. A. 1955. J. Chem. Phys. **23** (No. 1): 61.
SCHEFLAN, L. and JACOBS, M. 1953. The handbook of solvents. D. Van Nostrand Company, Inc., New York.
WEISSBERGER, A. and PROSKAUER, E. 1935. Organic solvents. Oxford at the Clarendon Press.
WEISSBERGER, A., PROSKAUER, E., REDDICK, J. A., and TOOPS, E. E. 1955. Organic solvents. Interscience Publishers, Inc., New York.

FINITE DISPLACEMENTS IN RHEOLOGICAL BODIES[1]

By A. E. Scheidegger

ABSTRACT

The study of the behavior of continuous matter is basic in many disciplines, such as in various branches of engineering and in the study of the Earth's interior. Herein, it is evidently necessary to have a sufficiently general mathematical formalism to encompass the behavior of *any* type of material under *any* mechanical conditions. Customary "rheological" theories suffer from various drawbacks; they are either (i) restricted to too specialized "ideal" materials, or (ii) restricted to too special displacements, or (iii) restricted to too specialized mathematical representations. The present paper attempts to fill the need for a summary of the representations of the dynamics of arbitrary materials. The displacement within the continuous medium is described by three "co-ordinate" functions as functions of three "parameters" and of time. Extensive use is made of the fact that, insofar as the expression of any physical statement is concerned, "co-ordinates" and "parameters" are entirely equivalent. Formulas are deduced which enable one to express the boundary conditions, the equations of motion, and any chosen rheological condition in either parameter space or co-ordinate space. The notion of finite strain is scrutinized.

1. INTRODUCTION

The study of the behavior of continuous matter is important in various disciplines. Engineers have been trying to describe the behavior of various materials using the model of continuous media, and so have geophysicists in connection with the investigation of the Earth's interior. If one surveys the existing theories of the dynamics of continuous matter, it appears that most of them refer to rather specialized "ideal" materials. These "ideal" materials constitute in many cases good approximations to "real" materials, but in others they do not. The "ideal" materials have been devised to describe, with reasonable accuracy, substances that are commonly encountered in everyday life, such as elastic bodies and viscous fluids. It is thus not surprising that, outside the domain of everyday experiences (such as in the Earth's interior), substances may be in existence for which the traditional theories are inadequate. It is, therefore, desirable to devise mathematical schemes which are sufficiently general to encompass the dynamics of *any* (continuous) material.

The science whose object is the macroscopic study of the dynamics of "any" type of material has been called "rheology". This science started at first by generalizing and modifying elasticity theory and classical hydrodynamics, which refer to the ideally elastic and to the ideally viscous medium, respectively. To these two materials, rheology added others in order to describe the behavior of various substances of increasing technological importance, such as paints, sols, gels. Rheology, thus, comprises theories of a variety of "ideal" materials, which are attempted approximations to certain "real" ones. A discussion of theories of materials according to the views generally accepted among rheologists has been given by Reiner (1949).

The mathematical structure of each "rheological theory", describing the

[1]Manuscript received November 25, 1955.
Published by permission of the Acting Deputy Minister, Department of Mines and Technical Surveys, Ottawa. Contributions from the Dominion Observatory, Ottawa, Vol. 1, No. 22.

dynamics of a specified "ideal" body, is such that there is (*a*) a set of equations describing displacements (called kinematical equations), (*b*) a set of equations expressing Newton's law of motion (called the equations of motion), and (*c*) an equation describing the connection between the local forces and the displacements characteristic for each ideal body (called rheological condition, e.g. Hooke's law for ideally elastic bodies; the "rheological condition" is often called "constitutive equations" by mathematicians). The *fundamental problem* in rheology is to find the displacements of a body of given external dimensions and subject to a given rheological condition as a function of time, under a set of given external forces which themselves may be functions of time, or vice versa.

It has been mentioned above that rheology started first as a generalization and modification of elasticity theory. Elasticity theory is essentially a theory of infinitesimal displacements, and therefore most rheological theories also, unconsciously, make the assumption of infinitesimal displacements. This came about by the acceptance of the notion of "strain" into rheology which, normally, presupposes infinitesimal displacements. This assumption of infinitesimal displacements, however, is not justified in general rheology since most displacements that are of interest are not small.

Generalizations of the concept of "strain" to finite displacements have been discussed by many authors starting from Cauchy (see Truesdell 1952); these seem, however, to bear only upon special aspects of the problem and do not contain complete discussions of the possible schemes for the description of finite displacements in arbitrary rheological bodies.

Various rheological bodies appear to have been catalogued first by Weissenberg (1931) and later by many others. However, these catalogues have since been shown to encompass only a tiny fraction of all possible rheological bodies, apart from their being, in many instances, incorrect. A more satisfactory discussion of possible rheological bodies has been given by Oldroyd (1950), using rather a special mathematical representation.

What is required, therefore, is a comparison and exposition of the various investigations mentioned above to yield a discussion of the general mathematical schemes suitable to describe finite displacements in arbitrary rheological bodies, embodying directions to express all the necessary physical conditions (equations of motion, etc., as outlined above) in a proper form. Although most of the formulas given in this paper have been published previously somewhere or other, it is believed that the compilation of the formulas relating "parameters" and "co-ordinates" to be presented here is given for the first time.

2. THE STRUCTURE OF A FINITE STRAIN THEORY

As mentioned in the Introduction, there are various steps that must be observed in order to obtain a description of the dynamics of continuous media.

In the first place, one must decide upon a description of the deformation. Once this has been achieved, one must express various physical laws: the condition of continuity, the law of motion, and boundary conditions.

We shall discuss these steps one by one.

(*a*) *Measure of Displacement*

Let us assume that a certain volume W (which may be infinite) of space is filled with matter. The volume W, and the way in which it is filled, changes with time t.

The points of space may be specified by giving three Cartesian co-ordinates x_i such that the line element is defined as follows:

$$ds^2 = dx_i\, dx_i. \tag{2.1}$$

In this formula, the summation convention has been used, which stipulates that one has to sum over all indices that occur twice.

The above scheme characterizes the geometrical space ("co-ordinate space") occupied or potentially occupied by the continuous medium. The next task is to characterize the medium. It is well known that this can be done (Truesdell 1952) by introducing three parameters ξ_α. The whole medium is characterized if the parameters run through all points of a volume Ψ in "parameter space" (i.e. the space of the ξ's).

We shall assume that the space Ψ of the parameters is endowed with a Cartesian metric, such that a line element $d\sigma$ can be defined:

$$d\sigma^2 = d\xi_\alpha d\xi_\alpha. \tag{2.2}$$

It is always possible to make such a parameter transformation that the parameters are equal to the co-ordinates of all the particles at a particular time, say t_0. It is often convenient to do this.

With the above characterization of a continuous medium and the geometrical space occupied by it, one can proceed to describe motions. The complete motion is obviously given if the geometrical co-ordinates of each particle of the medium are known for all times:

$$x_i = x_i(\xi_\alpha, t). \tag{2.3}$$

Thus, the specification of three functions of the three parameters plus time determines the motion. This type of description is often called the material form of the description of motion.

It is well known that one also could have provided a description of the motion in another way, viz. by solving Eqs. (2.3) for the ξ's:

$$\xi_\alpha = \xi_\alpha(x_i, t). \tag{2.4}$$

Physically, this means that one states which "particle" is at a given time at any given spot. This is called the spatial form of the description of motion.

Although the specification of the functions in Eqs. (2.3) completely describes the motion, it is often convenient to introduce various other quantities. This is so because it is cumbersome to express the equations of motion directly in terms of the quantities introduced heretofore.

An important kinematical notion is the concept of strain. Strain, in the finite theory, is defined by the difference of the squared distance between neighboring points in two states, one of which is arbitrarily called "state of zero strain". The element of distance between neighboring particles is:

$$ds^2 = \frac{\partial x_i}{\partial \xi_\alpha}\frac{\partial x_i}{\partial \xi_\beta} d\xi_\alpha d\xi_\beta = \kappa_{\alpha\beta} d\xi_\alpha d\xi_\beta \tag{2.5}$$

where

$$\kappa_{\alpha\beta} = \frac{\partial x_i}{\partial \xi_\alpha} \frac{\partial x_i}{\partial \xi_\beta}. \tag{2.6}$$

Thus, the element of distance between two particles defines a symmetric tensor $\kappa_{\alpha\beta}$ in parameter space. If we denote the (time-independent) tensor of the state of zero strain by $\zeta_{\alpha\beta}$, we can define the "material strains" as follows:

$$\epsilon_{\alpha\beta} = \tfrac{1}{2}(\kappa_{\alpha\beta} - \zeta_{\alpha\beta}) = \frac{1}{2}\left(\frac{\partial x_i}{\partial \xi_\alpha} \frac{\partial x_i}{\partial \xi_\beta} - \zeta_{\alpha\beta}\right). \tag{2.7}$$

Equation (2.5) permits a different interpretation of strain from that given above. For, this equation (2.5) can be taken as a fundamental metric form in a certain space $\Sigma(t)$ which has been called the material strain space. In this instance, one should note that the $d\xi$'s are contravariant vectors and could be expressed by using superscripts instead of subscripts (employing the notation of Riemannian geometry):

$$ds^2 = \kappa_{\alpha\beta}\, d\xi^\alpha d\xi^\beta. \tag{2.8}$$

The elements (points) of this strain space are the parameters; the line element is ds, which is the line element of the co-ordinates. The metric in strain space is a function of time. In the strain space $\Sigma(t)$, the tensor $\kappa_{\alpha\beta}$ can be used to raise and lower indices, if the contravariant metric tensor is defined as follows:

$$\kappa_{\alpha\beta}\kappa^{\beta\gamma} = \delta_\alpha{}^\gamma \tag{2.9}$$

where $\delta_\alpha{}^\gamma$ signifies the Kronecker symbol.

Because of equation (2.5), the metric in strain space must be flat. This means that the contracted Riemann–Christoffel curvature tensor in Σ must be zero. This imposes six conditions upon the κ's, and hence upon the strains. These conditions are very well known in the theory of elasticity, where they are called "compatibility conditions".

Henceforth, we shall consider $\kappa_{\alpha\beta}$ (and therewith $\epsilon_{\alpha\beta}$) as a tensor in parameter space, and not as a metric. The problem, therefore, will be to determine the components of a tensor "field" $\epsilon_{\alpha\beta}$ as a function of time.

As a final kinematical notion, one can introduce the concept of density. Postulating the medium as homogeneously of density ρ_0 in the unstrained state, we define, in accordance with the principle of continuity:

$$\begin{aligned} \rho(\xi_\alpha, t) &= \rho_0 \sqrt{\det \zeta} / \sqrt{\det \kappa} \\ &= \rho_0 \sqrt{\det \zeta_{\alpha\beta}} / \sqrt{\det (2\epsilon_{\alpha\beta} + \zeta_{\alpha\beta})}\,. \end{aligned} \tag{2.10}$$

The above definition of strain was termed "material" because it gives the line element ds at time t in terms of the parameters. It is customary in hydrodynamics to term all description of motion in terms of the parameters (which are identifiable with the co-ordinates at t_0) as "material" and this terminology is being retained in the present exposition.

Since parameter and co-ordinate spaces are entirely homologous, it is obviously possible to reverse the rôles played by the two (Deuker 1941; also Eckart 1948). Thus the line element $d\sigma$ of parameter space (i.e. the line element at time $t = t_0$) can be expressed in terms of the co-ordinates at time t:

$$d\sigma^2 = \frac{\partial \xi_\alpha}{\partial x_i}\frac{\partial \xi_\alpha}{\partial x_j} dx_i\, dx_j = k_{ij} dx_i dx_j \tag{2.11}$$

where

$$k_{ij} = \frac{\partial \xi_\alpha}{\partial x_i}\frac{\partial \xi_\alpha}{\partial x_j}. \tag{2.12}$$

This means that the distance $d\sigma$, which was taken up at t_0 by two points of the medium differing at time t by dx_i, is specified by a symmetric tensor k_{ij} in co-ordinate space.

It is fairly easy to calculate the connection between spatial and material (as defined above) distances. One obtains:

$$k_{ij} = \kappa_{\alpha\beta}\frac{\partial \xi_\alpha}{\partial x_m}\frac{\partial \xi_m}{\partial x_i}\frac{\partial \xi_\beta}{\partial x_r}\frac{\partial \xi_r}{\partial x_j}. \tag{2.13}$$

In particular, the state of zero strain is characterized by the following tensor:

$$z_{ij} = \zeta_{\alpha\beta}\frac{\partial \xi_\alpha}{\partial x_m}\frac{\partial \xi_m}{\partial x_i}\frac{\partial \xi_\beta}{\partial x_r}\frac{\partial \xi_r}{\partial x_j}. \tag{2.14}$$

Thus, one can define the "spatial strain" as follows:

$$\begin{aligned} e_{ij} &= \tfrac{1}{2}(k_{ij} - z_{ij}) \\ &\equiv \tfrac{1}{2}\left(\frac{\partial \xi_\alpha}{\partial x_i}\frac{\partial \xi_\alpha}{\partial x_j} - z_{ij}\right). \end{aligned} \tag{2.15}$$

In the above formulas, it should be noted that the tensor z_{ij} characterizing the state of zero strain is no longer time independent.

The spatial density becomes:

$$\begin{aligned} \rho(x_i, t) &= (\sqrt{\det z}/\sqrt{\det k})\rho_0 \\ &= \rho_0\sqrt{\det z_{ij}}/\sqrt{\det(2e_{ij}+z_{ij})}, \end{aligned} \tag{2.16}$$

which is the same as the material density. The latter statement is easy to check as the expression for z as well as k can be written as the product of the matrix ζ or κ, respectively, with the same matrices. Upon the formulation of the determinants, the determinants of these matrices can be factorized out and cancel as they are the same in numerator and denominator.

It will be noted that the tensor k_{ij} also, if taken as a metric tensor, describes a flat metric. Hence it must satisfy the condition that the Riemann–Christoffel curvature tensor, formed with k_{ij}, must be the zero tensor. This leads to six compatibility relations for k_{ij}, and hence for e_{ij}, as was the case with the material strains.

Finally, one may make a few remarks regarding "convected co-ordinates". We have seen above that the tensors $\kappa_{\alpha\beta}$ and k_{ij}, being symmetric tensors, can be thought of as metric tensors in certain spaces. This is the approach to finite displacement rheology which has been taken by Oldroyd (1950), at least with regard to the tensor $\kappa_{\alpha\beta}$ (Oldroyd did not consider the equivalent possibility of using the tensor k_{ij}). The tensor $\kappa_{\alpha\beta}$, in fact, can be regarded as describing the metric in a "convected" co-ordinate system, viz. in a system

whose co-ordinate lines are given at $t = t_0$ as Cartesian co-ordinate lines, and are moving along with the medium. If the motion is expressed in terms of such "convected co-ordinates", one has to introduce the whole formalism of Riemannian geometry, which is actually quite unnecessary in view of the fact that, after all, the medium is moving in an ordinary Euclidean space. "Convected co-ordinates", therefore, appear as a rather clumsy means of describing the dynamics of continuous matter.

(*b*) *Continuity Condition and Equations of Motion*

In order to derive the equations of motion, it is necessary to define time derivatives of the various quantities introduced above.

Owing to the occurrence of parameters and of co-ordinates, time differentiation of any function can be performed either with the parameters held constant, or with the co-ordinates held constant. Although the complete reciprocity between parameter space and co-ordinate space—and of the corresponding time derivatives—has already been demonstrated by Deuker (1941) (see also Green and Zerna 1950), this fact is not commonly borne to light in the customary presentation of rheological theories.

We shall denote[2] the time derivative of a scalar function of the parameters or co-ordinates, for constant parameters, by $\Delta/\Delta t$:

$$\Delta/\Delta t\, f(\xi, t) = \left.\frac{\partial f}{\partial t}\right|_{\text{constant } \xi} \tag{2.17}$$

and the time derivative with the co-ordinates held constant by D/Dt:

$$D/Dt\, f(x, t) = \left.\frac{\partial f}{\partial t}\right|_{\text{constant } x}. \tag{2.18}$$

With the definition of time derivatives, one is now in a position to formulate the continuity condition and the equations of motion. The continuity equation is, as is well known:

$$\frac{D\rho}{Dt} + \frac{\partial}{\partial x_i}\left(\rho \frac{\Delta x_i}{\Delta t}\right) = 0. \tag{2.19}$$

In this presentation of the continuity equation, care has been taken to indicate the various types of time derivatives, according to our notation. It becomes then apparent that the usual form of the continuity equation is somewhat cumbersome since it contains functions which have x as well as ξ as arguments.

A similar situation occurs in the equations of motion which are usually written as follows:

$$\frac{\partial \tau_{ik}}{\partial x_k} + \rho\left(f_i - \frac{\Delta^2 x_i}{\Delta t^2}\right) = 0 \tag{2.20}$$

where τ_{ik} is the stress tensor (a function of x) and f the specific volume force.

[2]It should be noted that the present notation is at variance with that in most textbooks on elasticity where D/Dt denotes the derivative with ξ held constant. This derivative has been denoted in the present paper by using *Greek* $\Delta/\Delta t$ to indicate that the parameters (*Greek* symbols) are held constant. Similarly, the *Latin* D/Dt has been chosen to indicate that the co-ordinates (*Latin* symbols) are to be held constant.

Again, $\ddot{x}_i$ $(= \Delta^2 x_i/\Delta t^2)$ should be expressed as a function of x which means that one should use $\ddot{\xi}$ rather than $\ddot{x}$.

(*c*) *Rheological Condition*

The relations noted heretofore are not sufficient to determine the behavior of continuous matter. What is needed is a connection between the kinematical quantities of Section 2(*a*) and the dynamical quantities of Section 2(*b*). Such relations are commonly termed "rheological conditions".

The rheological condition, being an equation of state, must be independent of the motion of the medium as a whole. It, therefore, appears as natural to use as kinematical variables the strains $\epsilon_{\alpha\beta}$, or the components of the tensor $\kappa_{\alpha\beta}$ describing the state of the medium in parameter space.

Many types of rheological equations have been postulated (see Reiner 1949), but it is to the credit of Oldroyd (1950) to have made a satisfactory enumeration of the possible variables and the form in which they may enter the rheological condition. Oldroyd states that, in its general form, the rheological condition *can be written as a set of integrodifferential equations in parameter space, of which six are independent, relating the stresses* τ_{ik}, *the finite strains* $\epsilon_{\alpha\beta}(\xi, t)$ (or else the components of the tensor $\kappa_{\alpha\beta}$), *the temperature* $\theta(\xi, t)$, *and such physical constants as may pertain to the medium.*

The quantities τ_{ik}, $\epsilon_{\alpha\beta}$, and θ are functions of time. The fact that it is permissible for the rheological condition to contain integrations of time (with fixed ξ) allows for the possibility of occurrence of effects which depend on the total previous strain-history at a certain point of the medium. In simple cases, the integrodifferential equations can be reduced to differential equations by the processes of rearrangement and differentiation.

3. THE POSSIBLE SCHEMES OF DYNAMICS

In order to solve a concrete dynamical problem, it is necessary to express all the equations in one type of independent variable. The necessary equations, as outlined above, are (i) the continuity equation, (ii) the equations of motion, (iii) the rheological condition, and (iv) boundary and initial conditions. The functions sought after will be either $x_i(\xi_\alpha, t)$ or $\xi_\alpha(x_i, t)$.

It is observed that the equations of motion and the boundary conditions (in most cases) can be more easily expressed in co-ordinate space than in parameter space. For the rheological condition, and in some cases for the boundary conditions (if there are free surfaces), the reverse is true. Before proceeding to a solution of a certain problem, one will therefore have to decide at this point whether it will be preferable to work in parameter space or in co-ordinate space. Oldroyd (1950) considered only the possibility of expressing everything in terms of the co-ordinates, which makes matters extremely clumsy; and it should, therefore, be remarked that parameter and co-ordinate space are, as always, entirely equivalent. It is only a matter of convenience of calculation whether one wants to use parameter or co-ordinate space. It appears rather as a trivial statement to say that one has two possibilities; either to express everything in terms of co-ordinates, or to express everything in terms of parameters. It is, therefore, interesting to observe that there

seems to be no place in the literature where the corresponding transformation formulas are conveniently put together, although most of them have been discussed previously somewhere or other. It is, therefore, believed that the present compilation is given here for the first time.

(*a*) *Transformation Formulas for Time Derivatives*

The all-important formulas establishing the connection between the various representations are based upon the definition of the time derivatives, (2.17) and (2.18).

One immediately observes that this yields the following connection between $\Delta/\Delta t$ and D/Dt:

$$\frac{D}{Dt}f = \frac{\Delta}{\Delta t}f + \frac{\partial f}{\partial \xi_\alpha}\frac{D\xi_\alpha}{Dt} \equiv \frac{\Delta}{\Delta t}f + \frac{\partial f}{\partial \xi_\alpha}\dot{\xi}_\alpha, \tag{3.1}$$

$$\frac{\Delta}{\Delta t}f = \frac{D}{Dt}f + \frac{\partial f}{\partial x_i}\frac{\Delta x_i}{\Delta t} = \frac{D}{Dt}f + \frac{\partial f}{\partial x_i}\dot{x}_i, \tag{3.2}$$

where the dot stands for partial time derivatives of the co-ordinates or parameters (there is no ambiguity since the parameters are always thought to be functions of the co-ordinates and time, and the co-ordinates functions of the parameters and time). The above relations also imply:

$$\frac{\partial f}{\partial \xi_\alpha}\dot{\xi}_\alpha = -\frac{\partial f}{\partial x_i}\dot{x}_i. \tag{3.3}$$

The above rules apply to time derivatives of scalars. There appears to be an additional difficulty if tensors in either parameter space or co-ordinate space are involved. As arguments of such tensors one can choose either the parameters, or the co-ordinates; and that irrespective of whether the tensor itself is a tensor in parameter space or a tensor in co-ordinate space. A change of variables from parameters to co-ordinates does not imply a transformation of a tensor from parameter space to co-ordinate space. Thus, one has, for example, for a tensor A_α in parameter space:

$$A_\alpha(\xi, t) = A_\alpha(x = x(\xi, t), t), \tag{3.4}$$

$$A_\alpha(x, t) = A_\alpha(\xi = \xi(x, t), t). \tag{3.5}$$

The time derivative $\Delta/\Delta t$ assumes fixed parameters; thus:

$$\frac{\Delta}{\Delta t}A_\alpha(\xi, t) \equiv \frac{\partial}{\partial t}A_\alpha(\xi, t) = \frac{DA_\alpha(x, t)}{Dt} + \frac{\partial A_\alpha(x, t)}{\partial x_k}\dot{x}_k\,. \tag{3.6}$$

Correspondingly:

$$\frac{D}{Dt}A_\alpha(x, t) = \frac{\partial}{\partial t}A_\alpha(x, t) = \frac{\Delta A_\alpha(\xi, t)}{\Delta t} + \frac{\partial A_\alpha(\xi, t)}{\partial \xi_\beta}\dot{\xi}_\beta. \tag{3.7}$$

Thus, one obtains the same formulas as if the components of A were scalars. In particular, the definitions of $\dot{x}$ and $\dot{\xi}$ are:

$$\dot{x}_i = \frac{\Delta}{\Delta t}x_i, \tag{3.8}$$

$$\dot{\xi}_\alpha = \frac{D}{Dt}\xi_\alpha, \tag{3.9}$$

which is what they ought to be.

The fact that Dx_i/Dt and $\Delta\xi_\alpha/\Delta t$ must be zero yields the following identities:

$$\frac{D}{Dt}x_i = 0 = \dot{x}_i + \frac{\partial x_i}{\partial \xi_\alpha}\dot{\xi}_\alpha, \tag{3.10}$$

$$\frac{\Delta}{\Delta t}\xi_\alpha = 0 = \dot{\xi}_\alpha + \frac{\partial \xi_\alpha}{\partial x_i}\dot{x}_i. \tag{3.11}$$

Similarly, one can define second-order time derivatives (accelerations):

$$\frac{\Delta^2}{\Delta t^2}x_i = \ddot{x}_i, \tag{3.12}$$

$$\frac{D^2}{Dt^2}\xi_\alpha = \ddot{\xi}_\alpha. \tag{3.13}$$

One can also define "mixed" types of accelerations. Thus, the following quantities make sense:

$$\frac{D}{Dt}\frac{\Delta}{\Delta t}x_i \equiv \frac{D}{Dt}\dot{x}_i = \ddot{x}_i + \frac{\partial \dot{x}_i}{\partial \xi_\alpha}\dot{\xi}_\alpha = \ddot{x}_i - \frac{\partial \dot{x}_i}{\partial \xi_\alpha}\frac{\partial \xi_\alpha}{\partial x_j}\dot{x}_j, \tag{3.14}$$

$$\frac{\Delta}{\Delta t}\frac{D}{Dt}\xi_\alpha \equiv \frac{\Delta}{\Delta t}\dot{\xi}_\alpha = \ddot{\xi}_\alpha + \frac{\partial \dot{\xi}_\alpha}{\partial x_i}\dot{x}_i = \ddot{\xi}_\alpha - \frac{\partial \dot{\xi}_\alpha}{\partial x_i}\frac{\partial x_i}{\partial \xi_\beta}\dot{\xi}_\beta. \tag{3.15}$$

The other "mixed" accelerations must vanish identically, and so must D^2x_i/Dt^2 and $\Delta^2\xi_\alpha/\Delta t^2$. This gives rise to the following identities:

$$0 = \ddot{x}_i + 2\frac{\partial \dot{x}_i}{\partial \xi_\alpha}\dot{\xi}_\alpha + \frac{\partial^2 x_i}{\partial \xi_\alpha \partial \xi_\beta}\dot{\xi}_\alpha\dot{\xi}_\beta + \frac{\partial x_i}{\partial \xi_\alpha}\ddot{\xi}_\alpha, \tag{3.16}$$

$$0 = \ddot{x}_i + \frac{\partial \dot{x}_i}{\partial \xi_\alpha}\dot{\xi}_\alpha + \ddot{\xi}_\alpha\frac{\partial x_i}{\partial \xi_\alpha} + \frac{\partial x_i}{\partial \xi_\alpha}\frac{\partial \dot{\xi}_\alpha}{\partial x_j}\dot{x}_j, \tag{3.17}$$

and to a similar set if x and ξ are interchanged. These identities enable one to express any time derivatives up to second order in terms of any other chosen ones of first and second order.

(*b*) *Representations of the Continuity Condition*

It has been mentioned earlier that the representation of the continuity condition in its usual form, as displayed in (2.19), is really quite unsatisfactory, owing to the fact that it contains the x's as well as the ξ's as arguments. It would appear as more consistent to introduce time derivatives of ξ instead of x, as then all occurring functions would consistently refer to x as arguments. If this is done, using the identities just established, one obtains:

$$\frac{D\rho}{Dt} - \frac{\partial}{\partial x_i}\left(\rho\dot{\xi}_\alpha\frac{\partial x_i}{\partial \xi_\alpha}\right) = 0. \tag{3.18}$$

This representation of the continuity equation has the x's as independent variables, and all time derivatives are obtained with x being held constant.

Reciprocally, one can express the law of continuity in parameter space. In fact, this has already been done implicitly on the occasion of the definition of "density". One obtains from (2.10):

$$\frac{\Delta}{\Delta t}(\rho\sqrt{\det \kappa}) = 0 \tag{3.19}$$

or, written out:

$$\frac{\Delta}{\Delta t}\left\{\rho(\xi, t)\sqrt{\det\left(\frac{\partial x_i}{\partial \xi_\alpha}\frac{\partial x_i}{\partial \xi_\beta}\right)}\right\} = 0. \tag{3.20}$$

(*c*) *Representations of the Equations of Motion*

Similar remarks pertain to the equations of motion. Again, their usual representation, as displayed in (2.20), contains functions of x as well as functions of ξ, which is somewhat unsymmetrical. One should express $\ddot{x}$ as a function of x, which means that one should use $\ddot{\xi}$ rather than $\ddot{x}$. Using the identities established above, one obtains:

$$\frac{\partial \tau_{ik}}{\partial x_k}+\rho\left(f_i+\frac{\partial x_i}{\partial \xi_\alpha}\ddot{\xi}_\alpha-2\frac{\partial x_i}{\partial \xi_\alpha}\frac{\partial x_j}{\partial \xi_\beta}\frac{\partial \dot{\xi}_\alpha}{\partial x_j}\dot{\xi}_\beta-\frac{\partial^2 x_i}{\partial \xi_\alpha \partial \xi_\beta}\dot{\xi}_\alpha\dot{\xi}_\beta\right) = 0. \tag{3.21}$$

The above expression of the law of motion (often referred to as "Newton's law of motion", but actually due to Cauchy) is in a form as it is commonly encountered: The independent variables are the x's and all time derivatives are obtained with x being held constant (this of course does not exclude the fact that the inverse functions, $\xi_\alpha(x_i, t)$, can occur in differentiations other than time differentiations). This form of the equations of motion is useful if the boundary conditions are fixed in the co-ordinates, such as pertaining to containers or fixed bearings. However, it can also occur that the boundary conditions are fixed in parameter space, e.g. forces acting upon "free surfaces" of the body. In such cases it is preferable to express the laws of motion and continuity in terms of the parameters.

Thus, the law of motion has now to be expressed in parameter space.

The expression of the equations of motion in terms of ξ is obtained if, in the argument of τ and f, x is expressed in terms of ξ:

$$0 = \frac{\partial \tau_{ik}(x = x(\xi, t))}{\partial \xi_\alpha}\frac{\partial \xi_\alpha}{\partial x_k}+\rho(\xi)\left\{f_i(x = x(\xi, t))-\frac{\Delta^2 x(\xi, t)}{\Delta t^2}\right\}. \tag{3.22}$$

It thus appears again that, with regard to the description of motion, parameter space and co-ordinate space are entirely equivalent. It will be found that the expression of the law of motion is simpler in terms of the co-ordinates, but this is only because of the definition of the usually employed stress-tensor in terms of the co-ordinates and not in terms of the parameters.

(*d*) *Representation of the Rheological Condition*

A general form of the rheological condition, as established by Oldroyd, has been discussed in Sec. 2. Other forms of the rheological condition have been proposed by Cotter and Rivlin (1955) and by Thomas (1955). If the rheological condition contains only time derivatives, one can use the identities established

above to express time derivatives with fixed ξ in terms of time derivatives with fixed x. If, however, the rheological condition contains time integrations with fixed ξ, one must express the latter in terms of time integrations with fixed x. The problem is therefore to find by what $(F(x, t))$ the integrand $(f(\xi, t))$ has to be replaced in a time integration with fixed ξ such that one can integrate with fixed x instead of with fixed ξ. The condition is:

$$\int_{\text{fixed } \xi} f(\xi, t)dt = \int_{\text{fixed } x} F(x, t)dt. \tag{3.23}$$

Differentiating this condition with fixed x yields:

$$f(\xi, t)+\dot{\xi}_\alpha \frac{\partial}{\partial \xi_\alpha} \int_{\text{fixed } \xi} f(\xi, t)dt = F(x, t). \tag{3.24}$$

Thus, in every time integral with fixed ξ, the integrand f has to be replaced by F according to Eq. (3.24), and then the time integral may be taken with fixed x instead of with fixed ξ. This completes all procedures necessary to express the rheological condition in co-ordinate space.

The above considerations take account of Oldroyd's rheological conditions. It is seen that a great variety of such conditions are possible. The simple catalogues of rheological equations devised by Reiner (1949), etc., are therefore seen to be entirely inadequate; they only constitute a few special cases out of an infinity of possibilities.

4. CONCLUSION

In conclusion, it may be well to summarize once more the important points in the analysis of displacements of a continuous medium.

In general, the behavior of a continuous medium is given by determining three functions (displacement functions, co-ordinate functions) of three parameters and time. The physical conditions pertinent to determining these functions are, firstly, the equation of continuity, secondly, Newton's law of motion, thirdly, the rheological condition of state, and fourthly, boundary and initial conditions.

The mathematical problem is to express all the physical conditions in a suitable form. In this connection, it should be noted that any infinitesimal-displacement theory is inadequate. If one wants to maintain the notion of "strain", one therefore has to generalize this notion to finite displacements. In fact, it is not convenient to use the components of strain as kinematical variables since they are not independent because they must fulfill the compatibility relations. It is, therefore, better to eliminate the strains altogether from the equations and to maintain only the displacement functions. The strains, however, are very useful in establishing rheological conditions, and therefore formulas must be found to connect the strains with other variables.

It can be shown that the simplest mathematical representation of the physics of the displacements in continuous matter is obtained either by expressing the displacement co-ordinates as functions of the parameters and time, or else by expressing the parameters as functions of the co-ordinates

and time. Both representations are equivalent, a fact which, although known, has not been sufficiently emphasized in the literature. The space of the parameters as well as the space of the co-ordinates is Euclidean and one sensibly will use Cartesian co-ordinates to describe them. There is no need to introduce Riemannian geometry. There is a connection between our "parameters" and "convected" co-ordinates introduced by other authors, but convected co-ordinates introduce the formalism of Riemannian geometry which in the end must again be eliminated since all physical events take place in ordinary, Euclidean space. It seems, therefore, superfluous to introduce the formalism of Riemannian geometry in the first place.

The scheme presented is not a simple one and is designed to take care of all imaginable rheological materials. It is strictly phenomenological in that there is no intrinsic motivation to assume one rheological condition over another. It, therefore, is designed to take care of any behaviors of materials that might be encountered in engineering science or in the physics of the Earth's interior, as long as the displacements are continuous.

REFERENCES

COTTER, B. A. and RIVLIN, R. S. 1955. Quart. Appl. Math. **13**: 177.
DEUKER, E. A. 1941. Deut. Math. **5**: 546.
ECKART, C. 1948. Phys. Rev. **73**: 373.
GREEN, A. E. and ZERNA, W. 1950. Phil. Mag. (7), **41**: 313.
OLDROYD, J. G. 1950. Proc. Roy. Soc. A, **200**: 523.
REINER, M. 1949. Twelve lectures on theoretical rheology. North-Holland Pub. Co., Amsterdam.
THOMAS, T. Y. 1955. Proc. Natl. Acad. Sci. U.S. **41**: 762.
TRUESDELL, C. 1952. J. Rational Mech. Anal. **1**: 125.
WEISSENBERG, K. 1931. Abhandl. deut. Akad. Wiss. Berlin, No. 2.

SCATTERING OF ELECTROMAGNETIC WAVES BY COAXIAL CYLINDERS[1]

By Albert W. Adey[2]

ABSTRACT

A scattering system comprising two coaxial, dielectric cylinders has been studied theoretically and experimentally. Calculations have been made of the forward and back scattered fields for several combinations of inner and outer radii. It has been found that, by covering a metal cylinder with a coaxial dielectric shield, it is possible to eliminate to some extent the deep near-field shadow. Experimental results obtained at a wavelength of 3.275 cm. using a parallel-plate transmission line are in good agreement with calculations.

INTRODUCTION

The formal solution of the problem of the scattering of a plane electromagnetic wave by a system of two coaxial, dielectric cylinders was suggested by Thilo (1920) in a study of radiation pressure. He gave no numerical results. No calculations on this configuration have been announced, as far as the present author is aware. Several authors (Keitel 1955; Montroll and Greenberg 1952) have, however, treated the problem of scattering by a dielectric cylinder for which the refractive index has a continuous but non-uniform radial distribution.

Experiments using free-space methods would be restricted for the most part to a core of liquid in a dielectric tube, because of the difficulty of fabricating coaxial structures of sufficient length to be considered "infinitely long". Several studies using such a system have been reported (Schaefer and Grossman 1910; Tamarkin 1949) but in each case the effect of the dielectric container was neglected in the calculations, and the results were presented as applying to scattering by a homogeneous cylinder. However, the recent introduction of the parallel-plate transmission line (El-Kharadly 1955; Row 1953) as a microwave measuring device has removed this restriction and has permitted the use of various combinations of cylinder materials with resulting accuracy of machining and economy of materials.

The problem is of some practical interest in a discussion of the radiation from a slot on a dielectric-coated cylinder and of the effect on the scattering by a cylindrical structure of, say, an ice coating.

In the present paper some calculated and experimental results will be presented for the case of a metal cylinder surrounded by a dielectric sleeve. The experiments were performed using a parallel-plate transmission line (Adey 1955) operating at a wavelength of 3.275 cm. and the results agreed satisfactorily with theoretical calculations.

---

[1]Manuscript received October 28, 1955.

This work was performed at the Imperial College of Science and Technology, London, England, and, with the exception of the results of Fig. 7, formed part of a thesis accepted by the University of London for the award of the Ph.D. degree, October, 1954. Presented at the joint Canadian Association of Physicists and American Physical Society meeting, Toronto, June 22, 1955.

[2]Present address: Defence Research Telecommunications Establishment, Radio Physics Laboratory, Defence Research Board, Shirley Bay, Ottawa, Ontario.

THEORETICAL SOLUTION

A plane wave, of amplitude unity for convenience, and having its electric vector polarized parallel to the cylinder axis, propagates in the direction $\phi = 0$ in a medium of permittivity ϵ_1 and permeability μ_1. It is incident on a cylinder with a core of radius a and coaxial sleeve of outer radius b. The sleeve has a permittivity ϵ_2 and permeability μ_2 and the core has the corresponding constants ϵ_3, μ_3. Fig. 1 illustrates the arrangement for a cylindrical system of

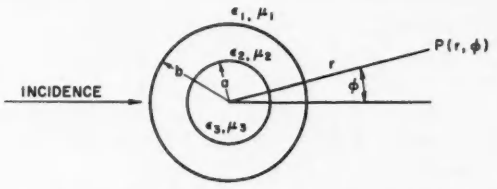

FIG. 1. Coordinate system for scattering by a coaxial cylinder.

coordinates (r, ϕ, z). A time factor of $e^{-i\omega t}$ is assumed and rationalized m.k.s. units are used.

The fields in the three regions can be represented by the following forms:

Region 1

$$E_{\text{inc}}(r, \phi) = e^{iK_1 r\cos\phi} = \sum_{n=0}^{\infty} e_n (i)^n J_n(K_1 r) \cos n\phi \tag{1}$$

$$E_1^{\text{sc}}(r, \phi) = \sum_{n=0}^{\infty} e_n B_n H_n^{(1)}(K_1 r) \cos n\phi \tag{2}$$

Region 2

$$E_2(r, \phi) = \sum_{n=0}^{\infty} e_n [D_n J_n(K_2 r) + C_n Y_n(K_2 r)] \cos n\phi \tag{3}$$

Region 3

$$E_3(r, \phi) = \sum_{n=0}^{\infty} e_n A_n J_n(K_3 r) \cos n\phi \tag{4}$$

where the J_n and the Y_n are the Bessel functions of the first and second kinds respectively, the $H_n^{(1)}$ are the Hankel functions of the first kind, and the K's are the wave numbers appropriate to the various regions ($K = 2\pi/\text{wavelength}$).

From the Maxwell equation for the magnetic field

$$H_\phi(r, \phi) = \frac{i}{\omega\mu} \frac{\partial}{\partial r} E(r, \phi) \tag{5}$$

and the application of the usual boundary condition of continuity of the

tangential electric and magnetic fields at the interfaces between the several regions there results the following expression for the scattered amplitudes B_n in (2):

$$(6)\quad -\frac{B_n}{(i)^n} = \frac{\begin{vmatrix} J_n(p), & -J_n(s), & -Y_n(s), & 0 \\ \frac{K_1}{\mu_1}J_n'(p), & -\frac{K_2}{\mu_2}J_n'(s), & -\frac{K_2}{\mu_2}Y_n'(s), & 0 \\ 0, & J_n(m), & Y_n(m), & -J_n(l) \\ 0, & \frac{K_2}{\mu_2}J_n'(m), & \frac{K_2}{\mu_2}Y_n'(m), & -\frac{K_3}{\mu_3}J_n'(l) \end{vmatrix}}{\Delta}$$

where $l = K_3 a$, $m = K_2 a$, $s = K_2 b$, $p = K_1 b$, and the prime indicates a differentiation with respect to the argument. Δ is obtained from the numerator of (6) by the following changes in the first column:

$$(7)\quad \begin{aligned} J_n(p) &\rightarrow H_n^{(1)}(p), \\ J_n'(p) &\rightarrow H_n^{(1)\prime}(p). \end{aligned}$$

The corresponding expressions for the amplitudes in the other regions are obtained in the same way.

The total external field is then obtained by substituting from (6) and (7) in (2) and adding to (1).

If $\epsilon_2 = \epsilon_3$ and $\mu_2 = \mu_3$ one obtains the usual expressions appropriate to scattering by a homogeneous cylinder.

Considerable simplification results when the central core is a highly conducting cylinder. The scattered field amplitudes then become

$$(8)\quad -\frac{B_n}{(i)^n} = \frac{\begin{vmatrix} J_n(p), & -J_n(s), & -Y_n(s) \\ 0, & J_n(m), & Y_n(m) \\ \frac{K_1\mu_2}{K_2\mu_1}J_n'(p), & -J_n'(s), & -Y_n'(s) \end{vmatrix}}{T}$$

and the amplitudes of the fields in the shell

$$(9)\quad D_n = P\,Y_n(m)/T,$$

$$(10)\quad C_n = -P\,J_n(m)/T,$$

$$(11)\quad P = (i)^{n-1}\cdot\frac{2}{\pi p}\cdot\frac{K_1\mu_2}{K_2\mu_1},$$

where T is obtained from the numerator of (8) by the changes indicated in (7).

The scattered amplitudes given by either (6) or (8) are thus of the form

$$(12)\quad B_n = -(i)^n\frac{a_n}{a_n + ib_n},$$

as was found previously for the homogeneous conducting and dielectric cylinders (Adey 1955).

THIN-SLEEVE APPROXIMATION

(*a*) *Conducting Core*

If the sleeve is thin, i.e., $t = b-a < a$, one can simplify (8) further. From the first two terms of the Taylor expansion for the Bessel function expressions

$$J_n(K_2b) = J_n(K_2a)+K_2t\,J_n'(K_2a), \tag{13}$$

$$Y_n(K_2b) = Y_n(K_2a)+K_2t\,Y_n'(K_2a), \tag{14}$$

and the Bessel function Wronskian (McLachlan 1941), relation (8) becomes

$$-\frac{B_n}{(i)^n} = \frac{J_n(p)\,.\,F + k\,J_n'(p)\,.\,G}{H_n'(p)\,.\,F + k\,H_n^{(1)\prime}(p)\,.\,G} \tag{15}$$

with

$$F = \frac{2b(b-2a)(n+1)+a^2n}{\pi mab}, \tag{16}$$

$$G = 2t/\pi a, \tag{17}$$

$$k = \frac{K_1\mu_2}{K_2\mu_1} = \sqrt{\frac{\mu_2\epsilon_1}{\mu_1\epsilon_2}}. \tag{18}$$

(*b*) *Dielectric Core*

By the same method as for (*a*) there results from (6) and (7)

$$-\frac{B_n}{(i)^n} = \frac{A}{B}, \tag{19}$$

$$\begin{aligned} A = J_n(p)\Bigg[\left(\frac{K_2}{\mu_2}\right)^2\left\{\frac{2t[b(m^2-n^2)-nt]}{\pi m^2ab}\right\}J_n(l) \\ +Z\left\{\frac{2[b(b-2a)(n+1)+a^2n]}{\pi mab}\right\}J_n'(l)\Bigg] \\ +\frac{K_1}{\mu_1}J_n'(p)\left[\frac{K_2}{\mu_2}\left(\frac{2}{\pi m}\right)J_n(l)+\frac{K_3}{\mu_3}\left(\frac{2t}{\pi a}\right)J_n'(l)\right], \end{aligned} \tag{20}$$

$$Z = \frac{K_2K_3}{\mu_2\mu_3} = \omega^2\sqrt{\epsilon_2\epsilon_3/\mu_2\mu_3}, \tag{21}$$

and B can be obtained from A by making the changes indicated in (7).

OTHER INCIDENT FIELD SYSTEMS

(*a*) *Perpendicular Polarization*

If the magnetic vector of the incident plane wave is oriented parallel to the cylinder axis, the results given previously apply if everywhere μ is replaced by ϵ, E by H, and H by $-E$. For incidence in a direction normal to the cylinder axis the field system for any orientation of the field vectors is then given as a superposition of the two separate results for parallel and perpendicular polarization.

(*b*) *Cylindrical Incident Wave*

If the incident wave is not plane, but is produced by a line source parallel to the cylinder axis and at a finite distance from it, the scattered field can be

found by applying a simple "curvature factor" correction to the plane wave results, this factor being identical with that found for the case of a homogeneous cylinder.

(*c*) *Oblique Incidence*

Only normal incidence has been considered here. The general case of oblique incidence has been analyzed more recently and is more complicated. The results differ in two respects from those presented here: (1) cross-polarization terms occur in the field expressions, as discussed by Sloan (1951) and Wait (1955*a*) for the homogeneous cylinders of metal and dielectric respectively, and (2) the solution is no longer of the simple form given by Eq. 12.

(*d*) *Spherical Incident Wave*

The case for spherical wave incidence does not appear to have been treated. Such a treatment could perhaps be based on the methods of Brick (1954) and Wait (1955*b*) who considered the homogeneous cylinder.

CALCULATED AND EXPERIMENTAL RESULTS

Calculations have been made of the total and the scattered fields for parallel incidence and for a conducting core surrounded by a polystyrene sleeve, for the following values of the parameters:

$$K_1a = 1.25,$$
$$K_1b = 2.5, 3, 4,$$
$$K_2/K_1 = 1.60,$$
$$\phi = 0, \pi/2, \pi.$$

The total shadow field results are given in Fig. 2. The phase curves indicate the change of phase at the field point due to the presence of the cylinder. Fig. 3 shows the behavior of the field amplitude in the sleeve on the shadow side of the core. The amplitude on the illuminated side of the cylinder and in the diametral plane normal to the direction of incidence is illustrated in Figs. 4 and 5 respectively. The scattered field calculations are given in Fig. 6, for three directions relative to the incidence direction.

Three points in particular are to be noted from the results:

(*a*) For the smallest cylinder there is an almost complete matching of the shadow field amplitude. If the metal core were replaced by polystyrene, the field amplitude would increase sharply on approaching the cylinder. If the polystyrene sleeve were removed, or replaced by metal, the shadow would extend to a considerable distance from the cylinder. This particular combination of metal and polystyrene effects a compensation of these two tendencies. For several other values of the polystyrene sleeve's outer radius it was found experimentally that a particular value of the metal core radius could be chosen that would give this matching tendency. Fig. 7 presents some of these results, for sleeves of polystyrene and a lossy plastic.

(*b*) Resonances in the scattering by a homogeneous dielectric cylinder appear to be somewhat neutralized by the presence of the metal core. This

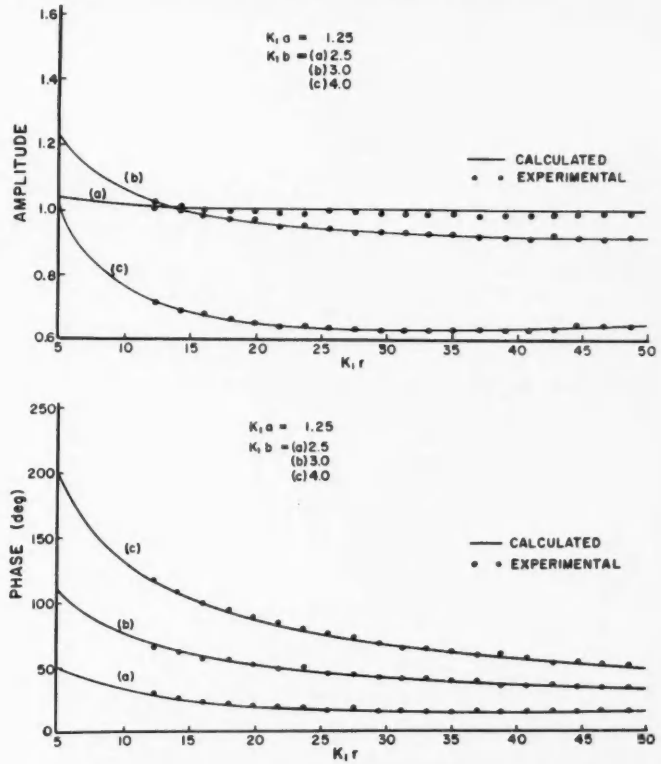

FIG. 2. Shadow field of a coaxial cylinder comprising a metal core and a polystyrene sleeve.

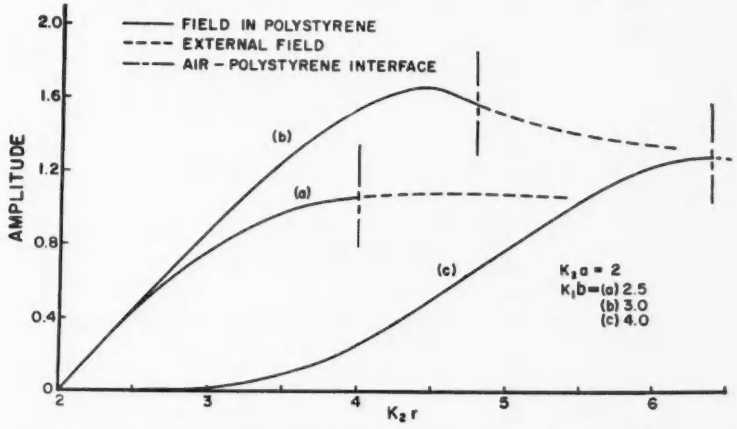

FIG. 3. Field amplitude in the shadow of the core of a coaxial cylinder comprising a metal core and a polystyrene sleeve.

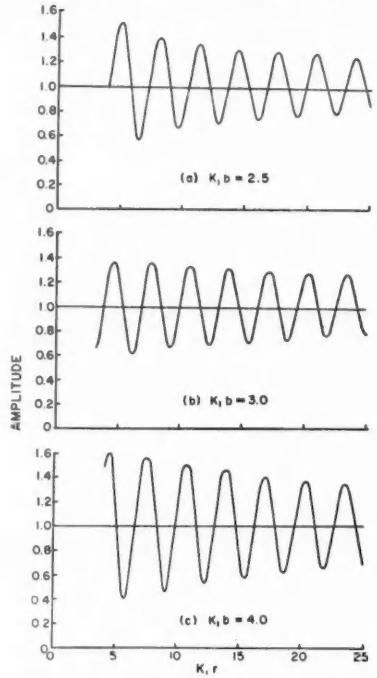

FIG. 4. Field amplitude on the illuminated side of a coaxial cylinder. Core—brass. Sleeve—polystyrene. $K_1a = 1.25$.

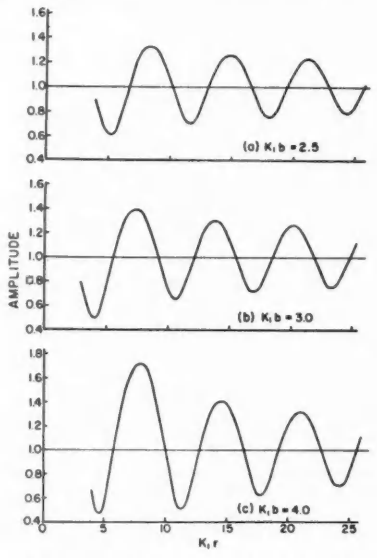

FIG. 5. Field amplitude in diametral plane normal to direction of incidence for coaxial cylinder. $K_1a = 1.25$. Core—brass. Sleeve—polystyrene.

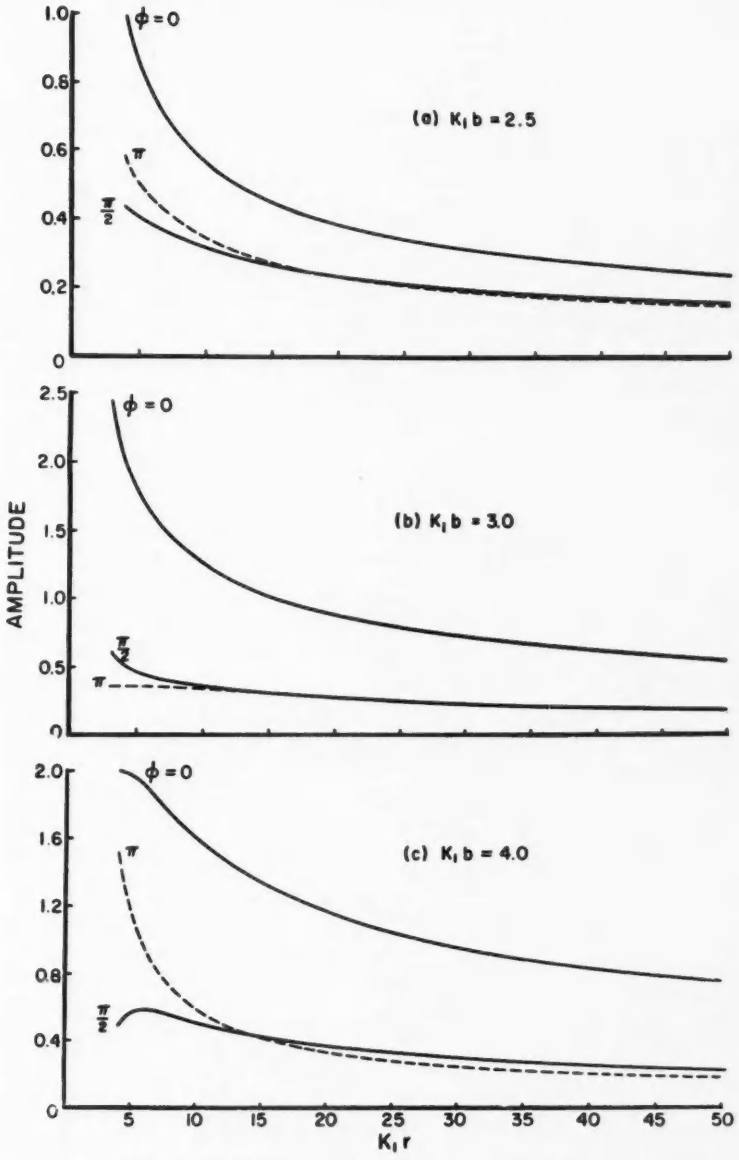

FIG. 6. Amplitude of the field scattered by a coaxial cylinder. $K_1a = 1.25$. Core—brass. Sleeve—polystyrene.

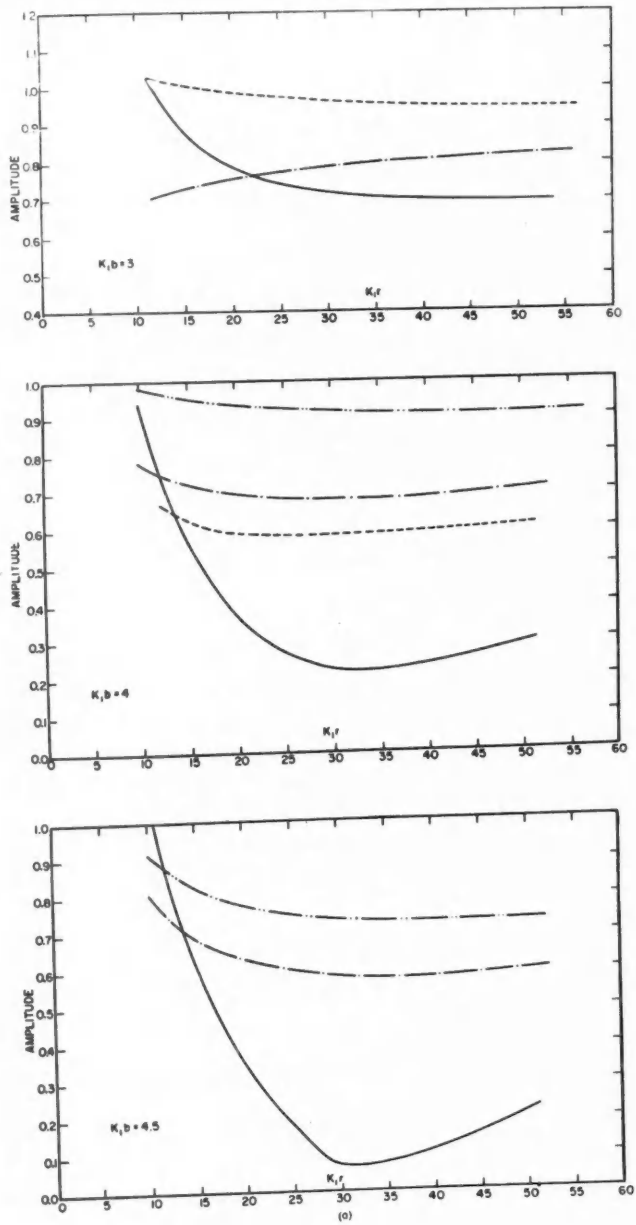

(a)

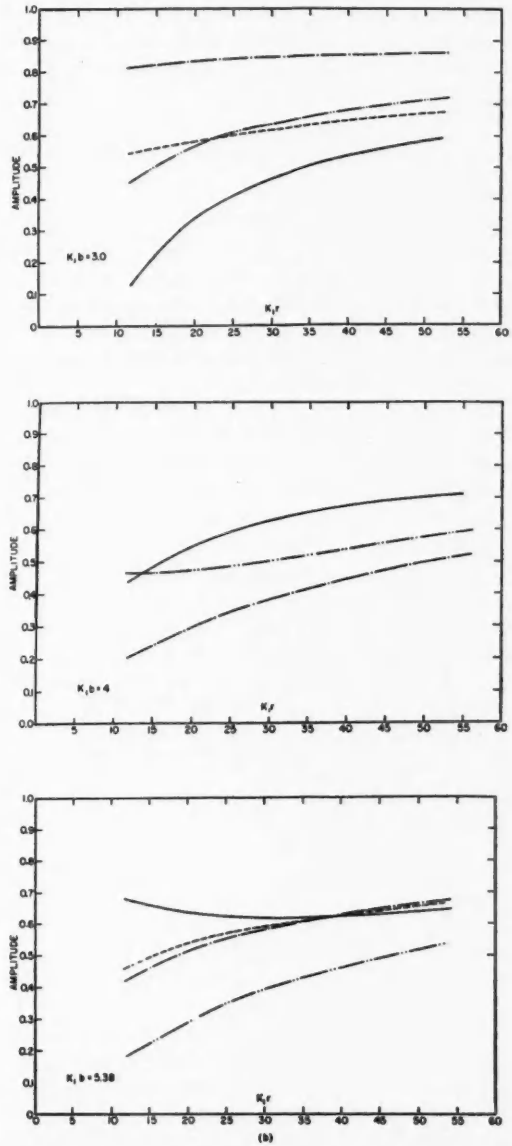

FIG. 7. Shadow field amplitude of a coaxial cylinder. (*a*) Core—brass. Sleeve—polystyrene. (*b*) Core—brass. Sleeve—plastic of permittivity $\epsilon_2 = 3.40(1+i\ 0.0581)\epsilon_1$.

———Homogeneous ($K_1a = 0$)
— — —$K_1a = 1.5$
——·——$K_1a = 2.0$
——··——$K_1a = 2.5$

is illustrated by the phase curve for $K_1b = 4$ in Fig. 2, which is of the smooth form found for a metal cylinder rather than of the rapidly-varying form found for this value of radius for a homogeneous polystyrene cylinder.

(*c*) The internal fields do not exhibit the rapid fluctuations characteristic of those for a homogeneous polystyrene cylinder, but rather resemble the shadow field for a metal cylinder (except for the fact that they rise above the incident field value).

CONCLUSIONS

The calculations have shown, and the experiments have verified, that the scattering behavior of a lossless dielectric cylinder can be highly modified by the presence of a metal core, particularly with regard to some of the resonance phenomena. It has also been seen that a significant reduction of the deep shadow existing behind a metal cylinder can be effected by surrounding the cylinder with a dielectric sleeve.

ACKNOWLEDGMENTS

The guidance of Dr. Willis Jackson and Dr. John Brown is acknowledged. Thanks are extended to the University of New Brunswick for the award of an Overseas Beaverbrook Scholarship, and its extension, and to the Canadian Defence Research Board for a study grant.

REFERENCES

ADEY, A. W. 1955. Can. J. Phys. **33**: 407.
BRICK, D. B. 1954. Cruft Lab. Sci. Rept. No. 1.
EL-KHARADLY, M. M. Z. 1955. Proc. I.E.E. **102, B**: 17.
KEITEL, G. H. 1955. Proc. I.R.E. **43**: 1481.
MCLACHLAN, N. W. 1941. Bessel functions for engineers. Oxford at the Clarendon Press.
MONTROLL, E. W. and GREENBERG, J. M. 1952. Phys. Rev. **86**: 889.
ROW, R. V. 1953. J. Appl. Phys. **24**: 1448.
SCHAEFER, C. L. and GROSSMAN, F. 1910. Ann. Physik, **31**: 455.
SLOAN, R. W. 1951. Tech. Rept. Ohio State Univ. Research Found.
TAMARKIN, P. 1949. J. Acoust. Soc. Amer. **21**: 612.
THILO, G. 1920. Ann. Physik, **62**: 531.
WAIT, J. R. 1955*a*. Can. J. Phys. **33**: 189.
——— 1955*b*. Appl. Sci. Research, B, **4**: 464.

A NOTE ON OPTICAL HYPERFINE STRUCTURE IN CD II

By F. M. Kelly and J. B. Sutherland

A hollow cathode light source, cooled with liquid nitrogen, was used to excite the resonance lines in the second spectrum of cadmium in order to observe the hyperfine structure of the ground level ($5s\ ^2S_{1/2}$). A Hilger medium quartz spectrograph was used with a Fabry-Perot interferometer mounted externally to the spectrograph. A fairly dense coating of aluminum was used on the interferometer plates (Burridge *et al.* 1953).

The Cd II resonance lines arise from the transitions $5s\ ^2S_{1/2} - 5p\ ^2P_{3/2,1/2}$ at 2144 and 2265 Å. Three different etalons were used. The patterns showed that each of the lines consisted of three components. A strong central component is ascribed to the unresolved even isotopes. The two weaker components are attributed to the unresolved odd isotopes and with a small correction give the splitting of the $5s\ ^2S_{1/2}$ level. The nuclear spins of the two odd isotopes are known to be 1/2 (Poss 1949). The line widths of the radiation produced in the source are larger than the anticipated isotope shifts in these lines so that the components due to the individual isotopes could not be resolved.

With one of the spacers (1.255 cm.) the components due to the odd isotopes could be measured on the same patterns without reference to inaccurate measurements of the overexposed component due to the even isotopes. The separation of the components due to the odd isotopes in 2144 Å is 0.519 ± 0.004 cm^{-1} and 0.491 ± 0.007 cm^{-1} in 2265 Å. The errors quoted are the average deviations from the mean of the individual measurements of eight or more separate exposures.

The average value of the nuclear magnetic moments of the two odd isotopes of cadmium can be calculated from the hyperfine structure separations using the Goudsmit (1933), Fermi–Segrè (1933) formula. In this formula the value of the factor $(1 - d\sigma/dn)$ is evaluated by the method of Crawford and Schawlow (1949). Substitution of numerical values in the formula gives $a(5s) = 0.419\ g_I$. When a small allowance is made for the unresolved ^2P structure we obtain $g_I = -1.28$ from 2144 Å and $g_I = -1.20$ from 2265 Å. Then the average value of the nuclear magnetic moment of the two odd isotopes of cadmium is $\mu = -0.62 \pm .02$ n.m.

This result gives a further test of the Fermi–Segrè factor, $1 - d\sigma/dn$, which is 1.16 for the $5s$ electron in Cd II. The test of the accuracy of the Fermi–Segrè factor may be made in two ways. The first is to compare the spectroscopic result with the results of the more accurate determinations by means of the nuclear induction method. From the results of Proctor and Yu (1950) the average value of the nuclear moments of the two odd isotopes is $\mu = -0.608$ n.m. Our result agrees with this within the experimental error, confirming the

evaluation of the Fermi–Segrè factor. The spectroscopic value should be increased by about 2% to account for the correction due to the finite volume of the nucleus (Rosenthal and Breit 1932) but this refinement is beyond the experimental accuracy of this method.

A second comparison can be made using the observed splitting of the $6s\ ^2S_{1/2}$ level of Cd II (Jones 1933). For the $6s$ electron the Fermi–Segrè factor is 1.03. Applying the correction for the unresolved ^2P structure in the lines used by Jones, and with the Fermi-Segrè factor, the calculated value of the nuclear moment from this level is $\mu = -0.63$ n.m. This agrees with our result but the experimental uncertainty is higher. The Fermi–Segrè factor has been confirmed within the experimental error of the spectroscopic determinations.

BURRIDGE, J. C., KUHN, H., and PERY, A. 1953. Proc. Phys. Soc. B, **66**: 963.
CRAWFORD, M. F. and SCHAWLOW, A. L. 1949. Phys. Rev. **76**: 1310.
FERMI, E. and SEGRÈ, E. 1933. Z. Physik, **82**: 729.
GOUDSMIT, S. 1933. Phys. Rev. **43**: 636.
JONES, E. G. 1933. Proc. Phys. Soc. A, **63**: 830.
POSS, H. L. 1949. Properties of atomic nuclei. I. Spins, magnetic moments and electric quadrupole moments. Brookhaven National Laboratory, Upton, New York.
PROCTOR, W. G. and YU, F. C. 1950. Phys. Rev. **76**: 1728.
ROSENTHAL, J. E. AND BREIT, G. Phys. Rev. **41**: 459.

RECEIVED NOVEMBER 28, 1955.
DEPARTMENT OF PHYSICS,
UNIVERSITY OF MANITOBA,
WINNIPEG, MANITOBA.

LETTERS TO THE EDITOR

Under this heading brief reports of important discoveries in physics may be published. These reports should not exceed 600 words and, for any issue, should be submitted not later than six weeks previous to the first day of the month of issue. No proof will be sent to the authors.

Absorption Spectrum of Free CH_3 and CD_3 Radicals[1]

Numerous attempts to obtain the absorption spectrum of the free CH_3 radical have been made in the spectral region 2200–9000 Å. It is possible that the failure of these attempts is due to the fact that the electronic transitions expected in this region are forbidden and therefore far too weak for detection, or to the fact that the upper state is unstable and therefore the absorption is continuous and consequently not easily detected. If CH_3 is planar, the first reason is very likely to apply (see Walsh 1953). It was therefore considered worth while to search for an absorption spectrum in the vacuum ultraviolet where strong allowed absorptions of the Rydberg type are expected.

The radicals were produced by the flash photolysis technique and the absorption spectrum was investigated with the 3 meter vacuum grating spectrograph of this laboratory. Using $Hg(CH_3)_2$ as the parent compound at a pressure of 0.04 mm. in an absorption tube of 50 cm. length, four narrow groups of diffuse absorption bands in the region 1510–1300 Å were found when absorption spectra were taken between 50 and 250 μsec. after the photolysis flash. Similar but slightly shifted band groups were observed in the flash photolysis of $Hg(CD_3)_2$. When, under the optimum conditions, the study of the spectrum was extended to the longer wavelength region, a further band was observed near 2160 Å in $Hg(CH_3)_2$ and near 2140 Å in $Hg(CD_3)_2$. In this region, the absorption of the parent compound is not as troublesome as in the 1500 Å region and therefore the 2150 Å bands can be obtained with considerable intensity by increasing the pressure. They are shown in Fig. 1. At the increased pressure, in $Hg(CD_3)_2$ two additional much weaker bands appear, one of which is visible in Fig. 1.

TABLE I

ABSORPTION BANDS OF CH_3 AND CD_3

n	CH_3		CD_3	
	ν_{obs} (cm^{-1})	ν_{calc} (cm^{-1})	ν_{obs} (cm^{-1})	ν_{calc} (cm^{-1})
	46205 46333 v.w.		46626 Q head 46675 R peak	
			47253 Q head 47304 R peak	
3	66536 v.s. 66717 s. 66811 s.	66536	66471 v.s. 66730 s.	66461
4	72168 s. 72329 s.	72250	72177 m. 72300 v.w.	72175
5	74852 m.	74852	74771 m.	74777
6	76252 m.	76252	76178 w.	76177
7	77088 w.	77090		

In Table I all the observed bands are listed. These bands occur only immediately (within less than 250 μsec.) after the photolysis flash which lasts about 50 μsec. They do not occur in undecomposed $Hg(CH_3)_2$ nor in the residue, say two minutes after photolysis. They must therefore be due to a molecule of short life that is produced by the photodecomposition. Since, from photochemical evidence (see Steacie 1954), it is known that $Hg(CH_3)_2$ splits off one or two CH_3 radicals in the primary act of photodecomposition, it appears probable that the observed spectra are due to free CH_3 and CD_3, respectively.

Further strong evidence for free methyl as the carrier of these spectra comes from the observation of the same bands (to the extent that they are not hidden by parent absorption) in the photolysis of CH_3CHO, $(CH_3)_2N_2$, $(CH_3)_2CO$, CH_3I, and CH_2Br. For all these molecules there is photochemical evidence that free CH_3 radicals are produced.

[1]Issued as N.R.C. No. 3955.

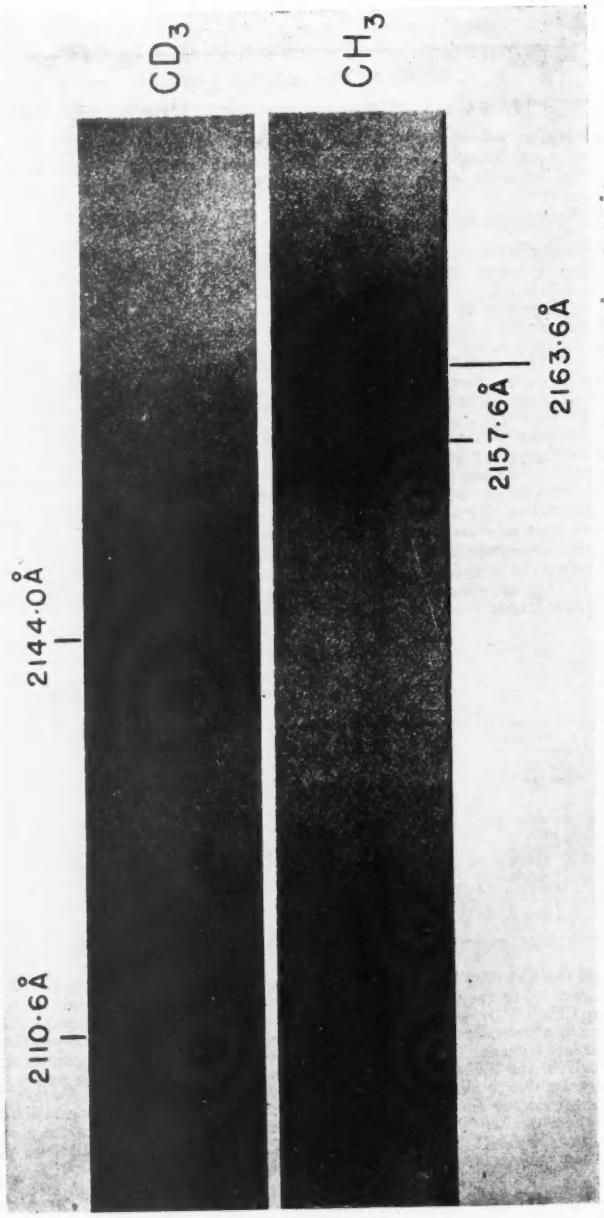

FIG. 1. Absorption spectra of CH_3 and CD_3. (The first wave length at the top should be 2115.6 Å not 2110.6 Å.)

The principal bands in the vacuum region form clear Rydberg series which can be represented by the formulae

$$CH_3: \quad \nu = 79380 - \frac{R}{(n - 0.077)^2}, \qquad n = 3, 4, 5, 6, 7, \ldots,$$

$$CD_3: \quad \nu = 79305 - \frac{R}{(n - 0.077)^2}, \qquad n = 3, 4, 5, 6, \ldots.$$

The wave numbers calculated from these formulae are included in Table I. The constant terms in these formulae represent the ionization potentials of CH_3 and CD_3. Converted to electron volts they are 9.840 and 9.832 $\pm$ 0.002 ev. The excellent agreement with the value obtained by various authors (Lossing, Ingold, and Henderson 1954; Langer, Hipple, and Stevenson 1954) from mass spectrometric measurements, namely 9.9$_6$$\pm$0.1 ev., makes it practically certain that the observed bands are due to free CH_3 and CD_3.

Further conclusive proof that the 2150 Å bands shown in Fig. 1 are due to CH_3 and CD_3 has been obtained by a study of these bands in the flash photolysis of isotopic mixtures of acetone containing 25, 50, and 75% deuterium. In these mixtures two additional bands appear in the space between the CH_3 and CD_3 bands, clearly belonging to CHD_2 and CD_2H. Thus there can be no doubt that the molecule responsible for the spectrum under discussion has three H atoms. The coarseness of the rotational structure of the 2140 Å bands of CD_3 (Fig. 1) excludes the presence of more than one C atom in the molecule. Therefore, one can safely and unambigiously conclude that the spectrum is due to the free methyl radical.

With one exception, the CD_3 band at 2140 Å, all observed bands are diffuse without any indication of fine structure. This diffuseness is clearly due to predissociation which, in the case of the 2140 Å CD_3 band, is apparently slowed down by a barrier which is less easily penetrated in CD_3 than in CH_3. The one resolved branch of the 2140 Å band shows a slight intensity alternation. Assuming the band to be a $\parallel$ band of a planar CD_3 molecule, a slight intensity alternation is expected since the subband with $K = 0$ would have a 10:1 intensity alternation while the other subbands have none, leaving a small alternation in the superposed subbands. The same would apply for a non-planar CD_3 molecule if the inversion doubling is large enough to give rise to separate bands for the two components, that is, if the deviation from the planar configuration is small; but no intensity alternation is expected if the inversion doubling is small, i.e., if the molecule is far from being planar.

The conclusion that the CH_3 molecule in its ground state is planar or nearly planar is in agreement with the predictions of molecular orbital theory (see Walsh 1953) and at the same time accounts in a satisfactory way on the basis of the Franck–Condon principle for the observation of a simple Rydberg series of bands rather than of complex band systems as exhibited by NH_3 in the region below 1500 Å.

With the CH_3 spectrum here observed it will be possible to search more readily for improved conditions of increased concentration and in this way it should be possible to find the expected forbidden transition in the visible region. If this transition occurs above about 2600 Å, it could not be predissociated and would therefore give more precise information on the geometrical structure of CH_3.

We are greatly indebted to Dr. L. C. Leitch for supplying us with the deuterated compounds and to Drs. A. E. Douglas, D. A. Ramsay, and S. R. Polo for critical comments and suggestions.

Langer, A., Hipple, J. A., and Stevenson, D. P. 1954. J. Chem. Phys. **22**: 1836.
Lossing, F. P., Ingold, K. U., and Henderson, I. H. S. 1954. J. Chem. Phys. **22**: 621.
Steacie, E. W. R. 1954. Atomic and free radical reactions. Reinhold Publishing Corp., New York.
Walsh, A. D. 1953. J. Chem. Soc. 2296.

Received March 20, 1956.
Division of Pure Physics,
National Research Council,
Ottawa, Canada.

G. Herzberg
J. Shoosmith

THE PHYSICAL SOCIETY

MEMBERSHIP of the Society is open to all who are interested in Physics.

FELLOWS pay an Entrance fee of £1 1*s*. ($3.00) and an Annual Subscription of £2 2*s*. ($6.00).

STUDENTS: A candidate for Studentship must be between the ages of 18 and 26, and pays an Annual Subscription of 5*s*. ($0.75).

MEETINGS: Fellows and Students may attend all Meetings of the Society including the annual Exhibition of Scientific Instruments and Apparatus.

PUBLICATIONS include the *Proceedings of the Physical Society*, published monthly in two sections, and *Reports on Progress in Physics*, published annually. Volume XVIII, 1955, is now available (price 50*s*. ($7.15)). Members are entitled to receive many of the Publications at a reduced rate.

Further information can be obtained from:

THE PHYSICAL SOCIETY

1, LOWTHER GARDENS, PRINCE CONSORT ROAD
LONDON, S.W.7, ENGLAND

CANADIAN JOURNAL OF PHYSICS

Notes to Contributors

Manuscripts

(i) ***General.*** Manuscripts, in English or French, should be typewritten, double spaced, on paper 8½ × 11 in. **The original and one copy are to be submitted.** Tables and captions for the figures should be placed at the end of the manuscript. Every sheet of the manuscript should be numbered.

Style, arrangement, spelling, and abbreviations should conform to the usage of this journal. Names of all simple compounds, rather than their formulas, should be used in the text. Greek letters or unusual signs should be written plainly or explained by marginal notes. Superscripts and subscripts must be legible and carefully placed.

Manuscripts and illustrations should be carefully checked before they are submitted. Authors will be charged for unnecessary deviations from the usual format and for changes made in the proof that are considered excessive or unnecessary.

(ii) ***Abstract.*** An abstract of not more than about 200 words, indicating the scope of the work and the principal findings, is required, except in Notes.

(iii) ***References.*** References should be listed **alphabetically by authors' names,** unnumbered, and typed after the text. The form of the citations should be that used in issues of this journal published in 1956; in references to papers in periodicals, titles should not be given and only initial page numbers are required. The names of periodicals should be abbreviated in the form given in the most recent *List of Periodicals Abstracted by Chemical Abstracts*. All citations should be checked with the original articles and each one referred to in the text by the authors' names and the year.

(iv) ***Tables.*** Tables should be numbered in roman numerals and each table referred to in the text. Titles should always be given but should be brief; column headings should be brief and descriptive matter in the tables confined to a minimum. Vertical rules should be used only when they are essential. Numerous small tables should be avoided.

Illustrations

(i) ***General.*** All figures (including each figure of the plates) should be numbered consecutively from 1 up, in arabic numerals, and each figure referred to in the text. The author's name, title of the paper, and figure number should be written in the lower left corner of the sheets on which the illustrations appear. Captions should not be written on the illustrations (see Manuscripts (i)).

(ii) ***Line Drawings.*** Drawings should be carefully made with India ink on white drawing paper, blue tracing linen, or co-ordinate paper ruled in blue only; any co-ordinate lines that are to appear in the reproduction should be ruled in black ink. Paper ruled in green, yellow, or red should not be used unless it is desired to have all the co-ordinate lines show. All lines should be of sufficient thickness to reproduce well. Decimal points, periods, and stippled dots should be solid black circles large enough to be reduced if necessary. Letters and numerals should be neatly made, preferably with a stencil (**do NOT use typewriting**) and be of such size that the smallest lettering will be not less than 1 mm. high when reproduced in a cut 3 in. wide.

Many drawings are made too large; originals should not be more than 2 or 3 times the size of the desired reproduction. In large drawings or groups of drawings the ratio of height to width should conform to that of a journal page but the height should be adjusted to make allowance for the caption.

The original drawings and one set of clear copies (e.g. small photographs) are to be submitted.

(iii) ***Photographs.*** Prints should be made on glossy paper, with strong contrasts. They should be trimmed so that essential features only are shown and mounted carefully, with rubber cement, on white cardboard with no space or only a **very** small space (less than 1 mm.) between them. In mounting, full use of the space available should be made (to reduce the number of cuts required) and the ratio of height to width should correspond to that of a journal page (4¾ × 7½ in.); however, allowance must be made for the captions. Photographs or groups of photographs should not be more than 2 or 3 times the size of the desired reproduction.

Photographs are to be submitted in duplicate; if they are to be reproduced in groups one set should be mounted, the duplicate set unmounted.

Reprints

A total of 50 reprints of each paper, without covers, are supplied free. Additional reprints, with or without covers, may be purchased.

Charges for reprints are based on the number of printed pages, which may be calculated approximately by multiplying by 0.6 the number of manuscript pages (double-spaced typewritten sheets, 8½ × 11 in.) and including the space occupied by illustrations. An additional charge is made for illustrations that appear as coated inserts. The cost per page is given on the reprint requisition which accompanies the galley.

Any reprints required in addition to those requested on the author's reprint requisition form must be ordered officially as soon as the paper has been accepted for publication.

Contents

Page

Structure of the Mass Increments of Isotopes—*G. A. Baker, Jr. and G. A. Baker, Sr.* - - - - - - - - - - - - - - - 423

Production of Cosmic Ray Mesons at Large Zenith Angles—*D. Jakeman* - - - - - - - - - - - - - - - - 432

A Study of Nucleon Forces with Repulsive Cores. II. Low Energy Properties, Particularly Charge Independence—*J. Shapiro and M. A. Preston* - - - - - - - - - - - - - - - 451

Kinetics of Solidification—*K. A. Jackson and Bruce Chalmers* - 473

The Electrical Conductivity of Chlorobenzene—*John Hart and A. G. Mungall* - - - - - - - - - - - - - - - 491

Finite Displacements in Rheological Bodies—A. E. Scheidegger - 498

Scattering of Electromagnetic Waves by Coaxial Cylinders—*Albert W. Adey* - - - - - - - - - - - - - - - - 510

Notes:

A Note on Optical Hyperfine Structure in Cd II—*F. M. Kelly and J. B. Sutherland* - - - - - - - - - - - - - - 521

Letters to the Editor:

Absorption Spectrum of Free CH_3 and CD_3 Radicals—*G. Herzberg and J. Shoosmith* - - - - - - - - - - - - - - 523

Printed in Canada *by* University of Toronto Press